Validation of ozone measurements from the Atmospheric Chemistry Experiment (ACE)

Article · January 2008

43 authors, including:

Eric Dupuy
National Institute for Environmental Studies
68 PUBLICATIONS 1,378 CITATIONS

SEE PROFILE

Jayanta Kar
Science Systems and Applications, Inc.
117 PUBLICATIONS 1,714 CITATIONS

SEE PROFILE

C. T. Mcelroy
York University
240 PUBLICATIONS 6,591 CITATIONS

SEE PROFILE

Ryan C. Hughes
University of Waterloo
12 PUBLICATIONS 230 CITATIONS

SEE PROFILE

Some of the authors of this publication are also working on these related projects:

Project Tropospheric Emissions: Monitoring of Pollution (TEMPO) View project

Project ESA's Climate Change Initiative - Ozone_cci View project

**Atmospheric
Chemistry
and Physics
Discussions**

Validation of ozone measurements from the Atmospheric Chemistry Experiment (ACE)

E. Dupuy[1], K. A. Walker[1,2], J. Kar[2], C. D. Boone[1], C. T. McElroy[2,3], P. F. Bernath[1,4], J. R. Drummond[2,5], R. Skelton[1], S. D. McLeod[1], R. C. Hughes[1], C. R. Nowlan[2], D. G. Dufour[6], J. Zou[2], F. Nichitiu[2], K. Strong[2], P. Baron[7], R. M. Bevilacqua[8], T. Blumenstock[9], G. E. Bodeker[10], T. Borsdorff[11], A. E. Bourassa[12], H. Bovensmann[13], I. S. Boyd[14], A. Bracher[13], C. Brogniez[15], J. P. Burrows[13], V. Catoire[16], S. Ceccherini[17], S. Chabrillat[18], T. Christensen[19], M. T. Coffey[20], U. Cortesi[17], J. Davies[3], C. De Clercq[18], D. A. Degenstein[12], M. De Mazière[18], P. Demoulin[21], J. Dodion[18], B. Firanski[22], H. Fischer[9], G. Forbes[23], L. Froidevaux[24], D. Fussen[18], P. Gerard[18], S. Godin-Beekman[25], F. Goutail[26], J. Granville[18], D. Griffith[27], C. S. Haley[28], J. W. Hannigan[20], M. Höpfner[9], J. J. Jin[29], A. Jones[30], N. B. Jones[27], K. Jucks[31], A. Kagawa[7,32], Y. Kasai[7], T. E. Kerzenmacher[2], A. Kleinböhl[13,24], A. R. Klekociuk[33], I. Kramer[9], H. Küllmann[13], J. Kuttippurath[13,25], E. Kyrölä[34], J.-C. Lambert[18], N. J. Livesey[24], E. J. Llewellyn[12], N. D. Lloyd[12], E. Mahieu[21], G. L. Manney[24,35], B. T. Marshall[36], J. C. McConnell[29], M. P. McCormick[37], I. S. McDermid[38], M. McHugh[36], C. A. McLinden[3], J. Mellqvist[30], K. Mizutani[7], Y. Murayama[7], D. P. Murtagh[30], H. Oelhaf[9], A. Parrish[39], S. V. Petelina[12,40], C. Piccolo[41], J.-P. Pommereau[26], C. E. Randall[42], C. Robert[16], C. Roth[12], M. Schneider[9], C. Senten[18], T. Steck[9], A. Strandberg[30], K. B. Strawbridge[22], R. Sussmann[11], D. P. J. Swart[43], D. W. Tarasick[3], J. R. Taylor[2], C. Tétard[15], L. W. Thomason[37],

A. M. Thompson[44], M. B. Tully[45], J. Urban[30], F. Vanhellemont[18], T. von Clarmann[9], P. von der Gathen[46], C. von Savigny[13], J. W. Waters[24], J. C. Witte[47,48], M. Wolff[2], and J. M. Zawodny[37]

[1]Department of Chemistry, University of Waterloo, Waterloo, ON, Canada

[2]Department of Physics, University of Toronto, Toronto, ON, Canada

[3]Environment Canada, Downsview, ON, Canada

[4]Department of Chemistry, University of York, Heslington, York, UK

[5]Department of Physics and Atmospheric Science, Dalhousie University, Halifax, Canada

[6]Picomole Instruments Inc., Edmonton, AB, Canada

[7]National Institute of Information and Communications Technology (NICT), Koganei, Tokyo, Japan

[8]Naval Research Laboratory, Washington, D.C., USA

[9]Institut für Meteorologie und Klimaforschung (IMK), Forschungszentrum Karlsruhe (FZK) and Universität Karlsruhe, Karlsruhe, Germany

[10]National Institute of Water and Atmospheric Research, Lauder, New Zealand

[11]Institut für Meteorologie und Klimaforschung Atmosphärische Umweltforschung (IMK-IFU), Forschungszentrum Karlsruhe, Garmisch-Partenkirchen, Germany

[12]Institute of Space and Atmospheric Studies, University of Saskatchewan, Saskatoon, SK, Canada

[13]Institut für Umweltphysik (IUP), Universität Bremen, Bremen, Germany

[14]NIWA - Environmental Research Institute, University of Massachusetts, Amherst, MA, USA

[15]Laboratoire d'Optique Atmosphérique, CNRS – Université des sciences et technologies de Lille, Villeneuve d'Ascq, France

[16]Laboratoire de Physique et Chimie de l'Environnement, CNRS – Université d'Orléans, Orléans, France

[17]Instituto di Fisica Applicata "N. Carrara" (IFAC) del Consiglio Nazionale delle Ricerche (CNR), Sesto Fiorentino, Italy

[18]Institut d'Aéronomie Spatiale de Belgique (BIRA-IASB), Bruxelles, Belgium

[19]Danish Climate Centre, Danish Meteorological Institute, Copenhagen, Denmark

[20]Earth and Sun Systems Laboratory (ESSL), National Center for Atmospheric Research (NCAR), Boulder, CO, USA

[21]Institut d'Astrophysique et de Géophysique, Université de Liège, Liège, Belgium

[22]Science and Technology Branch, Environment Canada, Centre For Atmospheric Research Experiments, Egbert, ON, Canada

[23]Environment Canada Sable Island, Dartmouth, Canada

[24]Jet Propulsion Laboratory (JPL), California Institute of Technology, Pasadena, CA, USA

[25]CNRS – Service d'Aéronomie (SA), Université Pierre et Marie Curie (UPMC) Paris VI, Paris, France

[26]CNRS – Service d'Aéronomie (SA), Verrières-le-Buisson, France

[27]School of Chemistry, University of Wollongong, Wollongong, Australia

[28]Centre for Research in Earth and Space Science, York University, Toronto, ON, Canada

[29]Department of Earth and Space Science and Engineering, York University, Toronto, ON, Canada

[30]Department of Radio and Space Science, Chalmers University of Technology, Göteborg, Sweden

[31]Harvard-Smithsonian Center for Astrophysics, Cambridge, MA, USA

[32]Fujitsu FIP Corporation, Koto, Tokyo, Japan

[33]Ice, Ocean, Atmosphere and Climate (IOAC) Program, Australian Antarctic Division, Kingston, Australia

[34]Earth Observation, Finnish Meteorological Institute, Helsinki, Finland

[35]New Mexico Institute of Mining and Technology, Socorro, NM, USA

[36]GATS, Inc., Newport News, VA, USA

[37]NASA Langley Research Center, Atmospheric Sciences Division, Hampton, VA, USA

[38]Jet Propulsion Laboratory, Table Mountain Facility, Wrightwood, CA, USA

[39]Department of Astronomy, University of Massachusetts, Amherst, MA, USA

[40]Department of Physics, La Trobe University, Victoria, Australia

[41]Atmospheric, Oceanic and Planetary Physics, Oxford University, UK

2515

[42]Laboratory for Atmospheric and Space Physics, University of Colorado, Boulder, CO, USA

[43]National Institute for Public Health and the Environment (RIVM), Bilthoven, The Netherlands

[44]Department of Meteorology, Pennsylvania State University, University Park, PA, USA

[45]Atmosphere Watch Section, Bureau of Meteorology, Melboune, Vic, Australia

[46]Alfred Wegener Institute for Polar and Marine Research, Research Unit Potsdam, Germany

[47]Science Systems and Applications, Inc., Lanham, MD, USA

[48]NASA Goddard Space Flight Center (GSFC), Greenbelt, MD, USA

Correspondence to: K. A. Walker (kwalker@atmosp.physics.utoronto.ca)

2516

Abstract

This paper presents extensive validation analyses of ozone observations from the Atmospheric Chemistry Experiment (ACE) satellite instruments: the ACE Fourier Transform Spectrometer (ACE-FTS) and the Measurement of Aerosol Extinction in the Stratosphere and Troposphere Retrieved by Occultation (ACE-MAESTRO) instrument. The ACE satellite instruments operate in the mid-infrared and ultraviolet-visible-near-infrared spectral regions using the solar occultation technique. In order to continue the long-standing record of solar occultation measurements from space, a detailed quality assessment is required to evaluate the ACE data and validate their use for scientific purposes. Here we compare the latest ozone data products from ACE-FTS and ACE-MAESTRO with coincident observations from satellite-borne, airborne, balloon-borne and ground-based instruments, by analysing volume mixing ratio profiles and partial column densities. The ACE-FTS version 2.2 Ozone Update product reports more ozone than most correlative measurements from the upper troposphere to the lower mesosphere. At altitude levels from 16 to 44 km, the mean differences range generally between 0 and +10% with a slight but systematic positive bias (typically +5%). At higher altitudes (45–60 km), the ACE-FTS ozone amounts are significantly larger than those of the comparison instruments by up to ∼40% (typically +20%). For the ACE-MAESTRO version 1.2 ozone data product, agreement within ±10% (generally better than ±5%) is found between 18 and 40 km for the sunrise and sunset measurements. At higher altitudes (45–55 km), systematic biases of opposite sign are found between the ACE-MAESTRO sunrise and sunset observations. While ozone amounts derived from the ACE-MAESTRO sunrise occultation data are often smaller than the coincident observations (by as much as −10%), the sunset occultation profiles for ACE-MAESTRO show results that are qualitatively similar to ACE-FTS and indicate a large positive bias (+10 to +30%) in this altitude range. In contrast, there is no significant difference in bias found for the ACE-FTS sunrise and sunset measurements. These systematic effects in the ozone profiles retrieved from the measurements of ACE-FTS

and ACE-MAESTRO are being investigated. This work shows that the ACE instruments provide reliable, high quality measurements from the tropopause to the upper stratosphere and can be used with confidence in this vertical domain.

1 Introduction

Ozone is a key molecule in the middle atmosphere because it absorbs solar ultraviolet (UV) radiation and contributes to the radiative balance of the stratosphere. Understanding changes occurring in the distribution of ozone in the atmosphere are, therefore, important for studying ozone recovery, climate change and the coupling between these processes (WMO, 2007). To this end, it is important to have continuous high quality measurements of ozone in the stratosphere. Profile measurements from satellite-borne instruments provide height-resolved information that can be used to understand changes in ozone concentrations occurring at different altitudes. For the past two decades, one of the primary sources for ozone profile information has been satellite-borne instruments making solar occultation measurements. The solar occultation technique provides self-calibrating measurements of atmospheric absorption spectra with a high signal-to-noise ratio and good vertical resolution. Thus, to extend this time series of measurements in a consistent way, it is crucial to conduct validation studies that compare the results from new instruments with those from older and more established instruments.

The newest satellite for solar occultation studies is the Atmospheric Chemistry Experiment (ACE). This Canadian-led satellite mission, also known as SCISAT, was launched on 12 August 2003 (Bernath et al., 2005). There are two instruments onboard the spacecraft that provide vertical profiles of ozone and a range of trace gas constituents, as well as temperature and atmospheric extinction due to aerosols. The ACE Fourier Transform Spectrometer (ACE-FTS) (Bernath et al., 2005) measures in the infrared (IR) region of the spectrum and the Measurement of Aerosol Extinction in the Stratosphere and Troposphere Retrieved by Occultation (ACE-MAESTRO) (McEl-

roy et al., 2007) operates in the UV/visible/near-IR. The main objective of the ACE mission is to understand the global-scale chemical and dynamical processes which govern the abundance of ozone from the upper troposphere to the lower mesosphere, with an emphasis on chemistry and dynamics in the Arctic. SCISAT, the platform carrying the ACE-FTS and ACE-MAESTRO, is in a circular low-Earth orbit, with a 74° inclination and an altitude of 650 km (Bernath et al., 2005). From this orbit, the instruments measure up to 15 sunrise (hereinafter SR) and 15 sunset (hereinafter SS) occultations each day. Global coverage of the tropical, mid-latitude and polar regions (with the highest sampling in the Arctic and Antarctic) is achieved over the course of one year and the ACE measurement latitude pattern repeats each year. When ACE was launched, there were several solar occultation satellite-borne instruments in operation: Stratospheric Aerosol and Gas Experiment (SAGE) II (Mauldin et al., 1985), SAGE III (SAGE ATBD Team, 2002a), HALogen Occultation Experiment (HALOE) (Russell et al., 1993), Polar Ozone and Aerosol Measurement (POAM) III (Lucke et al., 1999) and SCanning Imaging Absorption spectroMeter for Atmospheric CHartographY (SCIAMACHY) (Bovensmann et al., 1999). The first four instruments only make occultation measurements while SCIAMACHY operates in nadir, limb and occultation modes. Between August and December 2005, the SAGE II, SAGE III, HALOE, and POAM III measurements ended. Currently, ACE-FTS and ACE-MAESTRO are the only satellite-borne instruments operating exclusively in solar occultation mode, while SCIAMACHY provides occultation measurements in addition to its limb and nadir observations. To be able to extend the long-standing record of observations from the SAGE II, SAGE III, POAM III and HALOE instruments, it is important that the ozone measurements provided by ACE-FTS and ACE-MAESTRO be well characterized and their quality thoroughly assessed.

In this paper, we present extensive validation studies for the most recent ozone data products from ACE-FTS (version 2.2 Ozone Update) and ACE-MAESTRO (version 1.2). These are compared with measurements from satellite-borne instruments as well as ozonesondes and balloon-borne, airborne and ground-based instruments employing different observation techniques. Section 2 describes the ACE satellite mission,

2519

instruments, and the ozone data products. The coincidence criteria and the validation methodology are described in Sects. 3 and 4, respectively. The comparisons are organized by instrument platform in the following two sections, Sect. 5 for the satellites and Sect. 6 for the ozonesondes, balloon-borne, airborne and ground-based instruments. The overall results are summarized and discussed in Sect. 7 and conclusions are given in Sect. 8.

2 The ACE instruments and data products

2.1 ACE-FTS

The primary instrument for the ACE mission, the ACE-FTS, is a successor to the Atmospheric Trace MOlecule Spectroscopy (ATMOS) experiment (Gunson et al., 1996), an infrared FTS that operated during four flights on the Space Shuttle (in 1985, 1992, 1993 and 1994). ACE-FTS measures high-resolution (0.02 cm^{-1}) atmospheric spectra between 750 and 4400 cm^{-1} (2.2–13 μm) (Bernath et al., 2005). A feedback-controlled pointing mirror is used to target the centre of the Sun and track it during the measurements. Typical signal-to-noise ratios are more than 300 from ~900 to 3700 cm^{-1}. From the 650 km ACE orbit, the instrument field-of-view (1.25 mrad) corresponds to a maximum vertical resolution of 3–4 km (Boone et al., 2005). The vertical spacing between consecutive 2 second ACE-FTS measurements depends on the satellite's orbit geometry during the occultation and can vary from 1.5–6 km. The altitude coverage of the measurements extends from the cloud tops to ~100–150 km.

Vertical profiles of atmospheric parameters, namely temperature, pressure and volume mixing ratios (VMRs) of trace constituents, are retrieved from the occultation spectra. This is described in detail in Boone et al. (2005). Briefly, retrieval parameters are determined simultaneously in a modified global fit approach based on the Levenberg-Marquardt nonlinear least-squares method (see Boone et al., 2005, and references therein). The retrieval process consists of two steps. First, pressure and temperature

2520

profiles are derived from the ACE-FTS spectra, using microwindows containing CO_2 spectral lines. Then the pressure and temperature profiles are used to calculate the VMR profiles of the target species. In the current ACE-FTS data set (version 2.2 with updates for ozone, N_2O_5, and HDO), profiles are retrieved for more than 30 species using spectroscopic information from the HITRAN 2004 line list (Rothman et al., 2005). First-guess profiles are based on the results of the ATMOS mission, but the retrieval method is not sensitive to this information. The altitude range of the ozone retrievals typically extends from ~10 km to ~95 km. The final results are provided jointly on the measurement (tangent height) grid and interpolated onto a 1 km grid using a piecewise quadratic method. The latter form is used for all analyses presented in this study.

Initial validation comparisons for ACE-FTS version 1.0 ozone retrievals have been reported (Walker et al., 2005; Petelina et al., 2005a; Fussen et al., 2005; McHugh et al., 2005; Kerzenmacher et al., 2005). Version 2.1 ozone was used in the early validation studies for the Microwave Limb Sounder (MLS) on the Aura satellite (hereafter Aura-MLS) by Froidevaux et al. (2006). In these earlier ACE-FTS ozone retrievals (up to and including version 2.2), a set of microwindows from two distinct spectral regions (near ~5 μm and ~10 μm) was used. Because of apparent discrepancies in the spectroscopic data for these two regions, the vertical profiles near the stratospheric ozone concentration peak were found to have a consistent low bias of ~10% in comparisons with other satellite-borne instruments. This was corrected in an update to version 2.2 by removing from the analysis the microwindows in the 5 μm spectral region. A consistent set of 37 microwindows around 10 μm (from 985 to 1128 cm^{-1}, with the addition of one microwindow at 922 cm^{-1} to improve results for the interfering molecule CFC$-$12) is now used for ozone retrievals. This O_3 data product, "version 2.2 Ozone Update", is used in the comparisons presented here. These version 2.2 Ozone Update profiles were used in recent validation studies for Aura-MLS (Froidevaux et al., 2008) and the Michelson Interferometer for Passive Atmospheric Sounding (MIPAS) on Envisat (Cortesi et al., 2007). The agreement with Aura-MLS version 2.2 ozone profiles is within 5% in the lower stratosphere (with ACE-FTS ozone VMRs consistently larger

than those of Aura-MLS), but degrades with altitude with the largest difference in the upper stratosphere (up to ~25%) (Froidevaux et al., 2008). Relative differences with the MIPAS ESA operational ozone v4.62 data products are within ±10% between 250 and ~2 hPa (10–42 km) but increase above this range, with ACE-FTS reporting larger VMR values than MIPAS by up to +40% around 0.6 hPa (~53 km) (Cortesi et al., 2007).

2.2 ACE-MAESTRO

ACE-MAESTRO is a dual-grating diode-array spectrophotometer that extends the wavelength range of the ACE measurements into the near-IR to UV spectral region (McElroy et al., 2007). It records over a nominal range of 400–1010 nm with a spectral resolution of 1.5–2 nm for its solar occultation measurements. The forerunner of the ACE-MAESTRO is the SunPhotoSpectrometer instrument which was used extensively by Environment Canada as part of the NASA ER-2 stratospheric chemistry research program (McElroy, 1995; McElroy et al., 1995). ACE-MAESTRO uses the same sun tracking mirror as the ACE-FTS, receiving ~7% of the beam collected by the mirror. The ACE-MAESTRO instrument vertical field-of-view is ~1 km at the limb. The observation tangent altitudes range from the surface to 100 km with a vertical resolution estimated at better than 1.7 km (Kar et al., 2007).

The processing of ACE-MAESTRO version 1.2 occultation data is done in two stages and is described in McElroy et al. (2007). In summary, the raw data are converted to wavelength-calibrated spectra, corrected for stray light, dark current and other instrument parameters in the first step. The corrected spectra are then analyzed by a nonlinear least-squares spectral fitting code to calculate slant-path column densities for each spectrum, from which vertical profiles of O_3 and NO_2 VMRs are subsequently derived. The retrieval algorithm does not require any a priori information or other constraints (McElroy et al., 2007). The inversion routine uses the pressure and temperature profiles and tangent heights from the ACE-FTS data analysis to fix the tangent heights for ACE-MAESTRO. Vertical profiles for the trace gases are determined by adjusting an initial guess (high-vertical-resolution model simulation) using a nonlin-

ear Chahine relaxation inversion algorithm (see McElroy et al., 2007 and references therein). The final profiles are provided both on the tangent grid and interpolated onto a 0.5 km-spacing vertical grid. As is done for ACE-FTS, the latter profiles are used in the analyses presented in this work. The version 1.2 ACE-MAESTRO data products have been compared with the ACE-FTS version 2.2 Ozone Update profiles, as well as with SAGE III, POAM III and ozonesonde observations (Kar et al., 2007). Agreement is generally within ±5–10% from 20–40 km. At higher altitudes, there is a significant bias between the SR observations, for which ACE-MAESTRO reports less ozone than the comparison instrument, and the SS observations, which show a large positive bias for ACE-MAESTRO with respect to the coincident measurements (of up to 30% around 50 km) (Kar et al., 2007).

As described above, ACE-MAESTRO consists of two spectrophotometers and each can provide vertical VMR profiles for ozone. Following the previous validation study of Kar et al. (2007), this work presents only the comparisons made with the Visible-Near-IR (VIS) spectrometer ozone data product. The retrieved profiles from the VIS spectrometer are in good agreement with those obtained from the UV spectrometer over the altitude range where the UV data have good signal-to-noise (∼15–30 km). The VIS profiles provide results over a larger vertical range, necessary for studies in the upper stratosphere and lower mesosphere.

3 Temporal and spatial criteria for coincidences

The nominal time period chosen for this study extends over 2.5 years from 21 February 2004 to 31 August 2006. The start date is the first day for which routine, reliable measurements were available for both ACE-FTS and ACE-MAESTRO. This time period includes the 2004, 2005, and 2006 Canadian Arctic ACE Validation Campaigns (e.g., Kerzenmacher et al., 2005; Walker et al., 2005; Sung et al., 2007; Manney et

2523

al., 2007a; Fraser et al., 2007; Fu et al., 2008; Sung et al., 2008[1]) and the final period of measurements from the SAGE II, SAGE III, POAM III and HALOE instruments. Based on availability of correlative measurements, this time period has been adjusted for some comparisons.

Common coincidence criteria were used to search for correlative observations to compare with ACE-FTS and ACE-MAESTRO. In addition to the spatial and temporal criteria discussed below, it was also required that there were profiles available for both ACE instruments for each coincidence. This provided a consistent distribution of comparisons for ACE-FTS and ACE-MAESTRO. For satellite comparisons, a maximum absolute time difference of ±2 h between the ACE observation and the correlative measurement, and maximum latitude and longitude differences of ±5° and ±10°, respectively, were generally used. All time differences were calculated using Universal Time (UT). The geographic coincidence criteria correspond to maximum distances of ∼600 km at high latitudes and about twice this value near the equator. Note that the measurement density is lower at low latitudes because of the high inclination of the ACE orbit and, therefore, we have significantly fewer coincidences available in the tropics and subtropics. These criteria provide good statistics consisting of a few hundred to several thousand events for most satellite-borne instruments. The list of the correlative datasets, time periods, number of coincidences and mean values of the distance and of the time, latitude and longitude differences is given in Table 1. Analysis of the variation of the differences (not shown) between the profiles from ACE-FTS and the comparison instruments, as a function of altitude and of the relative distance or other geometric parameters, did not reveal any consistent systematic biases. For the sparser data sets from ozonesondes and airborne, balloon-borne and ground-based instruments, it is more difficult to find coincidences using the criteria listed above. In those cases, a

---

[1]Sung, K., Strong, K., Mittermeier, R. L., Walker, K. A., et al.: Partial and total column SFIT2 retrievals from Eureka DA8 spectra in spring 2004 and 2005, including comparisons with PARIS-IR and ACE Satellite measurements, Atmos. Chem. Phys. Discuss., in preparation, 2008.

2524

similar fixed distance criterion was used (800 km for ozonesondes, 500 to 1000 km for other ground-based instruments) but the time criterion was relaxed to ±24 h. This was done in an effort to maximize the number of coincident profiles while at the same time avoiding biases in the atmospheric sampling.

To test the sensitivity of the comparison results to the temporal and geolocation criteria of the correlative measurements, we also performed comparisons within shorter time periods and smaller geographical regions: typically, comparisons were done for each month of the 2.5-year period and in five latitude bands: four (two in each hemisphere) for mid- and high latitudes (latitudes 30°–60° and 60°–90°, respectively) and a larger one for the tropics and subtropics (30° S–30° N). No systematic latitudinal dependence of the differences was found during these comparisons. The time series of the ACE-FTS latitudes for coincidences with SAGE III in 2005 is shown as an example, together with the comparison of the latitude values for both instruments (Fig. 1). There is no visible latitude bias (e.g., ACE-FTS latitudes systematically higher or lower than those of SAGE III) between the instruments for this particular data set. Careful examination of the time series of the relative differences, as a function of the distance or of the observation geometry, also did not reveal significant biases that might have required the use of narrower coincidence criteria.

It should be noted that broad criteria such as those defined here may result in multiple coincident observations for a particular ACE occultation, for instance when the ACE orbit footprint is close to the satellite ground-track of the correlative instrument or when the allowed time difference is large (e.g., 24 h). In such cases, each coincident pair (the same occultation measured by ACE-FTS or ACE-MAESTRO paired with a distinct observation from the comparison instrument) is treated as an independent event, except for the statistical comparisons with ozonesondes (see Sect. 6.5) and MicroWave Radiometers (MWRs) (see Sect. 6.9). However, the number of multiple matches did not exceed a few hundred for the largest comparison sets (e.g., for comparisons with SABER), with no more than 6–8 distinct comparison measurements coinciding with a single observation from the ACE instruments.

2525

Furthermore, for comparisons with satellite-borne solar occultation instruments, we analyzed the SR and SS occultations separately, for both ACE-FTS or ACE-MAESTRO and the correlative dataset. Since these comparisons did not reveal a significant SR/SS bias for ACE-FTS (Sect. 5.1), data from all occultations were averaged together for subsequent comparisons for ACE-FTS. For ACE-MAESTRO, comparisons were made separately for all data sets because there is a known SR/SS bias.

Day/night differences in ozone VMR can have an impact on the comparison results in the mesosphere (e.g., Schneider et al., 2005). For the comparisons presented hereafter, we did not use any photochemical model for the ACE measurements to account for these diurnal variations. However, in two cases, a photochemical correction was applied to the correlative data (Sects. 5.4.1 and 5.4.2).

4   Validation methodology

The satellite data used in the following comparisons have vertical resolutions ranging from 0.5 to 5 km, which is the same order of magnitude as those of the ACE instruments (∼3–4 km for ACE-FTS and better than 1.7 km for ACE-MAESTRO). Therefore, coincident profiles are linearly interpolated onto the ACE vertical grid (with a spacing of 1 km for ACE-FTS or 0.5 km for ACE-MAESTRO) for the comparison. Tests with other interpolation methods, or by comparing at the actual ACE tangent heights, did not yield any significant differences.

Secondly, for high-resolution measurements such as those from ozonesondes or other instruments measuring in situ, it is necessary to smooth the comparison data. In this case, two techniques were used, either a smoothing function was applied or an integration method was used.

For most in situ and high-resolution profile comparisons, smoothing (convolution) functions were created for ACE-FTS, consisting of triangular functions of full width at the base equal to 3 km and centered at the tangent heights of each occultation. This value was chosen to account for the smoothing effect of the limited ACE-FTS resolution,

2526

whilst allowing for simplified but valid systematic analysis. Furthermore, it accounts for the vertical spacing of the tangent heights in a retrieved ACE-FTS profile. The spacing varies with altitude (including refraction below ~30 km) and with the beta angle for the occultation (angle between the satellite orbital plane and the Earth-Sun vector). The minimum spacing is about 1.5 km at low altitudes for a high-beta occultation and increases to a maximum value of ~6 km at mesospheric heights for a low-beta event. High-resolution correlative measurements are convolved with these triangular functions for each ACE tangent height z_i:

$$x_s(z_i) = \frac{\sum_{j=1}^{n_{hr}} w_j \cdot x_{hr}(z_{hr})}{\sum_{j=1}^{n_{hr}} w_j}, \tag{1}$$

where $x_s(z_i)$ is the smoothed mixing ratio for the high-resolution instrument at tangent height z_i, x_{hr} is the VMR value of the high-resolution profile at altitude z_{hr}, w_j the associated weight (function of $z_{hr} - z_i$), and n_{hr} the number of points from the high-resolution profile found in the 3 km layer centered at z_i. The resulting smoothed profile is subsequently interpolated onto the 1 km grid. For ACE-MAESTRO comparisons, the high-resolution profiles are smoothed by convolution with a Gaussian filter of full width at half-maximum (FWHM) equal to 1.7 km, which is the upper limit for the vertical resolution of the instrument. The smoothed profiles are then interpolated onto the ACE-MAESTRO 0.5 km grid.

An alternative method is used in some comparisons with ozonesondes and lidars (Sect. 6.6). To account for the higher vertical resolution of the ozonesonde and lidar measurements, these profiles are first integrated to obtain partial columns calculated within layers centered at the ACE measurement grid levels (tangent heights). To calculate the partial column corresponding to altitude z_i, the layer edges are defined as the mid-points between tangent heights z_{i-1} and z_i (lower limit) and z_i and z_{i+1} (upper

limit). Then these partial columns are reported on the interpolated grids of ACE-FTS (1 km) and of ACE-MAESTRO (0.5 km).

Thirdly, for ground-based measurements with lower vertical resolution than the ACE instruments (Fourier Transform IR spectrometers (FTIRs) and MWRs), the ACE-FTS and ACE-MAESTRO profiles are smoothed using the averaging kernels calculated during the ground-based retrieval process, following the method of Rodgers and Connor (2003):

$$x_S = x_a + \mathbf{A}(x_{ACE} - x_a), \tag{2}$$

where x_{ACE} is the original ACE profile (ACE-FTS or ACE-MAESTRO), x_S is the smoothed profile, and x_a and $\mathbf{A}$ are the a priori profile and the averaging kernel matrix of the ground-based instrument, respectively.

For the analysis, data are screened to reject either the whole profile or identified low-quality measurements at some altitudes. First, the data from each instrument are filtered according to the recommendations provided by each calibration/processing team. The profiles which do not meet the quality requirements are rejected as a whole. Then, altitude levels for which the stated error represents more than 100 % of the profile value, or which exhibit unphysical VMR values – outside of the relatively broad interval of [−10; +20] ppmv – are excluded from the analysis. This generally leads to a lower number of comparison pairs at the lowermost and uppermost altitude levels. Negative VMR values are not systematically rejected as they can be produced by the retrieval process as an artifact due to noise in the measurements, especially at altitudes where O_3 abundance is naturally low. Finally, visual examination is used to remove erroneous profiles that were not rejected during the aforementioned analysis (a maximum of 5–6 per comparison set).

Differences are calculated for each individual pair of profiles, at the altitude levels where both instruments satisfy the screening criteria described above. The difference

at a given altitude z is expressed as

$$\delta_i(z) = \frac{x_{\text{ACE}}(z) - x_{\text{comp}}(z)}{x_{\text{ref}}(z)}, \quad (3)$$

where $x_{\text{ACE}}(z)$ is the VMR at altitude z for ACE (ACE-FTS or ACE-MAESTRO), $x_{\text{comp}}(z)$ the corresponding VMR for the comparison instrument, and $x_{\text{ref}}(z)$ is given by

$$
\begin{aligned}
x_{\text{ref}}(z) \quad &= 1 &\text{(abs.)} \\
&= x_{\text{comp}}(z) &\text{(rel.–gb+o3s)} \\
&= (x_{\text{ACE}}(z) + x_{\text{comp}}(z))/2 &\text{(rel.–others)}
\end{aligned}
$$

The first line is the value of $x_{\text{ref}}(z)$ for absolute difference calculations. The second and third lines give the denominator for calculations of relative differences for the ozonesondes and the ground-based instruments and for all other comparisons, respectively. There are two exceptions. For the comparisons with the Airborne SUbmillimeter Radiometer (ASUR, Sect. 6.1), $x_{\text{ref}}(z)=x_{\text{ACE}}(z)$ was used. In comparisons between ACE and the Global Ozone Monitoring by Occultation of Stars (GOMOS, Sect. 5.4.1) instrument, $x_{\text{ref}}(z)=x_{\text{GOMOS}}(z)$ was used as the denominator.

The resulting average differences for a complete set of coincident pairs of profiles are calculated as

$$\Delta(z) = \frac{1}{N(z)} \sum_{i=1}^{N(z)} \delta_i(z), \quad (4)$$

where $N(z)$ refers to the number of coincidences at altitude z and $\delta_i(z)$ is the difference (absolute or relative) for the ith coincident pair calculated using Eq. (3). The mean relative difference is given in percent in the following sections.

In some cases, notably for ACE-MAESTRO, there may seem to be a discrepancy between the apparent differences given by the mean profiles and the sign of the relative differences, or between the signs of the absolute and relative differences. The reader is reminded that the average differences are not calculated from the mean VMR profiles

2529

but from each pair of coincident profiles (Eq. 3). Thus, it is possible, if some profiles exhibit unusually low VMR values at certain altitude levels or if the VMRs for both instruments are of the same magnitude but of opposite signs, that the resulting mean relative differences become negative even though the absolute differences are positive (e.g., for the ACE-MAESTRO comparisons with the OSIRIS SaskMART data, Fig. 11).

5   Comparisons – satellites

5.1   Solar occultation instruments

5.1.1   SAGE II

SAGE II (Mauldin et al., 1985) was launched in October 1984 aboard the Earth Radiation Budget Satellite (ERBS) and remained operational until August 2005, thus providing a nearly continuous dataset over 21 years. ERBS was in a 610 km altitude circular orbit with an inclination of 56°. SAGE II performed two occultation measurements per orbit (1 SR and 1 SS), thus sampling two narrow latitude circles each day. Over the course of a month, observations were recorded between about 75–80° S and 75–80° N.

The SAGE II dataset comprises profiles of O_3, NO_2, H_2O and aerosol extinction, measured using seven channels centered at wavelengths from 0.385 to 1.02 μm. The ozone retrievals use data from the center of the Chappuis absorption band measured by the 0.603 μm channel. The retrieval algorithm is described in detail by Chu et al. (1989).

Data versions prior to version 6.00 have been the subject of several publications, including an extensive study of version 5.96 in the first Stratospheric Processes And their Role in Climate assessment report (SPARC, 1998). In 2000, a major revision of the retrieval algorithm corrected long-standing data issues (version 6.00). Version 6.00 was used in detailed comparisons with HALOE (Morris et al., 2002) and several other instruments (Manney et al., 2001). Subsequent improvements, versions 6.10 and

2530

6.20, were made and have been extensively validated (Wang et al., 2002; Kar et al., 2002; Iyer et al., 2003; Randall et al., 2003; Wang, P. H., et al., 2006). The current version (version 6.20) shows good agreement with correlative measurements – within 5% above ∼18 km – but exhibits a low bias below the tropopause (e.g., Borchi et al., 2005; Nazaryan and McCormick, 2005; Froidevaux et al., 2008). This version (v6.20) was used for the comparisons with ACE-FTS and ACE-MAESTRO.

Applying the coincidence criteria (±2 h, ±5° in latitude and ±10° in longitude), we found 229 matches in the period between August 2004 and early May 2005. Among these, 199 correspond to SR occultations for both instruments, and 30 to both SS observations. The ACE-FTS comparison results are shown in Fig. 2 for the SR/SR (top panel) and the SS/SS (bottom panel) comparisons. ACE-FTS reports consistently higher ozone values than SAGE II at all altitudes. Relative differences are on the order of 10–17% in the range 12–18 km, similar to the low bias of SAGE II ozone values previously reported (e.g., Borchi et al., 2005; Wang, P. H., et al., 2006). The agreement is better than 10% between 18 and 42 km for both SR and SS events, with typical values of +5% or less. Above 42 km, both SR and SS comparisons show larger positive differences of up to 20%. Comparisons for SS events yield generally better agreement, with smaller differences notably around 12 km and in the range 38–44 km (<3%). This analysis (as well as the comparisons for ACE-MAESTRO detailed below) provides an incomplete test of biases in the ACE-FTS (or SAGE II) dataset since the ACE-FTS SR (SS) occultations are all coincident with SAGE II SR (SS) occultations.

Figure 3 shows the comparisons between the SAGE II and ACE-MAESTRO ozone retrievals for the ACE-MAESTRO SR (top panel) and SS (bottom panel) profiles respectively. For the SR cases, the agreement is very good between 15 km and 55 km with fractional differences within ±3% throughout, except near 20 km. For the ACE-MAESTRO SS events, the agreement is again quite good (within ±5% between 16 and 45 km), except for a significant positive bias between 45 km–55 km, reaching a maximum of 17% at 54 km. This is much larger than the SR bias at these altitudes.

2531

5.1.2 UARS/HALOE

The Upper Atmosphere Research Satellite (UARS) (Reber et al., 1993) was deployed from the Space Shuttle Discovery in September 1991. The satellite circled the Earth at an altitude of 585 km with an orbital inclination of 57°. HALOE (Russell et al., 1993) remained in operation until November 2005 and performed two occultation measurements per orbit. A nearly-global latitude range (75–80° S to 75–80° N) was sampled in about 36 days.

HALOE observations used 8 channels to measure infrared absorption bands between 2.45 and 10.04 μm, providing VMR profiles of trace constituents (including O_3, H_2O, NO_2, and CH_4) with a vertical resolution of ∼2 km. O_3 profiles are retrieved with an onion-peeling scheme from the 9.6 μm channel, which provides an accurate product from the upper troposphere to the mesopause (Russell et al., 1993).

Extensive validation studies have been conducted for previous versions of the HALOE dataset (e.g., for version 17: Brühl et al., 1996; for version 18: Bhatt et al., 1999). The latest version, version 19 (hereinafter V19) has also been compared to numerous correlative measurements. Good agreement, to within ∼10%, was found in comparisons with various satellite-borne instruments for the mid-latitudes in November 1994 (Manney et al., 2001). Differences of 4 to 11% were found between HALOE V19 and SAGE II version 6.10 throughout the stratosphere (Randall et al., 2003). The differences with the POAM III version 3 ozone profiles were typically smaller than 5% and always within ±10% (Randall et al., 2003). Comparisons with the MIPAS IMK-IAA version V3O_O3_7 retrievals show a global agreement within 10% in the middle and upper stratosphere (Steck et al., 2007). The agreement of the HALOE V19 O_3 profiles with the most recent release (version 2.2) of the Aura-MLS ozone data product is ∼5% between 68 and 2 hPa (∼20–42 km) but degrades to 15% at 100 and 147 hPa (∼15 and ∼14 km, respectively), with Aura-MLS values larger than the HALOE values (Froidevaux et al., 2008). In this study, we use the HALOE V19 ozone retrievals.

In the comparisons, only 49 pairs of coincident profiles were found using ±2 h, ±5°

2532

in latitude and ±10° in longitude for the coincidence criteria. As for SAGE II, there are no SR/SS collocations, but only SR/SR and SS/SS events (respectively 8 and 41 coincidences). In Fig. 4, we present the results for the SS/SS comparisons only because of the limited number of coincidences for the SR events. The ACE-FTS mixing ratios exhibit a positive bias over most of the altitude range. Differences for the SS comparisons are within +4 to +13% in the range 15–42 km, increasing to about 28% at 60 km. These larger positive differences above ∼42 km are similar to those noted with SAGE II and are a persistent feature in most of the profile comparisons presented in this paper.

The ACE-MAESTRO comparisons were also done separately for SR and SS events. As for ACE-FTS, only the comparison between ACE-MAESTRO SS and HALOE SS results is shown (Fig. 5). For this comparison, there is good agreement (within 5–10%) between 15 km and 40 km. The deviation increases thereafter to a maximum of about 27% near 55 km. This is generally similar to the ACE-FTS-HALOE comparison shown above.

5.1.3 POAM III

POAM III (Lucke et al., 1999) was launched in March 1998 onboard the fourth Satellite Pour l'Observation de la Terre (SPOT-4) in a sun-synchronous orbit, with an altitude of 833 km, an inclination of 98.7° and ascending node crossing at 22:30 (local time). It is a solar occultation instrument able to provide high-resolution (∼1 km) vertical profiles of O_3, NO_2, H_2O and aerosol extinction using nine filter channels from 0.353 to 1.02 μm. POAM III measured in high latitude ranges throughout the year (∼55°–71° N and ∼63°–88° S), with satellite sunrises in the northern hemisphere and satellite sunsets in the southern hemisphere. POAM III was operational from April 1998 to early December 2005.

Briefly, the retrieval algorithm for POAM III consists of a spectral inversion for species separation, followed by the limb (vertical) inversion. Ozone is retrieved primarily from the 0.603 μm channel where the Chappuis absorption dominates the total optical depth

between 15 and 60 km.

The retrieval and error budget for the version 3 (v3) data products are described in detail in Lumpe et al. (2002). The ozone v3 retrievals have been extensively compared and validated using observations from aircraft, balloon and satellite-borne instruments (see Randall et al., 2003, and references therein). They were shown to be highly accurate from 13 to 60 km with a typical agreement of ±5%. A possible slight bias of ∼5% was noted between the SR (northern hemisphere) and SS (southern hemisphere) profiles, and a high bias (up to 0.1 ppmv) was found below 12 km (Randall et al., 2003). For these comparisons, we use version 4 (hereinafter v4) of the POAM III retrievals. This version was improved to account for problems in the POAM III v3 retrievals, due in part to unexpected instrument degradation over the course of the mission. Comparative studies similar to those conducted with v3 show that the general conclusions of Randall et al. (2003) can be applied to POAM III v4 ozone data (http://eosweb.larc.nasa.gov/PRODOCS/poam3/documents/poam3_ver4_retrievals_status.pdf).

The quality flag implemented for the POAM III v4 O_3 product (http://eosweb.larc.nasa.gov/PRODOCS/poam3/documents/poam3_ver4_documentation.pdf) was used for data screening: altitude levels with non-zero values of the quality flag were excluded from the calculations. We used ±2 h, ±5° in latitude and ±10° in longitude for the coincidence search. A total of 376 coincidences was found in the comparison period, with about 1/3 in the northern hemisphere (POAM III SR) and the remainder in the southern hemisphere (POAM III SS).

Results are shown in Fig. 6 for the ACE-FTS SR (top) and SS (bottom) occultations. Agreement within ±10% (typically +4%) is found from ∼12–42 km in all cases. In particular, the ACE-FTS SS/POAM III SS results show an excellent agreement within ±2.5% in the range 9–41 km. The largest differences are found for the ACE-FTS SR/POAM III SS comparisons (109 coincidences, with typical values of +7% and a maximum difference of about 13%). Below 16 km, ACE-FTS measures consistently less ozone than POAM III, with large percent differences corresponding to absolute differences of less than 0.1 ppmv. Above 42 km, differences increase to a maximum of 34% around

60 km, with ACE-FTS VMR values larger than those of POAM III. The largest relative differences are found for the ACE-FTS SR/POAM III SS events in the range 42–48 km and for the ACE-FTS SS/POAM III SR pairs (~230 coincidences) above 42 km.

The ACE-MAESTRO and POAM III comparisons were done by Kar et al. (2007) using measurements from February 2004 to September 2005. This slightly shorter comparison period did not significantly lower the statistics of the analysis. Therefore, a short summary will be given but the reader is referred to the analysis of Kar et al. (2007) for more information and to their Fig. 6a and b for illustration of the results. ACE-MAESTRO SR events show consistently smaller (by 5–15%) VMRs from 20–50 km when compared to POAM III SR or SS profiles. The comparisons of the ACE-MAESTRO SS profiles with POAM III yield differences within ±10% in the altitude range ~18–40 km, with smallest differences (<4% from 20–35 km) for the comparisons of ACE-MAESTRO SS and POAM III SR. Above ~40 km, the ACE-MAESTRO SS profiles show larger ozone values than POAM III (up to 20% for POAM III SR and 30% for POAM III SS). As for SAGE II or HALOE, the shape of the relative difference profile above ~45 km for the ACE-MAESTRO SS events is qualitatively similar to the results obtained for ACE-FTS at high altitudes.

5.1.4   SAGE III

SAGE III was an upgraded version of SAGE II and was launched in December 2001 aboard the Russian Meteor-3M satellite. The satellite is in a sun-synchronous orbit at an altitude of 1000 km, with an inclination of 99.3° and an ascending node crossing at 09:00 (local time). It used solar and lunar occultation as well as limb scatter to make measurements in 87 spectral channels (at wavelengths from 280 to 1035 nm) using a grating spectrometer (SAGE ATBD Team, 2002a). The solar occultation observations produced high-resolution (~1 km) profiles of O_3, NO_2, H_2O and aerosol extinction. The SAGE III solar occultation measurements occured at high latitudes in the northern hemisphere (45° N–80° N, satellite SS) and at mid-latitudes in the southern hemisphere (60° S–25° S, satellite SR). This provided increased opportunities for mea-

surements coincident with ACE occultation events, particularly in the northern hemisphere. SAGE III took measurements from May 2002 through December 2005.

Two different processing algorithms have been used for SAGE III ozone retrievals in the upper troposphere and the stratosphere. One is a SAGE II type (least-squares) algorithm using only a few wavelengths and the second one employs a multiple linear regression technique (MLR) to retrieve ozone number densities from the Chappuis absorption band (SAGE ATBD Team, 2002b). The recent study of Wang, H. J., et al. (2006), using the latest release (version 3.0) of the retrievals, showed that both products are essentially similar from 15 to 40 km. When compared to correlative measurements, the SAGE II type retrievals provide better precision above 40 km and do not induce artificial hemispheric biases in the upper stratosphere, whereas the MLR retrieval yields slightly better accuracy in the upper troposphere/lower stratosphere (UT/LS) region. Comparisons with ozonesondes, SAGE II and HALOE show that the estimated precision of SAGE III for the least-squares retrieval algorithm is better than 5% between 20 and 40 km and ~10% at 50 km, and the accuracy is ~5% down to 17 km. In particular, excellent agreement was found with SAGE II from 15 to 50 km, with ozone values reported by SAGE III systematically higher than those of SAGE II by only 2–3%. Below 17 km, SAGE III ozone VMR values are systematically higher than those of the comparison instruments, by 10% at 13 km (Wang, H. J., et al., 2006). We use version 3.0 of the ozone data product from the SAGE II type algorithm for the comparisons detailed hereafter.

Of the solar occultation instruments, the most coincidences were found with SAGE III (648 events). There is very good overall agreement between ACE-FTS and SAGE III, as shown in Fig. 7. Fractional differences are within ±6% from 12–42 km (except for the ACE-FTS SR/SAGE III SR results at 17 km), with typical values of ±1–2% throughout. Above 42 km, ACE-FTS reports larger VMRs than SAGE III (by 10–20%). This is consistent with other comparisons presented in this study. There is no noticeable bias between the ACE-FTS SR and SS occultations below 42 km, but the results differ by 2 to 8% above this altitude. However, the number of coincidences between the ACE-FTS

SR profiles and the SAGE III observations is considerably lower than for the ACE-FTS SS occultations and thus no conclusions can be drawn as to possible SR/SS biases in the ACE-FTS retrievals based on these comparisons.

As for POAM III, comparisons of ACE-MAESTRO with SAGE III were conducted by Kar et al. (2007) using narrower geographic criteria (maximum distance of 500 km) and will not be reproduced here. Agreement within ±5% is found from 15 to 36–40 km for the statistically significant samples (ACE-MAESTRO SS/SAGE III SR and ACE-MAESTRO SS/SAGE III SS). Above this range, the ACE-MAESTRO SS profiles exhibit a large positive bias of up to 20–30%, similar to that found for ACE-FTS but of larger magnitude. The ACE-MAESTRO SR measurements show a persistent low bias of −5 to −15% in the altitude range 28–55 km. This is shown in Fig. 5 of Kar et al. (2007).

5.2 Odin

The Swedish-led Odin satellite, launched in February 2001, is in a sun-synchronous, near-terminator orbit at ~600 km with a 97.8° inclination and an ascending node crossing time at 18:00 (local time) (Murtagh et al., 2002). This orbit provides the limb-scanning instruments with latitudinal coverage in the orbit plane from 82.2° N to 82.2° S. Odin serves both astronomy and aeronomy objectives and, while in normal operation, it shares time equally between aeronomy and astronomy measurements. The stratospheric mode (measured for one day out of every three) scans the Earth's limb from 7 to 70 km with a vertical speed of 0.75 km per second.

5.2.1 Odin/OSIRIS

The Optical Spectrograph and InfraRed Imaging System (OSIRIS) is one of the two instruments on Odin. It measures limb-scattered solar radiance in the spectral range 280–810 nm with ~1 nm resolution (Llewellyn et al., 2004). The instrument's vertical field-of-view is ~1 km at the tangent point. OSIRIS provides approximately 30 ozone

profiles per orbit over the sunlit hemisphere (about 60 profiles per orbit during orbital equinox periods).

There are presently two versions of the OSIRIS ozone data product. The retrieval algorithm for the first product is developed and maintained at York University (Toronto, Canada). It applies the inversion technique developed by Flittner et al. (2000) and McPeters et al. (2000) to OSIRIS radiances measured at three wavelengths in the Chappuis absorption band (von Savigny et al., 2003). The resulting ozone number density profiles, version 3.0 (v3.0), are provided from 10–46 km with a 2 km spacing. The York v3.0 data products are described in Haley and Brohede (2007). These will be referred to as the "York retrievals" hereinafter. There were two previous releases of the York ozone product (v1.2 and v2.4), yielding very similar results (agreement better than 3%). Version 1.2 has been validated against coincident ozonesonde and satellite measurements (Petelina et al., 2004, 2005a). These comparisons showed a good agreement of the OSIRIS York data product with correlative measurements, within ±5–7% over the altitude range 16–32 km.

The second OSIRIS ozone retrieval algorithm, SaskMART, is developed and maintained at the University of Saskatchewan (Saskatoon, Canada). We also compare the ACE-FTS and ACE-MAESTRO ozone profiles with version 2.1 (v2.1) of this product (hereinafter "SaskMART retrievals"). The SaskMART algorithm combines information from the Chappuis and the Hartley-Huggins bands to infer the ozone number density from the cloud tops to the lower mesosphere. It is described by Roth et al. (2007) and uses a Multiplicative Algebraic Reconstruction Technique (MART) and the SASKTRAN radiative transfer model (Bourassa et al., 2007). SaskMART zonal mean profiles were compared with SAGE II v6.20 and SAGE III v3.0 O_3 profiles by Roth et al. (2007). Results show an overall agreement within ±5% for SAGE II and ±10% for SAGE III from 20–40 km, with OSIRIS reporting less ozone over most of the altitude range. The full analysis, with the complete OSIRIS dataset and an altitude range extended to ~65 km, will be the subject of further publication (Degenstein et al., 2008[2]). Preliminary results

---

[2]Degenstein, D. A., Bourassa, A. E., Roth, C. Z., and Llewellyn, E. J.: A Method for the

over the full altitude range show a substantial low bias (10–30%) above 50 km (C. Roth, personal communication).

Since the comparisons with solar occultation instruments did not show evidence for a SR/SS bias in the ACE-FTS dataset, averages (without SR/SS separation) will be shown for the ACE-FTS analyses in the following sections. For OSIRIS, the ACE-FTS profiles were first compared with the York retrievals (Fig. 8). Following the developers' recommendation, only profiles for which the measurement response is greater than 0.9 (i.e., where 90% or more of the information content comes from the observation and not from the a priori (Rodgers, 2000)) were included in the analysis. Furthermore, the data were screened to exclude altitude levels for which the estimated vertical resolution is >5 km. A total of 913 coincidences was found with criteria of ±2 h, ±5° in latitude and ±10° in longitude. ACE-FTS consistently reports more ozone than the OSIRIS York retrievals from 11–40 km. Differences are within +4 to +11% throughout, with a typical value of +7%, and largest differences at 18 and at 37 km (~11%).

Results of the comparison of ACE-FTS with the SaskMART retrievals are presented in Fig. 9. In these comparisons, the ACE-FTS VMR values are also consistently larger than those of OSIRIS, but there is very good agreement (<+6%) in the altitude range 12–45 km (except around 18 km where the difference is about +9%). Above 45 km the differences increase, up to 44% at 60 km. Considering the low bias previously noted in the comparisons of OSIRIS SaskMART with SAGE II and SAGE III, this suggests that this large positive difference may be the combination of the persistent high bias of ACE-FTS between ~45 and 55–60 km and of a low bias of the SaskMART retrievals above ~50 km. Since OSIRIS measures exclusively during daytime, the diurnal variations of the O_3 VMR in the mesosphere might account for part of this bias in the SaskMART ozone data product.

Figure 10 shows the results of the comparison between ACE-MAESTRO and the York retrievals, for ACE-MAESTRO SR (top panel) and SS (bottom panel) occultations.

Retrieval of Ozone Profiles from 10 to 60 km Using Limb Scattered Sunlight, Atmos. Chem. Phys. Discuss., in preparation, 2008.

2539

For both types of events, there is good agreement with the York retrievals from 16–40 km. Differences are within ±5% below ~26 km and from +6 to +12% between 26 and 40 km. However, the ACE-MAESTRO SR profiles around 37 km seem to have a larger positive bias compared to the SS profiles, which is opposite to the known SR/SS bias seen with the solar occultation comparisons. The reason for this is not clear at this time.

The comparison results for ACE-MAESTRO and OSIRIS SaskMART retrievals are shown in Fig. 11 for ACE-MAESTRO SR (top) and SS (bottom) events. The agreement is quite good for the SR events, with fractional differences within ±7% over the altitude range 18–59 km. For ACE SS events, ACE-MAESTRO ozone mixing ratios have a significant positive bias above 40 km, similar to comparisons with most other instruments. However, the maximum deviation of ~15% near 53 km is somewhat smaller than the corresponding positive bias for ACE-FTS at this altitude. A SR/SS bias in ACE-MAESTRO ozone measurements can be seen, particularly in the upper stratosphere. The fact that the relative differences at the uppermost levels are negative while the absolute differences are small but positive is due to very low VMR values in the ACE-MAESTRO retrievals for more than half (~240 out of ~450 coincidences) of the individual events.

5.2.2 Odin/SMR

The Sub-Millimetre Radiometer (SMR) is the second instrument on board the Odin satellite. It uses four tunable heterodyne radiometers to observe thermal limb emission from atmospheric molecules, in the frequency range 486–581 GHz. In the stratospheric mode, SMR measures several species related to stratospheric ozone processes in two frequency bands centered at 501.8 GHz and 544.6 GHz, namely O_3, HNO_3, ClO and N_2O (Urban et al., 2005).

The current best ozone data product for SMR is version 2.1 of the operational processing developed at the Chalmers University of Technology, Gothenburg, Sweden (hereinafter Chalmers-v2.1). It uses the observations of a weak O_3 line near 501.5 GHz

to retrieve ozone VMRs mainly in the stratosphere (above ∼17–18 km at mid-latitudes), with a retrieval scheme based on the Optimal Estimation Method (Rodgers, 2000). The vertical resolution achieved is on the order of 2.5–3.5 km below ∼40–45 km. Chalmers-v2.1 and two previous operational ozone data products (v1.2 and v2.0) were compared with ozonesondes and with the MIPAS ozone profiles retrieved with the ESA Level 2 processor prototype (Raspollini et al., 2006) version 4.61 in the recent study of Jones et al. (2007). The SMR ozone v2.1 is very similar to the older versions in the altitude range 20–45 km, but is significantly improved below 20 km and above ∼45 km. Comparisons with MIPAS show percent differences of about −10% (smaller than 0.4 ppmv) between 17 and 55 km, with SMR reporting VMR values systematically smaller than those of MIPAS. Absolute differences with ozonesonde measurements are typically within ±0.3 ppmv below 27 km, but the SMR ozone VMRs are smaller than the ozonesonde measurements in the tropics around 30 km (by more than 10% or 0.9 ppmv; Jones et al., 2007). We used the Chalmers-v2.1 SMR ozone data product for the comparisons with the ACE instruments.

The comparisons were made with coincidence criteria of ±2 h, ±5° in latitude and ±10° in longitude. Following the recommendations of the retrieval team, only SMR data with a profile quality flag value of 0 were used at altitude levels where measurement response was greater than 0.9 (see Urban et al., 2005, for a description of the measurement response and the quality flag). The vertical range was limited to altitudes where the SMR measurements have a good signal-to-noise ratio (∼20–55 km). A total of 1161 coincidences was found in the comparison period. The results are presented in Fig. 12. The agreement is better than +14% (0.5 ppmv) below ∼25 km. Between 25 and ∼55 km, ACE-FTS consistently reports more ozone than SMR. The percent differences are within 13–20% between 25 and 40 km. In the altitude range 40–55 km, the differences are larger (+20 to +30%), which is consistent with the other comparisons presented in this study.

Similar comparisons were conducted with ACE-MAESTRO and are presented in Fig. 13. Overall, the fractional differences for the SR and SS events are similar and

2541

comparable to those of ACE-FTS. Relative differences are lower than +10% below 25 km and on the order of +10–20% in the altitude range ∼25–46 km (25–41 km) for the ACE-MAESTRO SR (SS) events. The ACE-MAESTRO SR data show more ozone below 33 km than the SS data, which translates into higher differences with SMR (by up to 5%) at these altitudes. A larger positive bias is also observed in the ACE-MAESTRO – SMR comparisons between 40 and ∼50 km, with a maximum difference of about +28%. Above 50 km, the differences rapidly decrease and become lower than +5% at the top of the comparison range (∼55 km).

5.3   TIMED/SABER

The Sounding of the Atmosphere using Broadband Emission Radiometry (SABER) instrument is one of the four instruments onboard the Thermosphere, Ionosphere, Mesosphere Energetics and Dynamics (TIMED) satellite. TIMED was launched in December 2001 into an orbit with an altitude of ∼625 km and an inclination of 74° (Russell et al., 1999). The latitude coverage alternates between 54° S–82° N and 82° S–54° N, and the local time coverage is ∼22 h in about 60 days. SABER uses ten channels in the near- and mid-IR spectral region (1.27–15 μm) to perform broadband limb emission measurements of pressure, temperature, the $O_2(^1\Delta)$ and OH Meinel volume emission rates, as well as VMR profiles for CO_2, O_3 and H_2O. The retrieval code takes into account non-local thermodynamic equilibrium (non-LTE) effects in the emissions measured above ∼55 km (Mertens, 2001). The ozone profiles are retrieved from the 9.6 μm channel, in the vertical range ∼12–∼100 km with a vertical spacing of ∼0.4 km.

The temperature and wind data have been extensively used for comparisons and scientific publications (e.g., Sica et al., 2008; Forbes et al., 2006; Petelina et al., 2005b; Mertens et al., 2004). However, at the time of writing, there are no published comparisons for the SABER trace gas data. The present study thereby constitutes the first large-scale intercomparison for the SABER ozone dataset. The SABER O_3 data product available at the time of writing, version 1.06 (hereinafter v1.06), is used for the comparisons. A new version (v1.07) is currently being developed, but the reprocess-

2542

ing was not completed in time for this analysis. Version 1.07 should show significant changes in the SABER temperature and ozone retrievals. For O_3, it should yield lower VMR values (by a few percent) in the stratosphere and a larger decrease (by 10% or more) in the mesosphere (B. T. Marshall, personal communication).

Results for the ACE-FTS and SABER comparisons are shown on Fig. 14. The shape of the difference profile is significantly different from the comparisons presented above. A total of 6210 coincidences was found between ACE-FTS and SABER with the criteria: ±2 h and ±5° and ±10° for the latitude and longitude differences, respectively. Narrower coincidence criteria did not induce significant changes in the results. Very good agreement (within ±6%) is found from 18–46 km. ACE-FTS reports less ozone than SABER around the peak in ozone VMR (31–42 km), but shows larger VMRs in the lower stratosphere and at altitudes between 41 and 56 km. Below 20 km and above 56 km, the O_3 VMRs measured by ACE-FTS are systematically lower than those of SABER. The amplitude of the fractional differences steadily decreases with increasing altitude between 12 and 20 km, from a largest value of −54% at 12 km. Conversely, it increases with increasing altitude between 55 and 70 km (up to −48% at 70 km). The expected decrease in the ozone VMR for the SABER v1.07 ozone data product should significantly reduce the discrepancies, notably in the mesospheric part of the comparison range. However, the reasons for this particular behavior cannot be explained at this time.

The comparisons of the ACE-MAESTRO retrievals with the SABER ozone profiles are shown in Fig. 15. Large negative differences are found at the top and at the bottom of the altitude range for both the SR and the SS events (below ~22 km and above ~54 km). Between 22 and 54 km, there is a significant difference between the results of the comparison for the ACE-MAESTRO SR and SS profiles. The ACE-MAESTRO SR profiles show good agreement of ±7% or less with SABER in this altitude range (Fig. 15, top panel). The percent differences decrease with increasing altitude in this vertical range, from a maximum value of +7% around 27 km to −7.5% at 51 km. The relative difference profile for the SS occultations (Fig. 15, bottom

2543

panel) is closer in shape to the results found for ACE-FTS. For those, a good agreement within ±4% is found between 22 and 42 km. From 42–54 km, ACE-MAESTRO SS measurements show VMR values significantly larger than those of SABER, by up to 16% around 48 km. As noted for the comparisons between ACE-MAESTRO and OSIRIS SaskMART in Sect. 5.2.1, the percent differences at the uppermost levels of the comparison vertical range are negative for ACE-MAESTRO SS occultations. This is also explained by unusually low values of the retrieved ACE-MAESTRO VMRs.

5.4 Envisat

The ESA Environmental Satellite (Envisat) was launched in March 2002 into a quasi-polar, sun-synchronous orbit at an altitude of 800 km, with an inclination of 98.6° and an ascending node crossing at 22:00 (local time). For most of the onboard sensors, this allows complete coverage of the Earth in one to three days. Three of the ten instruments are dedicated to atmospheric chemistry: the GOMOS, MIPAS and SCIAMACHY instruments.

5.4.1 Envisat/GOMOS

GOMOS is a stellar occultation instrument, that has been in operation since the launch of Envisat (see Kyrölä et al., 2004, and references therein). It is a UV/visible/near-IR grating spectrometer that can measure about 100 000 star occultations per year with a vertical sampling of better than 1.7 km. From these observations, atmospheric concentration profiles are retrieved for O_3, NO_2, NO_3, H_2O, O_2, Na, OClO and stratospheric aerosols. The range of latitudes sampled by GOMOS depends on the suitable stars available during each orbit and thus varies throughout the year. GOMOS sounds the atmosphere at different local solar times depending on the position of the star that is being observed.

The ozone measurements are made in the 250–687 nm spectral range. GOMOS ozone profiles are produced using a two step retrieval process (Kyrölä et al., 2004,

2544

2006). First, the spectral inversion uses a nonlinear Levenberg-Marquardt method to fit the refraction-corrected atmospheric spectra simultaneously at all wavelengths. Then, the onion-peeling method is used to perform the vertical inversion to obtain profiles. The typical altitude range of the GOMOS ozone retrievals is 15–100 km. The GOMOS precision is strongly influenced by both the star magnitude and temperature as these can both impact the signal-to-noise ratio of the measured spectra. The daytime (bright-limb) occultations suffer from additional noise from scattered solar light. Because of this, the comparisons shown here will be restricted to nighttime (dark limb) observations. The GOMOS ozone profiles have been validated using measurements from ozonesondes, lidars and MWRs (Meijer et al., 2004). Between 14 and 64 km, the differences were found to be 2.5–7.5% with GOMOS measuring less ozone than the comparison instrument. In comparisons with MIPAS and SCIAMACHY, the agreement for GOMOS dark limb profiles was −5% from 20–50 km and +1% from 20–40 km, respectively (Bracher et al., 2005). The level 2 data product used for these comparisons was version 6.0a. Version IPF 5.00 is used for the comparisons with ACE-FTS.

The approach taken for the GOMOS comparisons differs from that used for the other satellite instruments. Instead of calculating the mean of the relative differences for the GOMOS and ACE-FTS comparisons, the weighted median difference is determined. This approach, used in earlier GOMOS validation studies (e.g., Fussen et al., 2005), was adopted because outliers in either data set can significantly influence the results of the comparison. The weighted median difference, m, is calculated by minimizing the expression,

$$D(m) = \sum_i w_i \cdot |x_{ACE}(i) - x_{GOMOS}(i) - m|, \tag{5}$$

with respect to m, where $x_{ACE}(i)$ and $x_{GOMOS}(i)$ are the profile values at a given altitude, for coincidence i and for ACE-FTS and GOMOS, respectively, and w_i is the weighting factor that combines the estimated experimental errors from ACE-FTS and GOMOS. Figure 16 shows the dependence of the weighted median difference at 24.5 km on the number of collocated events and the spatial and temporal coincidence criteria used for

2545

the comparisons. From these results, it can be seen that a larger data set improves the statistical significance although a slight linear bias is apparent. Using criteria of ±12 h and 500 km, 1240 pairs of collocated profiles were identified for the comparisons.

Because both data sets extend into the mesosphere (60–80 km), we have used the Simulation of Chemistry, Radiation, and Transport of Environmentally important Species (SOCRATES) model to correct the GOMOS data for diurnal variations between the observation time and the local sunset or sunrise. SOCRATES is a two-dimensional chemistry-climate model which extends from the surface to the lower thermosphere. The version used here is optimized to study the heat budget and the photochemistry in the mesosphere (Chabrillat and Fonteyn, 2003; Kazil et al., 2003). Because the present study requires a precise representation of the chemical composition at sunrise and sunset, the model was run with a photochemical time step of 5 min over a whole year with solar flux conditions representative of the year 2004. Each GOMOS observation was scaled by the modeled ratio between ozone density at local sunset or sunrise and ozone density at the observation time.

The results of the ACE-FTS – GOMOS comparisons are presented in Fig. 17. A good agreement (<10%) can be observed in the stratosphere (15–40 km) with a slight positive bias increasing slowly with altitude. However, there exists a more important bias (up to 40%) between 40 and 60 km, similar to other comparisons. Above 60 km, the positive bias increases significantly when comparing the ACE-FTS and corrected GOMOS profiles. Without applying the photochemical correction, ACE-FTS reports significantly less ozone than GOMOS (by more than 50%). Because of the photochemical correction method used and the low ozone number densities, it is difficult to draw conclusions about the accuracy of the ACE-FTS profiles in the mesosphere based on these relative differences.

Since the GOMOS observations have better vertical resolution than the ACE-FTS profiles, an additional comparison was performed. For this, we applied an empirical triangular smoothing function to the GOMOS data to reduce the profile resolution (from 0.3–1.7 km) in order to better match ACE-FTS. This considerably improved the agree-

2546

ment between both data sets, as seen in Fig. 17, but necessitated a smoothing function with a FWHM as large as 10.5 km.

5.4.2 Envisat/MIPAS

MIPAS is a mid-IR Fourier transform emission spectrometer designed to perform global-scale continuous (day/night) limb-sounding measurements of VMR profiles for a range of atmospheric species (Fischer et al., 2007). For this purpose, it acquires spectra in five frequency bands over the range 685–2410 cm^{-1} (14.6–4.15 μm). Global measurements are achieved every day (Cortesi et al., 2007). The pointing system allows MIPAS to observe atmospheric parameters in a maximum altitude range of 5–160 km with a vertical spacing of 1–8 km depending on the altitude and on the measurement mode (Fischer et al., 2007). Operational measurements at full spectral resolution (0.025 cm^{-1}) were conducted from July 2002 to March 2004. However, anomalies affecting the interferometer slide mechanism led to the suspension of operations on 26 March 2004. Observations were resumed in January 2005 with a new operation mode, on a finer vertical grid and with reduced spectral resolution (0.0625 cm^{-1}). The following analyses present the comparisons of the ACE-FTS data product with three MIPAS datasets: the operational ESA processor (MIPAS full resolution mission; Cortesi et al., 2007), the ESA prototype processor used for validation purposes (reduced resolution observations) and the IMK-IAA scientific processor (full resolution observations; von Clarmann et al., 2003). During the time period corresponding to the full resolution observations, ACE-FTS acquired data from SS occultations only. Therefore, there are no ACE-FTS SR events in the comparisons with the ESA operational retrievals and the IMK-IAA retrievals.

Comparison of ACE-FTS with the operational ESA retrievals

The algorithm used for the ESA near-real time Level 2 analysis is based on the Optimised Retrieval Model (ORM) scientific prototype (Raspollini et al., 2006; Ridolfi et al.,

2000). Given the redundancy of measurements in MIPAS limb-scanning sequences, vertical profiles do not need constraints such as a priori information. Complementary information, when available, can however be used to improve the quality of the retrieved parameters (Ridolfi et al., 2000). The retrieval uses a set of microwindows designed to obtain maximum information on the target species while minimizing the total error and the computing cost (Raspollini et al., 2006). The microwindow selection algorithm is described by Dudhia et al. (2002). The standard products of the ESA processor are the atmospheric pressure and temperature profiles along with the volume mixing ratio profiles of 6 "key species": H_2O, O_3, HNO_3, CH_4, N_2O and NO_2. These are provided at the tangent heights of the MIPAS measurements during the full resolution mission, i.e., from 68–6 km with a variable vertical spacing ranging from 3 km below 42 km to 8 km above 52 km. A detailed validation analysis of the data acquired during the full resolution mission can be found in Cortesi et al. (2007). Briefly, the MIPAS profiles retrieved with the ESA operational processor (version 4.61 and 4.62) showed very good agreement with the correlative datasets in the middle and upper stratosphere, with relative differences within ±10% in the altitude range between ∼20 and ∼50 km (50–1 hPa). In the UT/LS, MIPAS profiles show a significant positive bias of +5 to +25% with respect to the coincident observations (Cortesi et al., 2007).

Here, MIPAS operational ozone data version 4.62 (ESA-v4.62) are compared with ACE-FTS. We found a total of 138 events at latitudes 70°–80° N, using coincidence criteria of ±6 h and 300 km. The time constraint was relaxed to 6 h (instead of the typical 2 h) in order to increase the statistics of the comparison since it did not introduce notable biases in the atmospheric sampling. For MIPAS, only profiles associated with a successful pressure/temperature and target species retrievals have been considered. The results of the comparison are summarized in Fig. 18. Percent differences are within ±10% between 10 and 41 km, with a local maximum of +9.9% (+0.44 ppmv) at 30 km which cannot be accounted for by the combined systematic uncertainty estimates. From 35 to 48 km, ACE-FTS reports increasingly larger ozone values, with a pronounced maximum around 48 km corresponding to differences of +58% (about

+1.4 ppmv). The amplitude of this peak is larger than the high altitude bias noted in other comparisons, but is limited to a narrower altitude range.

Comparison of ACE-FTS with the reduced-resolution mission ESA data product

New measurement scenarios were adopted for the reduced resolution mission. These scenarios are characterized by a finer vertical limb scanning step of 1.5 km from 6–21 km, 2 km from 21–31 km, 3 km from 31–46 km (i.e., equal to the instrument field-of-view) and 4 km above 46 km. A detailed description of these measurement scenarios can be found in Ceccherini et al. (2006). Since the retrieval is performed at the tangent altitudes, the use of a limb scanning step smaller than the width of the instrument field-of-view introduces instabilities in the retrieval and requires a regularization to avoid oscillations in the retrieved profiles. For this reason, the ORM retrieval code was modified to implement a Tikhonov regularization scheme that is described in detail by Ceccherini et al. (2007). Furthermore, a new set of microwindows, optimised for the new measurement mode, was selected using the same algorithm as for the full resolution observations. In particular, a larger number of spectral points is considered, in order to compensate for the loss of information content caused by the reduced spectral resolution. Comparison of the results obtained for the full and reduced resolution measurements showed that the new algorithm yields improved spatial resolution (horizontal and vertical) and lower retrieval errors (Ceccherini et al., 2006).

For this comparison, we used ±5° and ±10° for the latitude and longitude criteria, respectively. Here also, the time criterion was relaxed to ±6 h to increase the number of coincident pairs. A total of 160 coincidences was found. We used the MIPAS profiles retrieved with the ESA MIPAS Level 2 processor prototype (version ML2PP/5.0). These are a preliminary set of data that ESA generated for validation purposes. Figure 19 shows the results of the comparison. They are qualitatively consistent in the stratosphere with those from the full resolution observations. Differences are within ±8–10% between 14 and 45 km, with closest agreement around 20 and 38 km (relative differences within ±3%). At and above 45 km, ACE-FTS reports larger ozone

values than those of MIPAS, with a maximum difference of ∼25% around 58 km. This is consistent with the comparisons with other satellite sensors.

Comparison of ACE-FTS with the IMK-IAA scientific processor

The IMK-IAA retrieval scheme (von Clarmann et al., 2003, and references therein) is a scientific processor complementary to ESA's near-real-time analysis. It is based on regularized inversion using a first-order Tikhonov-type smoothing constraint (von Clarmann et al., 2003) and optionally includes non-LTE calculations, implemented at the IAA, to analyse cases (specific molecular species and/or altitude levels) where the LTE assumption is not verified. Ozone retrievals use a set of 10 microwindows within the spectral ranges 740–800 cm^{-1} and 1060–1110 cm^{-1} where non-LTE emissions are mostly negligible (Glatthor et al., 2006). The retrieved profiles are provided on a vertical grid with finer spacing than the tangent height distances: 1 km up to 44 km and 2 km from 44 to 70 km (von Clarmann et al., 2003). For the analysis presented here, the current IMK-IAA ozone data product (V3O_O3_7) is used for the full spectral resolution observation period. This product was compared by Steck et al. (2007) with ground-based instruments, ozonesondes and observations from HALOE and POAM III. They found mean percent differences within ±10% in the stratosphere, a precision of 5-10% and an accuracy of 15–20%. Below 18 km, the precision was reduced to 20% or more (Steck et al., 2007).

Using criteria of ±9 h and 800 km, we found a total of 333 (348) coincidences between ACE-FTS and the daytime (nighttime) measurements from MIPAS. The results of the comparisons are shown in Fig. 20, for daytime (top panel) and nighttime (bottom panel) MIPAS profiles. To take into account diurnal variations in the ozone abundance, the retrieved MIPAS data were corrected using the KArlsruhe SImulation model of the Middle Atmosphere (KASIMA) chemistry and transport model (Kouker et al., 1999). Differences between ACE-FTS and the MIPAS data are within ±8% from 12 to 43 km in both the KASIMA-corrected and uncorrected cases, with typical values of +3–4% and ACE-FTS VMRs generally larger than those of MIPAS. This is also consistent with

the results for the ESA retrievals from the full and reduced resolution data products. Above 40 km, the KASIMA correction generally improves the comparison. In general, the relative differences become larger with increasing altitude, with values of ∼30–40% (0.8–0.9 ppmv) at 48 km. For daytime MIPAS measurements, a sharp decrease of the absolute differences can be noted around 52 km.

5.4.3 Envisat/SCIAMACHY

SCIAMACHY is a limb- and nadir-viewing imaging spectrometer, also capable of occultation measurements. It uses eight channels in the UV, visible and near-IR spectral range from 240 to 2380 nm, with a moderate resolution of 0.2–1.5 nm (Bovensmann et al., 1999). Number density profiles of several atmospheric species (such as O_3, NO_2, BrO, OClO), as well as polar stratospheric clouds and noctilucent clouds, are routinely retrieved from the limb measurements from the surface to ∼92 km with a vertical spacing of 3.3 km (e.g., Brinksma et al., 2006).

The retrievals of stratospheric ozone density profiles in the 15–40 km altitude range from SCIAMACHY limb scattering measurements, used in this study, are the scientific retrievals done at the Institute of Environmental Physics (IUP, Bremen, Germany). They use version 1.63 of the Stratozone retrieval code (von Savigny et al., 2005a). Stratozone employs limb radiance profiles at three discrete visible wavelengths (525 nm, 600 nm, 675 nm) and exploits the differential absorption signature of ozone between the center and the wings of the Chappuis absorption band. A nonlinear iterative Optimal Estimation scheme drives the radiative transfer model SCIARAYS (Kaiser and Burrows, 2003), which is used as the forward model.

As the SCIAMACHY limb tangent heights are affected by errors of up to 2.5 km (von Savigny et al., 2005b), in this study we used tangent height retrievals using the Tangent height Retrieval by UV-B Exploitation (TRUE) algorithm (Kaiser et al., 2004) version 1.7 to correct the tangent heights prior to the O_3 profile retrieval. TRUE version 1.7 uses pressure and temperature data from the European Center for Medium-range Weather Forecast (ECMWF) for the location, date and time of each limb measure-

2551

ment. The ozone profile information required for the tangent height retrieval is taken from the dynamic ozone climatology of Lamsal et al. (2004), providing ozone profiles as a function of total ozone columns for five latitude regimes, in combination with total ozone column measurements from the Earth Probe – Total Ozone Mapping Spectrometer (EP-TOMS, http://toms.gsfc.nasa.gov/index_v8.html) for the location and date of each SCIAMACHY limb measurement. The tangent height offsets derived for tropical latitudes, where TRUE provides the most accurate results, are applied to all limb measurements in the corresponding orbit. The mean tangent height offset for 2004 is about −1.5 km. Previous SCIAMACHY IUP ozone profiles (version 1.6) have been validated extensively with lidars, ozonesondes, MWRs and SAGE II and SAGE III data (Brinksma et al., 2006). Results showed that the SCIAMACHY-IUP v1.62 data product is biased low between 16 and 40 km, by a few percent (3–6% with a standard deviation of ∼10%). In this analysis, we use version 1.63 of the IUP ozone number density profiles for SCIAMACHY.

The criteria chosen for the ACE-FTS and SCIAMACHY comparisons are a maximum difference of ±6 h and a maximum distance of 500 km. This gives a total of 734 coincidences between March and December of 2004, with more than 75% occurring in the Arctic polar region in the latitude range 60°–82° N, out of which 90% or more of the SCIAMACHY events are measured at high solar zenith angle (70°–85°). The overall results are shown in Fig. 21. The vertical range was limited to 17–41 km, since the retrieval below and above this range is dominated by the a priori and there is no information from the measurement. Over the full altitude range, the agreement is within ±4%, except around 30 km where ACE-FTS reports higher ozone values than those of SCIAMACHY (by up to 15%). This large bias around 30 km is noted in the high-solar zenith angle SCIAMACHY observations, mostly in the Arctic (564 events), but is not seen in other regions.

2552

5.5 Aura-MLS

The Aura satellite (Schoeberl et al., 2006) was launched in July 2004 in a sun-synchronous, quasi-polar orbit, with an altitude of ~700 km, an inclination of 98° and ascending node crossing at 13:45 (local time). MLS aboard Aura scans the Earth's limb to measure thermal emission at millimeter and submillimeter wavelengths, using seven radiometers designed to cover five broad spectral regions from 118 GHz to 2.5 THz. The Aura-MLS instrument, calibration and performance for the different channels are described by Jarnot et al. (2006), Cofield and Stek (2006) and Pickett (2006). The orbit geometry provides global coverage from 82° S to 82° N each day. 240 vertical scans are performed during each orbit, allowing the retrieval of ~3500 profiles per day for 17 primary atmospheric parameters: pressure, temperature and cloud ice water content, as well as 14 trace constituents such as O_3, H_2O and CO. An overview of the instrument and observation characteristics, main spectral lines and target species can be found in Waters et al. (2006).

The retrieval scheme is based on the Optimal Estimation Method (Rodgers, 2000). Taking advantage of the forward-looking geometry of the instrument with respect to the spacecraft, the innovative approach of the Aura-MLS retrievals resides in the combination of ~5–10 subsequent scans to retrieve atmospheric parameters on a two-dimensional grid, in the vertical direction and along the line-of-sight. This retrieval approach is detailed by Livesey et al. (2006). The vertical retrieval is provided on a standard pressure grid with 6 pressure surfaces per decade change in stratospheric pressure, and 3 levels per decade for pressures smaller than 0.1 hPa. The corresponding vertical resolution is 3–5 km. The ozone volume mixing ratio is retrieved from the observations of the radiometer centered at 240 GHz.

The Aura-MLS ozone version 1.5 dataset was compared with numerous correlative datasets (including SAGE II, HALOE, POAM III and the previous data version (v2.1) of ACE-FTS O_3) in the early validation study of Froidevaux et al. (2006) and with Odin/SMR (Bordeaux version 222 processor) by Barret et al. (2006). An overall agree-

2553

ment of 5–10% was found throughout the stratosphere, with Aura-MLS biased high in the lower stratosphere but low in the upper stratosphere. Extensive validation of the Aura-MLS version 2.2 (hereinafter v2.2) ozone product, with a limited time coverage, showed better results than version 1.5 with respect to the correlative datasets, with an agreement of 5–8% in the stratosphere (Froidevaux et al., 2008; Boyd et al., 2007; Jiang et al., 2007).

The comparisons presented here extend the analyses of Froidevaux et al. (2008) to the full Aura-MLS v2.2 dataset processed (as of May 2007) and include comparisons with ACE-MAESTRO. At the time of the analysis, coincidences were available on 465 dates, with very few in 2004 (19) and the remainder evenly distributed in the other years. A total of 3180 coincidences was found using the coincidence criteria: ±2 h, ±5° in latitude and ±10° in longitude. We used the recommended parameters for screening the Aura-MLS data: quality value >0.4, positive precision, even values of the status flag, and convergence <1.8 (Froidevaux et al., 2008). We also limited the vertical range of the comparisons to the altitudes ~10–65 km as recommended for Aura-MLS and ACE-MAESTRO. For the comparison, the Aura-MLS vertical profiles were interpolated in log(pressure) onto the ACE-FTS pressure levels and subsequently reported on the ACE-FTS or ACE-MAESTRO altitude grid.

The results of the comparisons for ACE-FTS are shown in Fig. 22. ACE-FTS reports consistently more ozone than Aura-MLS over the comparison range. Between 12 km and 42 km (~2 hPa), the relative differences are lower than +8%, with a typical value of +5%. Above 42 km, the differences increase up to a maximum of +25% at 53 km (~0.6 hPa). This is consistent with the findings of Froidevaux et al. (2008) and with the other comparisons presented in this paper.

The results for ACE-MAESTRO are presented in Fig. 23. The ACE-MAESTRO SR profiles show larger VMRs than Aura-MLS in the range 21–57 km, with relative differences lower than +16% and typically around +7%, in closest agreement with the Aura-MLS data around 38 km (<+2.5%). Above and below this range, the SR retrievals report VMR values significantly smaller than those of Aura-MLS, with negative

2554

differences rapidly increasing to about -50% at the limits of the comparison range. In the case of the ACE-MAESTRO SS events, the relative differences increase with altitude. The percent difference values range from about -10% (15 km or $\sim$120 hPa) to a maximum of $+21\%$ at 52 km ($\sim$0.7 hPa).

6 Comparisons with airborne, balloon-borne and ground-based instruments

6.1 Aircraft measurements from ASUR

ASUR is a microwave receiver operating in a tunable frequency range between 604.3 and 662.3 GHz (von Koenig et al., 2000). It measures atmospheric emission from various trace gas molecules including O_3, N_2O, HNO_3 and CO. Stratospheric measurements performed with the Acousto-Optical Spectrometer (AOS) are used in this intercomparison exercise. The total bandwidth of the AOS is 1.5 GHz and its resolution is 1.27 MHz. The heterodyne sensor is operated on board a high-flying research plane to avoid strong absorption signals from tropospheric water vapor. The instrument looks upwards at a stabilized constant solar zenith angle of 78°. Measured spectra are integrated during up to 80 s, which leads to a horizontal resolution of about 18 km along the flight path. Vertical abundance profiles are retrieved on a 2 km-spacing altitude grid using the Optimal Estimation Method (Rodgers, 2000). Vertical resolution of the ozone measurements is about 6–18 km, and the vertical range is 16–50 km. The precision of a single measurement is 0.1 ppmv and the accuracy (including systematic uncertainties) is 15% or 0.3 ppmv, whichever is greater. Details about the measurement technique and retrieval theory can be found in Kuttippurath et al. (2007).

The ASUR ozone measurements used in this study were performed aboard the NASA DC-8 aircraft during the Polar Aura Validation Experiment (PAVE) (http://www.espo.nasa.gov/ave-polar/). These were compared with ACE-FTS and ACE-MAESTRO using coincidence criteria of ±12 h and 1000 km. This resulted in a total of 39 (37) coincident ASUR measurements with ACE-FTS (ACE-MAESTRO), from 5 flights out of

2555

Portsmouth (New Hampshire, USA) reaching northern high latitudes ($\sim$65° N) on 24, 29 and 31 January and 2 and 7 February 2005. The corresponding ACE-FTS and ACE-MAESTRO occultations were obtained exclusively at sunrise. The ACE-FTS and ACE-MAESTRO VMR profiles were convolved with the ASUR averaging kernels to account for the lower vertical resolution of the ASUR profiles.

Figure 24 shows the results from the comparison between ACE-FTS and ASUR. The relative difference is less than 18% (0.45 ppmv) over the full altitude range. The ACE-FTS ozone values are larger than those of ASUR from 22–50 km, with largest values ($>+7\%$) around 25 km and in the upper stratosphere. Below 22 km, the ACE-FTS VMRs are slightly lower than the ASUR values, by up to -8% (-0.20 ppmv). The agreement between the datasets is very good at the altitudes of the peak in ozone VMR.

The results from the comparison between ACE-MAESTRO and ASUR are presented in Fig. 25. The mean difference is less than ±16% ($<\pm0.33$ ppmv) at all altitudes. The fractional differences are within ±3% from 22–38 km. Below 22 km, ACE-MAESTRO reports less ozone than ASUR, by up to -12% (-0.30 ppmv). Above 38 km, the VMRs reported by ACE-MAESTRO are increasingly larger than those of ASUR by up to $+16\%$ ($+0.33$ ppmv). Here too, there is very good agreement around the ozone VMR peak (32–34 km). The apparent discrepancy between the results shown in the mean VMR profiles and mean difference profiles (Fig. 25: left and middle/right panels, respectively) is because we present the mean of the individual differences rather than the difference of the mean profiles as discussed in Sect. 4.

6.2 Balloon-borne observations from FIRS-2

The Far-InfraRed Spectrometer (FIRS)-2 is a remote-sensing FTIR spectrometer designed and built at the Smithsonian Astrophysical Observatory. It measures thermal emission from the atmosphere in the wavelength range 8–120 μm ($\sim$80–700 cm^{-1}), with a spectral resolution of 0.004 cm^{-1} (Johnson et al., 1995). The balloon-borne observations are performed in the limb-sounding geometry. To analyse the data, first,

2556

the atmospheric pressure and temperature profiles are retrieved using the 15 μm band of CO_2. Then, vertical profiles of about 30 trace constituents are retrieved from the float altitude (typically 38 km) down to the tropopause, using a nonlinear Levenberg-Marquardt least-squares algorithm (Johnson et al., 1995). Uncertainty estimates for FIRS-2 contain random retrieval error from spectral noise and systematic components from errors in atmospheric temperature and pointing angle (Jucks et al., 2002; Johnson et al., 1995). In the case of the O_3 profile used in this analysis, the total error is 10–20% below 20 km and 5–8% above. Balloon flights of FIRS-2 have been used to validate observations from the Improved Limb Atmospheric Spectrometer (ILAS) on board the Japanese Advanced Earth Observing Satellite (ADEOS) (e.g., Nakajima et al., 2002) as well as from the MLS, HALOE and the Cryogenic Limb Array Emission Spectometer (CLAES) instruments aboard UARS (Jucks et al., 2002, and references therein). Results from FIRS-2 were also compared more recently with Aura-MLS observations (Canty et al., 2006).

We compared a FIRS-2 observation acquired on 24 January 2007 ($\sim$68° N, $\sim$22° E) with the ACE-FTS and ACE-MAESTRO profiles from the SR occultation sr18561 (64.7° N, 15.0° E, distance: $\sim$481 km) measured on 23 January 2007 at 08:25 UT (Fig. 26). Since the FIRS-2 data is reported on a 1 km-spacing altitude grid, we simply interpolated the FIRS-2 profile onto the altitude grids of ACE-FTS (1 km) and ACE-MAESTRO (0.5 km). For this particular observation, the float altitude of the balloon carrying FIRS-2 was lower than usual, leading to an upper limit of the vertical range of the comparison at 31 km. The differences between the O_3 profiles from FIRS-2 and ACE-FTS range from -12 to $+15$% over the vertical range 13–31 km, with largest differences at the limits of the vertical range. ACE-FTS generally reports larger VMR values than those of FIRS-2 above 16 km, except around 26 km. The comparisons with ACE-MAESTRO yield similar results, with relative differences within ±15% at altitudes between 15–31 km, but as large as -19% at lower altitudes.

6.3 SAOZ-balloon measurements in the tropics

The Système d'Analyse par Observation Zénitale (SAOZ) sonde is a light-weight UV-visible diode array spectrometer measuring the atmospheric absorption of sunlight during the ascent of the balloon and during a sunset occultation from float altitude (Pommereau and Piquard, 1994). Spectral analysis is performed using the Differential Optical Absorption Spectroscopy (DOAS) technique which uses least-squares fitting of the spectra with laboratory cross-sections. Ozone is measured in the Chappuis band (visible spectral range at 450–620 nm) where the absorption cross-section is not sensitive to temperature. The profiles are retrieved in the altitude range 10–28 km with a vertical resolution of 1.4 km, using the onion peeling method within 1 km-thick atmospheric shells. Data contaminated by clouds are removed by looking at the atmospheric extinction at 615 nm. For O_3, the estimated precision is 1.5% at 20 km, degrading to 5% at 17.5 km, 10% at 15 km and 23% at 10 km. Accuracy is evaluated by adding a systematic error of 1.5% (uncertainty from the ozone absorption cross-sections) to the precision values. The SAOZ ozone profiles have been compared to a number of satellite and sonde observations and were found to be very consistent with the most accurate data available (Lumpe et al., 2003; Haley et al., 2004; Borchi and Pommereau, 2007).

The three SAOZ flights used in this study were part of the African Monsoon Multidisciplinary Analysis (AMMA) balloon campaign (Redelsperger et al., 2006) undertaken within the framework of the Stratospheric-Climate Links with Emphasis on the Upper Troposphere and Lower Stratosphere (SCOUT-O3) European project (http://www.ozone-sec.ch.cam.ac.uk/scout_o3/). They occured in August 2006 in Niamey, Niger (13.48° N, 2.16° E) during the wet season. The first flight ($\sim$13.8° N, $\sim$0.8° E on 7 August 2006) reached a float altitude of 22 km, while the other two ($\sim$14.0° N, $\sim$0.0° E on 10 August 2006 and $\sim$13.9° N, $\sim$0.0° E on 19 August 2006) reached 28 km. The measurements (ascent and occultation) occured for all three flights around 18:00 (UT). The six resulting profiles (3 for ascent and 3 occultation profiles at float altitude) are

2558

compared with the spatially coincident ACE profiles from SS occultation ss16090 (8 August 2006 at 17:40 UT). Since the vertical resolution of the SAOZ balloon instrument is comparable to that of the ACE instruments, the SAOZ profiles were simply interpolated onto the vertical grids of ACE-FTS (1 km) and ACE-MAESTRO (0.5 km).

The results for ACE-FTS are presented in Fig. 27. Percent differences are within ±10% (<0.4 ppmv) above 19 km for all ascent (solid lines) and occultation (dotted lines) SAOZ profiles. Below 19 km the differences increase to 40–60% around 16 km, with VMR values reported by ACE-FTS smaller than those of SAOZ.

Figure 28 shows the comparison for ACE-MAESTRO. The ACE-MAESTRO and the SAOZ profiles are in good agreement (between −15 and +5%) above 19 km. As was found for ACE-FTS in the range 15–19 km, ACE-MAESTRO reports significantly less ozone than SAOZ with maximum relative differences larger than −70%. Below 16 km, the ACE-MAESTRO VMRs are considerably larger than those of SAOZ.

The large differences noted for ACE-FTS as well as for ACE-MAESTRO below ~18 km may be explained by the fact that the SAOZ measurements used in this study were deliberately performed in the vicinity of high altitude (up to 18 km) convective clouds. At higher altitudes, it is possible that the retrieved altitudes for the ACE instruments are slightly shifted with respect to those of SAOZ (for which the pointing accuracy was better than 50 m).

6.4 Balloon-borne SPIRALE observations

The SPectroscopie Infra-Rouge d'Absorption par Lasers Embarqués (SPIRALE) instrument is operated from a balloon-borne gondola by the Laboratoire de Physique et Chimie de l'Environnement (LPCE, Orléans, France) and is routinely used at all latitudes, in particular as part of European validation campaigns for the Odin and Envisat missions. The six tunable diode lasers absorption spectrometer (TDLAS) has been previously described in detail (Moreau et al., 2005). In brief, it can perform simultaneous in situ measurements of about ten chemical species in the vertical range 10–35 km. The high frequency sampling (~1 Hz) yields a vertical resolution of a few

2559

meters, depending on the ascent rate of the balloon. The diode lasers emit at mid-IR wavelengths (3–8 μm) and the beams are injected into a multipass Heriott cell, located under the gondola and largely exposed to ambient air. The cell (3.5 m long) is deployed during ascent when the pressure is lower than 300 hPa. The multiple reflections obtained between the two cell mirrors give a total optical path of 430.78 m. Species concentrations are retrieved from direct IR absorption, by fitting experimental spectra with spectra calculated using the HITRAN 2004 database (Rothman et al., 2005). Specifically, the ro-vibrational lines at 2086.0191 and 2086.4294 cm^{-1} were used for the SPIRALE O_3 retrievals. Simultaneous measurements of pressure and temperature onboard the gondola allow the number densities to be converted to VMRs. Estimates of the uncertainties in the SPIRALE measurements were detailed by Moreau et al. (2005). Total root-sum-square uncertainties are about 6% above 18 km (<80 hPa) and 8% below (>80 hPa).

For this study, we compared a SPIRALE profile (obtained during ascent) from 20 January 2006 (17:34–19:47 UT) with the coincident ACE-FTS and ACE-MAESTRO profiles from the SR occultation sr13151. The SPIRALE O_3 vertical range was 10.8–27.3 km. The balloon position remained rather constant around a mean location of 67.6±0.2° N and 21.55±0.2° E. The ACE occultation occurred 13 h later (on 21 January 2006 at 08:00 UT) and was located at 64.28° N–21.56° E at a distance of 413 km from the SPIRALE mean position. Potential vorticity (PV) maps were calculated with the Modélisation Isentrope du transport Méso-échelle de l'Ozone Stratosphérique par Advection (MIMOSA) contour advection model (Hauchecorne et al., 2002). They confirmed that SPIRALE and ACE sounded similar air masses in the well established polar vortex at this time, for the whole range of altitudes, with PV differences of less than 10%.

Since the vertical resolution for SPIRALE is on the order of meters, we smoothed the SPIRALE data using convolution functions as described in Sect. 4. The ACE-FTS and SPIRALE O_3 profiles are in good agreement over the full altitude range, with relative differences within ±7% (Fig. 29). Above 21 km, the ACE-FTS VMR values are

2560

systematically larger than those reported by SPIRALE (by +2 to +6%). The results for ACE-MAESTRO are presented in Fig. 30. Here also, there is very good agreement, with percent differences within ±5% above 16 km and slightly larger below (−7%).

6.5 Ozonesonde measurements

Ozonesondes are balloon-borne instruments launched (typically) weekly from various stations around the globe. They perform in situ measurements of pressure, temperature, humidity and O_3 abundances from the surface to the balloon's burst altitude (typically ∼35 km) with a resolution of 100–150 m. There are three types of ozonesondes currently in operation: the Electrochemical Concentration Cell (ECC) (Komhyr et al., 1995), Brewer-Mast (BM) (Brewer and Milford, 1960) and Carbon-Iodine (CI) (Kobayashi and Toyama, 1966) ozonesondes. The accuracy of ozonesonde observations is generally estimated to ±5% (e.g., SPARC, 1998) but in fact depends on numerous parameters (for instance, for ECC ozonesondes, the concentration of the sensing solution or the manufacturer influence the accuracy). Depending on the type of ozonesonde and the altitude, typical values for the precision and accuracy are ∼3–8% and ∼5–15%, respectively, up to 30 km (see Smit et al., 2007, and references therein).

For the statistical comparison of ACE-FTS and ACE-MAESTRO with ozonesonde observations, we used measurements from the World Ozone and Ultraviolet Data Center (WOUDC), the Southern Hemisphere ADditional OZonesonde (SHADOZ) archive and the 2004 INTEX Ozonesonde Network Study (IONS) campaign (see Table 2 for URLs and references). We defined coincidence criteria of ±24 h and 800 km. Table 2 lists the stations for which coincidences were found. Because of their high vertical resolution, the ozonesonde data were smoothed using the convolution functions described in Sect. 4. When several ACE-FTS or ACE-MAESTRO profiles were coincident with the same ozonesonde measurement, they were averaged and the resulting mean profile was compared with the ozonesonde data. From the initial total of 547 coincidences, we compared 376 profiles.

Figure 31 shows the results for the comparison with ACE-FTS. There is good agreement with the ozonesonde observations in the altitude range 12–36 km. In this range, ACE-FTS reports systematically larger VMRs than the ozonesondes with smallest differences of about 4.6% around 12 km. The relative differences are smaller than +7% from 12–17 km and within +7 to +11% between 18 and 36 km. Below 12 km, the variability is high and the differences increase significantly. Above 35 km, the number of coincident events drops sharply and the statistical significance of the results is limited, therefore these results are not shown.

Comparison results for ACE-MAESTRO are shown in Fig. 32 for the SR (top panel) and SS (bottom panel) events. The overall agreement is within ±5% from 15–29 km, with increasing deviations above and below this altitude range. Using a rather limited sample, Kar et al. (2007) had earlier shown a small bias between the ACE-MAESTRO SR and SS retrievals in the altitude range 20–30 km, when compared with the ozonesondes. The relative differences for the ACE-MAESTRO SR events were found to be more positive (by about 5%) than those calculated for the comparison between the SS observations and the ozonesondes. This bias seems to be somewhat reduced for this larger sample of coincidences but remains significant in terms of absolute differences, with the SS retrievals showing a larger negative bias between 15–29 km. The large relative differences below 15 km, reaching −20% (SS) and −40% (SR) at the lowest altitudes, with ACE-MAESTRO reporting consistently lower VMRs than the ozonesondes, are primarily due to the small VMR values at these altitudes.

6.6 NDACC ozonesonde and lidar measurements

Detailed comparisons were performed for individual sites with two types of ozone profiling instruments, ozonesondes and lidars. These are operated within the framework of the Network for the Detection of Atmospheric Composition Change (NDACC, formerly the Network for the Detection of Stratospheric Change or NDSC), a major component of the World Meteorological Organization's Global Atmosphere Watch program (WMO-GAW). The ozonesonde measurements have been described in the previous section.

DIfferential Absorption Lidar (DIAL) systems provide the vertical distribution of night-time ozone number density at altitudes between ~10 km and ~45 km, with a vertical resolution of 300 m to 3 km, depending on the altitude. Typical values for lidar accuracies are 3–7% between 15 and 40 km. At 40 km and above, due to the rapid decrease in signal to noise ratio, the errors increase and a significant bias of up to 10% may appear (Godin et al., 1999; Keckhut et al., 2004).

Coincidence criteria of ±12 h and 500 km were used to select available data from a total of 31 ozonesonde stations (Table 2) and 5 lidar stations (Table 3). Figure 33 shows the time and latitude coverage of all coincidences stored in the database used for this study. However, only stations for which at least three coincidences were found with the ACE instruments were included in the analyses. Therefore, stations visible in Fig. 33 but for which there were less than three coincident observations are not listed in Tables 2 and 3.

The analyses were conducted in three steps. First, the individual coincident events were examined to check the quality of the retrieved profiles. Then, time series for the ACE and the ground-based measurements and their relative differences were analyzed. This allowed time periods to be identified in which homogeneous results, and hence meaningful statistics, could be obtained. Finally, the vertical structure of the differences was investigated within these homogeneous time periods, by grouping the stations where similar results were found. The second and third steps will be described below. The integration methodology applied in smoothing the high-resolution ozonesonde and lidar profiles is described in Sect. 4.

In the detailed analysis of the time series, agreement between the ACE-FTS profiles and the ground-based data was within ±10%, with mean difference values of ±6%, in the altitude range 11–30 km for the ozonesondes and ranging from −4% to +10% in the range 10–42 km for the lidars. For ACE-MAESTRO, the relative differences with ozonesondes were mostly negative (with ACE-MAESTRO VMRs smaller than the ozonesondes) with mean values of −10 to +0.3% from 15–30 km and up to −16% below. When compared to lidars, ACE-MAESTRO reported less ozone between

15 and 37 km (mean difference of about −7%), whilst mean differences of up to −18% were observed below 15 km and positive differences (~+8%) in the range 37–41 km, with ACE-MAESTRO reporting larger VMRs than the lidars. This analysis showed that the temporal variations of the ozone layer are well captured by ACE-FTS and ACE-MAESTRO, but the limited temporal sampling does not allow finer-scale variations to be revealed. Within the stratosphere, no important structure or seasonal variation was identified in the time series which allowed us to derive meaningful statistics for the ACE-FTS and ACE-MAESTRO ozone data products by combining the three years of the comparison period.

We also investigated the height-resolved statistical differences over the full comparison time period for each station. For the ACE-FTS and ozonesonde comparisons, the mean difference was found to be ±7% over the range 10–35 km, increasing to 20% or more below 10 km. For the comparisons with lidars, a mean agreement within ±10% was observed from 10–15 km to 45 km. An example of these relative difference profiles is shown in Fig. 34 for the coincidences between ACE-FTS and lidar measurements for the Haute-Provence station. Figure 35 shows a similar example for ACE-MAESTRO and the ozonesonde data obtained at Eureka. The observed differences in the comparisons of ACE-MAESTRO retrievals with ozonesondes or lidar observations are globally negative, with a mean value of about −7% above 15 km. Below this altitude, ACE-MAESTRO reports significantly less ozone than either of the ground-based instruments, with mean differences of 20–40%. The standard deviation of the differences, for both ACE-FTS and ACE-MAESTRO, is within ±10% in the stratosphere but much larger in the troposphere.

The overall comparison results are summarized as zonally averaged (within 5° bins) distributions shown in Figs. 36 and 37 for ACE-FTS and ACE-MAESTRO, respectively. Figure 36 shows the averages of the relative differences between ACE-FTS and NDACC ozonesondes (top panel) and lidars (bottom panel). From ~10 km up to 30 km, the observed mean difference between the ACE-FTS VMRs and the ozonesonde data is small. For the comparisons with lidar profiles, similar small differences are found in

the altitude range 15–40 km. The global results for ACE-MAESTRO are summarized in Fig. 37. Between 15 km and 30 km, negative mean differences of −6 to −8% are observed between ACE-MAESTRO and the ozonesondes (top panel). Below 15 km, larger differences are observed. The results for the comparison of ACE-MAESTRO are comparable, with mean differences of about −7% over the altitude range 15–40 km.

6.7 Eureka DIAL measurements

A DIAL instrument has been in operation at the Arctic Stratospheric Ozone (AStrO) Observatory/Polar Environmental Atmospheric Research Laboratory (PEARL) in Eureka (80.05° N, 86.42° W) since 1993. In February–March 2004, 2005 and 2006, it measured temperature and ozone profiles as part of the Canadian Arctic ACE Validation Campaigns (Kerzenmacher et al., 2005; Walker et al., 2005; Sung et al., 2007; Manney et al., 2007a; Fraser et al., 2007; Fu et al., 2008; Sung et al., 2008[1]). The measurements use radiation from a XeCl excimer laser at two wavelengths, one with a strong absorption signature of O_3 (the "on" wavelength, 308 nm for the Eureka lidar) and one with little absorption (the "off" wavelength, hydrogen Raman-shifted to 353 nm at Eureka) (Donovan et al., 1995). A detailed description of the system is given by Carswell et al. (1991). The Eureka DIAL is operated exclusively at night and provides vertical profiles of ozone from the tropopause level to ∼45 km with a vertical resolution of 300 m and an estimated accuracy for ozone of 1–2% (e.g., Bird et al., 1997).

Data from the Eureka DIAL measurements obtained during the 2004 Canadian Arctic ACE Validation Campaigns were used for validation of the previous release of the ACE-FTS and ACE-MAESTRO data (Kerzenmacher et al., 2005). Comparisons of the DIAL temperature profiles with ACE observations can also be found in companion papers (e.g., Manney et al., 2007a; Sica et al., 2008). We present the comparisons of DIAL O_3 with ACE-FTS and ACE-MAESTRO. We used coincidence criteria of ±12 h and 500 km, yielding 10 (8) coincidences for ACE-FTS (ACE-MAESTRO) for the 2004–2006 winters.

The results are presented in Fig. 38 for ACE-FTS and Fig. 39 for ACE-MAESTRO.

The agreement between the lidar measurements and the ACE-FTS profiles is within −12 to +4% (less than −0.8 ppmv) in the range 14–35 km, where ACE-FTS reports ozone VMRs consistently lower than those of the Eureka DIAL except for small positive differences at 15 and 34 km. At the lowermost altitudes, the differences are higher (−12 to −27%). Above 35 km, the lidar profiles appear very noisy and the low statistics prevent us from drawing meaningful conclusions The shape of the difference profile for the comparison with ACE-MAESTRO is quite similar, but ACE-MAESTRO shows a larger negative bias with respect to the Eureka DIAL observations. Relative difference values range from −20 to −6% in the range 12–35 km (except at 34 km where the percent difference is about +7%), with typical values of about −14% between 19–32 km and a maximum absolute difference of about −1.1 ppmv at 28 km. These results are qualitatively comparable with those described in Sect. 6.6 for other lidars and show an unusual (especially for ACE-FTS) low bias of the ACE instruments with respect to the Eureka DIAL.

6.8 Ground-based FTIR observations

In this section, we compare partial columns derived from the ACE-FTS and ACE-MAESTRO observations with ground-based measurements obtained by FTIR spectrometers, at ten NDACC stations (Table 4). Although the coarse vertical resolution of FTIR measurements limits their use for profile comparisons, they provide regular observations at different locations under clear-sky conditions and offer possibilities that complement the ozonesonde and lidar measurements for evaluating the temporal variations of the ACE dataset.

The FTIR instruments involved in the comparisons use microwindows in the range 780–3060 cm^{-1} and have spectral resolutions ranging from 0.001 to 0.012 cm^{-1}. They provide information on numerous species including O_3 from the lower troposphere to the middle and upper stratosphere. Two different retrieval codes are used (depending on the station): SFIT2 (Pougatchev and Rinsland, 1995; Pougatchev et al., 1995; Rinsland et al., 1998) and PROFITT92 (Hase, 2000). They were compared by Hase

et al. (2004), who found that these algorithms are in excellent agreement (generally better than 1%) for both VMR retrievals and total column calculations. Both processing codes are based on the Optimal Estimation Method (Rodgers, 2000), thus providing averaging kernels which are useful for determining the information content and for smoothing higher vertical resolution measurements such as those from ACE-FTS and ACE-MAESTRO.

In this study, we used the coincidence criteria listed in Table 4. Because of the limited number of coincidences at some stations, the time period for the comparison exercise was extended to the end of 2006. The ACE-FTS and ACE-MAESTRO profiles were interpolated on the FTIR retrieval grid for each station and extended below the lowest retrieved altitude using the FTIR a priori VMR values. The resulting composite profile was smoothed using the FTIR averaging kernels and a priori profile, as described in Sect. 4. Partial columns were calculated for a specific altitude range for each station. To calculate the ACE-FTS and ACE-MAESTRO partial columns, we used the atmospheric density derived from the ACE-FTS measurements. For the FTIR instruments, we calculated a density profile from the pressure and temperature profiles used in their retrievals.

The lower limit of the partial column range was given by the ACE-FTS or ACE-MAESTRO lowest measured altitude, while the upper limit was determined from the sensitivity of the FTIR measurements. We used an approach similar to that of Vigouroux et al. (2007): the sensitivity (also called measurement response) at one altitude is given by the area under the corresponding averaging kernel. The useful range for the FTIR is defined as the altitudes where the FTIR sensitivity is greater than 0.5 (i.e., where the information comes primarily from the measurement). The resulting vertical ranges vary from station to station and for ACE-FTS and ACE-MAESTRO, with lower limits of 10–18 km and upper limits of 38–47 km. For the partial columns, this yields a number of degrees of freedom for signal (DOFS, defined as the trace of the averaging kernel matrix over the altitude range of the partial column) ranging from ∼1.7 for Toronto to ∼3.9 for Izaña.

2567

In Figs. 40 (for ACE-FTS) and 41 (for ACE-MAESTRO), we present time series of the partial columns and relative differences for the comparisons with each FTIR instrument. In some cases, the comparison period is limited to several days of measurements in 2004 (Poker Flat and La Réunion). The partial columns derived from the ACE-FTS profiles are in acceptable agreement (±20%) with the FTIR values, with mean differences ranging between −10 and +7%. The results are similar for ACE-MAESTRO, with average relative differences values from −9 up to +2%. Furthermore, the scatterplots presented in Fig. 42 for ACE-FTS and in Fig. 43 for ACE-MAESTRO show very good correlation between the O_3 partial columns for the ACE instruments and the ground-based FTIR spectrometers, with correlation coefficients of 0.88 for ACE-FTS and 0.84 for ACE-MAESTRO. When comparing the results for the northern high latitude stations, a larger scatter in the relative differences (especially for ACE-MAESTRO) can be noted for Thule than for Kiruna. This is most likely due to the coincidence criteria which were broader for Thule than for Kiruna (Table 4). Additional tests were done with a stricter distance criterion (500 km) for comparison with Thule and showed significantly less scatter. However, it did not modify the mean agreement between the ACE data and the ground-based measurements. The results of the analysis for ACE-FTS and ACE-MAESTRO are presented in Table 5, showing the altitude range used for the calculations, the DOFS values, and the mean relative differences and associated standard deviations for each ground-based station. The latter are useful for qualitative evaluation of the results, even though the statistical relevance is limited by the low number of coincidences.

6.9   Comparison with ground-based microwave radiometer measurements

Stratospheric and mesospheric profiles from the MWRs at the Lauder, New Zealand and Mauna Loa, Hawaii NDACC sites have been compared with ACE-FTS and ACE-MAESTRO measurements. These have also been used to perform non-coincident comparisons with other satellite-borne and ground-based instruments, in a manner previously employed by Boyd et al. (2007). This method allows comparison of datasets

2568

that would otherwise have limited or no coincident or collocated measurements. Here we compare a set of historical and current satellite-borne datasets as well as ground-based lidar measurements with the MWR measurements and, by using the MWRs as transfer standards, determine the agreement between the ACE instruments and a consensus of these other instruments.

The MWR instruments (Parrish et al., 1992; Parrish, 1994) observe atmospheric thermal emission of ozone at 110.836 GHz and the pressure-broadened line shape is analyzed to obtain the altitude distribution of ozone using the Optimal Estimation Method of Rodgers (2000). The observations are made 24 h a day and routinely averaged over 4–6 h to provide up to four VMR profiles per day. The lower altitude limit for the profiles is about 20 km based on the influence of the a priori on the retrieval, and the quality of the measurement averaging kernels. The upper altitude limit is between 64 km for daytime measurements and about 72 km during night, due to the increased mesospheric ozone signal. The expected precision is 4–5% between 20 and 57 km, and 7% at about 64 km. The expected accuracy (i.e., combined random and systematic error) is 6–9% between 20 and 57 km and 11% at about 64 km. The vertical resolution of the MWR profiles is 6–10 km between 20 and 50 km and about 13 km at 64 km. A detailed description of the error analysis approach used for this work is included in the work of Connor et al. (1995).

In the ACE − MWR comparisons, broad coincidence criteria of ±24 h, ±6° latitude and ±12° longitude were used to increase the number of coincidences available. In the event that there was more than one ACE measurement fitting this criterion, the one closest in time to the MWR measurement is chosen. To avoid the effects of the significant diurnal variations in ozone amounts in the upper stratosphere and mesosphere, comparisons are restricted to below 52 km. To account for the different vertical resolutions of the instruments each ACE measurement is convolved with the averaging kernels of the MWR measurement as described by Connor et al. (1995), using Eq. (2) (Sect. 4). The profiles used here are interpolated onto an altitude grid with 2 km vertical spacing. The differences in the VMR profiles are determined with respect to the

2569

correlative dataset ((ACE−MWR)/MWR).

The differences between the ACE and MWR measurements, as well as the corresponding mean ozone VMR profiles, are presented in Fig. 44. Despite the small number of comparison pairs at Mauna Loa (less than 15), the difference profiles at both sites are generally similar. Below 44 km, the agreement between the ACE instruments and the MWRs is within ±10%, and often better than ±5%, except for the ACE-MAESTRO − MWR differences at Lauder from 32–36 km, which are between +10 and +15%. Above 42 km, the ACE instruments have a positive bias, compared with the MWR, of between +3 and +25%, with differences for ACE-FTS larger than those of ACE-MAESTRO by 5–8%. Apart from a region between about 28 and 38 km at Lauder, ACE-FTS ozone retrievals yield larger VMRs than ACE-MAESTRO, though the differences are always within the indicated error bars.

A noticeable feature in the plots is the oscillation in the profile around the VMR peak at 34 km. This feature is also seen in comparisons between MWR measurements and those made with other instruments, as shown in Fig. 45, and can therefore be attributed to the MWR. Ground-based microwave measurements tend to produce retrievals with a small oscillatory component. The origin of this oscillation is discussed in Boyd et al. (2007) and Connor et al. (1995). These are effects of systematic spectral measurement errors that propagate through the process of averaging multiple spectra and can produce artifacts in difference profiles such as those seen in the figure.

To extend our validation comparisons, the MWR measurements were used as a transfer standard. The method compares data from the SAGE II, HALOE, Aura-MLS, GOMOS, and MIPAS satellite-borne instruments, as well as ground-based lidars, with the MWRs at Mauna Loa and Lauder. The difference profiles from these comparisons are then averaged to obtain a consensus difference profile. Also included in the averaging are MWR-MWR "zero-line" profiles so that the MWRs, themselves, are included in the consensus. These are then subtracted from the ACE-FTS − MWR and ACE-MAESTRO − MWR difference profiles from Fig. 44, to obtain profiles which show the agreement between the ACE instruments and the consensus of the other instruments.

2570

Instrument comparisons with the MWRs were made using criteria similar to those used for the ACE – MWR comparisons discussed above, except the geolocation window for the satellite-borne measurements extends to ±5.0° latitude and ±10.0° longitude of the two sites. All the instruments have relatively high vertical resolutions compared to the MWRs and have been convolved using the MWR averaging kernels for the comparison.

All available measurements made by the satellite- and ground-based instruments, in the three year period from 2004 through to the end of 2006, were used to determine the difference profiles. Table 6 summarizes the data sets used in this study, including the processing version number, the number of collocated pairs used in determining the difference profiles presented here and the gaps in the data sets. Results from the comparisons between the various instruments and the MWRs are presented in Fig. 45 for Mauna Loa (panel a) and for Lauder (panel b).

The resulting ACE-consensus difference profiles are again generally similar at both sites. Below 40 km, ACE-FTS shows a consistent positive bias, relative to the consensus, of between 2 and 7% at Mauna Loa and 4 to 8% at Lauder. ACE-MAESTRO also shows a generally positive bias of between 1 and 9%, in this region, at Lauder. At Mauna Loa, ACE-MAESTRO differences with the consensus are within 5% up to 40 km, starting as a small negative bias but then tending positive. Above 40 km, both ACE instruments have an increasing positive bias, with differences between ACE-FTS and the consensus of up to 24% and for ACE-MAESTRO, up to 19%. Diurnal variation in ozone amounts becomes a factor above about 45 km, with rapid changes in ozone occurring around sunrise and sunset. The solar occultation SAGE II instrument has a small positive bias above this height, compared to the other consensus instruments, but still measures less ozone than the ACE instruments, suggesting other systematic errors are contributing to the higher positive bias in the ACE instruments. While HALOE is also a solar occultation instrument, the HALOE retrieval incorporates a photochemical model intended to account for diurnal variation of ozone along the instrument's line of sight at sunrise and sunset.

2571

7 Summary – discussion

Here we summarize and discuss the VMR profile and partial column comparison results described in the previous sections. The relative differences from the vertical profile comparisons are presented in Figs. 46 and 47 for ACE-FTS and ACE-MAESTRO, respectively. In these plots, the vertical range has been limited to 60 km except for the comparisons with the Eureka DIAL, where the plotting limit was set to 38 km because of the large oscillations noted above this altitude. Only statistical comparisons are included in these summary plots, hence the comparisons with individual FIRS-2, SAOZ and SPIRALE measurements are not included.

7.1 ACE-FTS

The VMR comparisons for ACE-FTS show remarkably consistent results, with very good agreement in the stratosphere between ∼16 km and 44 km (Fig. 46). In this vertical range, ACE-FTS reports on average about +5% more ozone than the comparison instruments. The spread of the relative differences is on the order of ±5% around this typical value. In this altitude range, two outliers for which much larger relative differences were found can be noted. In one case the differences are larger and positive, while in the other case the percent values are large but negative. The former profile is the result of the comparison with Odin/SMR, for which the ACE-FTS VMR is consistently 10–20% larger than that of SMR in the stratosphere, and the latter was obtained when comparing ACE-FTS with the Eureka DIAL, which yields large negative differences of about −10%. The low bias of SMR ozone was noted in the validation study of Jones et al. (2007). The reason for the significant negative differences between ACE-FTS and the Eureka DIAL is still unclear. The individual comparisons with the balloon-borne instruments (not included in the figure) show a similar agreement (within ±10%). In addition, the comparison of partial columns derived from the ACE-FTS and ground-based FTIR measurements provide an alternate test of the overall quality of the ACE-FTS retrievals in the stratosphere. The typical partial column relative differences

2572

are within ±10% and generally positive, except for Thule (−9.1%) and Jungfraujoch (mean difference of −9.9%). There is a very good global correlation (∼0.87) between the values derived from the ACE-FTS measurements and those calculated for the FTIR observations.

Below 16 km, the relative differences are more scattered. This can be explained by both geophysical and instrumental factors. The lower stratosphere is an atmospheric region with intrinsically large variability in the ozone VMR, where the observations can be contaminated by clouds or where the sensitivity of satellite sensors can decrease. Therefore, it is difficult to assess the quality of the ACE-FTS measurements at the lowest levels of the comparison.

The persistent high bias of ACE-FTS in the mesosphere (45–60 km), noted frequently in previous sections, is clearly seen in Fig. 46, with a typical value of ∼20% at an altitude of about 55 km. Similar high VMR values were already noted in the initial validation for version 1.0 of the ACE-FTS data product (e.g., Walker et al., 2005; McHugh et al., 2005). The natural diurnal cycle of ozone in the mesosphere may be a factor in explaining the discrepancies, since the nighttime VMR values can be as much as 30 to 60% higher than the daytime values in the range 48–60 km (Schneider et al., 2005). However, these large differences are observed for comparisons with different instruments operating from different platforms, in different spectral ranges and with different viewing geometries. Therefore, it is unlikely that this difference at altitudes between ∼40 and 60 km arises solely due to the ozone diurnal cycle.

Several tests were performed with the ACE-FTS retrieval scheme to evaluate potential sources for a bias. The next processing version of the ACE-FTS software features an improved instrumental line shape (ILS) for the instrument. The ILS used for ACE-FTS version 2.2 processing gave an apparent 3–5% high bias in retrievals above ∼40 km for N_2 and HCl (and presumably other molecules as well). There is also an improvement in the retrieval process for pressure and temperature developed for the next version of the ACE-FTS analysis software. Neither the new ILS nor the improvements in the pressure/temperature processing fix the systematic high bias in ACE-FTS

2573

O_3 retrievals for the altitude region 45–60 km. A more promising explanation for the high bias may be spectroscopy for the microwindows employed in the retrievals. An alternative set of microwindows was tested for this altitude region that appears to yield improved agreement with other data sets, but this issue remains under investigation.

Finally, no systematic difference has been found between the ACE-FTS SR and SS profiles for all comparisons. There is very good consistency between the comparisons for ACE-FTS SR and SS occultations, as seen in Fig. 46.

7.2 ACE-MAESTRO

The current analyses have extended the results of Kar et al. (2007) to a broader range of correlative data sets. Figure 47 shows the relative differences of all comparisons. These are separated into ACE-MAESTRO SR and ACE-MAESTRO SS events. For completeness, we have included the results of Kar et al. (2007) for POAM III and SAGE III in this plot.

The most obvious result is the bias between the MAESTRO SR and SS observations, at all altitudes between ∼25 and 55 km. The amplitude of this bias varies with altitude and with the comparison instrument. In the range 25–30 km, most of the SR retrievals show generally positive and larger differences than the SS results. Above 30–35 km and up to ∼55 km, the ACE-MAESTRO SR observations are systematically lower than the SS results for the same correlative dataset, and yield more scattered relative difference values. The SR/SS bias is largest for POAM III and SAGE III around 50 km. For these instruments, the discrepancy can reach 25–30%, with relative differences of −10% for the ACE-MAESTRO SR occultations and +20% for the ACE-MAESTRO SS occultations. It should be noted that the ACE-MAESTRO measurements are known to have a timing error of up to one second with respect to the ACE-FTS measurements. Since the ACE-MAESTRO retrievals use the tangent heights retrieved for ACE-FTS, this can lead to an offset of a few kilometers in the ACE-MAESTRO tangent heights, resulting in VMR profiles that can be significantly lower or higher than those retrieved from ACE-FTS or the comparison instrument (Manney et al., 2007b). This issue is un-

2574

der investigation and has not been resolved yet. In particular, the v1.2 ACE-MAESTRO data used in the present study have not been corrected for this timing error. While this affects both SR and SS profiles, the effect is more pronounced for the SR profiles. This might explain the fact that in general, the standard deviations of the differences for the comparisons involving the ACE-MAESTRO SR profiles are significantly larger than those obtained using the ACE-MAESTRO SS profiles. Part of the large spread in the SR differences seen in Fig. 47 might also be attributed to this.

For most instruments apart from POAM III and SAGE III, the comparisons with ACE-MAESTRO SR measurements show a relatively constant low bias, typically within ±5% over the altitude range 25–55 km. However, the spread in the difference values (of ±10% around the typical difference) is larger than for ACE-FTS. In contrast, the ACE-MAESTRO SS results are more consistent. They show very good agreement (within ±5%) from 20–40 km. The mean relative difference values increase with increasing altitude, from about –5% at 20 km to +5% at 40 km. As was found for ACE-FTS, the largest discrepancies in the altitude range ∼20–35 km are seen in the comparisons with Odin/SMR (with positive differences of +5 to +20%) and with the Eureka DIAL (with negative differences of about –18%). It is interesting to note that the SR/SS bias is not apparent in the comparisons with SMR.

In the upper stratosphere/lower mesosphere altitude range, the ACE-MAESTRO SS occultations show significantly more ozone than the comparison instrument, typically by up to +20%. This is comparable to the high altitude positive bias already noted for ACE-FTS in the mesosphere. Potential explanation for this similarity between the ACE-FTS and the ACE-MAESTRO SS results may reside in the fact that the pressure and temperature profiles used in the ACE-MAESTRO retrievals are the profiles calculated from the ACE-FTS observations. This is also under investigation but is unlikely to account fully for this bias.

Below ∼18 km and above ∼55 km, the relative differences increase in magnitude and reach large negative values. Above 55 km, the low signal-to-noise ratio in the O_3 Chappuis band affects the retrievals and may be responsible for the larger negative

2575

differences noted at these altitudes.

Finally, comparisons of partial columns with the ground-based FTIR instruments show very good agreement in the range used for calculations, with typical (mean) differences within ±9% but generally around ±1–2%, and a correlation coefficient (0.83) slightly lower than that for the ACE-FTS comparisons.

8 Conclusions

We have completed a comprehensive validation study for the ozone profiles retrieved from measurements by the Atmospheric Chemistry Experiment satellite-borne instruments, namely the ACE-FTS version 2.2 Ozone Update and the ACE-MAESTRO version 1.2 data products. These data sets have been compared with VMR profiles from eleven satellite-borne instruments as well as ozonesondes and aircraft, balloon-borne and ground-based observations, over a time period of 1.5–3 years. Moreover, partial columns derived from the ACE measurements were compared with ground-based FTIR instruments. In these analyses, efforts were made to use consistent coincidence criteria, comparison methodology and data filtering (including selection of events with simultaneous observations from ACE-FTS, ACE-MAESTRO and the comparison instrument) in order to better assess the overall quality of the ACE-FTS and ACE-MAESTRO O_3 data products. The overall results of the intercomparisons are summarized in Table 5 (partial columns comparisons with ground-based FTIR instruments) and Table 7 (profile comparisons).

The analyses show generally very good agreement and good consistency between ACE-FTS, ACE-MAESTRO and the correlative instruments. Biases were identified over particular altitude domains in both data sets. The main findings for the ACE-FTS version 2.2 Ozone Update product are that there is very good agreement with the correlative measurements in the stratosphere, with a slight positive bias of about 5% between 15 and 45 km and a larger well-characterized systematic bias above 42–45 km. The analyses are remarkably consistent for the range of data products used in

2576

the comparisons, with a few exceptions which are generally accounted for by known biases of the comparison instrument. For the ACE-MAESTRO version 1.2 data product obtained from the VIS spectrometer, there is a noticeable bias between observations performed at sunrise and at sunset. Agreement for the SS measurements is generally better (within ±5%) in the range 20–40 km than that found for the SR events (typical value is close to zero but with a large scatter of ±15%), but there is a high bias above ~45 km similar to the one noted for ACE-FTS. The SS difference profiles more closely resemble the results found for the ACE-FTS analyses. For both ACE-FTS and ACE-MAESTRO, comparisons of partial columns with ground-based FTIR instruments confirm the overall results and show comparable agreement with all stations.

Studies were done to investigate the sensitivity of the comparisons to the coincidence criteria (time difference, distance), to the observation geometry (beta angle), and to the analysis methodology (e.g., interpolation method). These have shown that the results are mostly insensitive to such parameters. Time series using measurements over one to three years did not reveal any temporal degradation of the measurement quality for either ACE instrument. The biases in the ACE-FTS and ACE-MAESTRO profiles have been identified and well-characterized. Tests with a preliminary version of the next generation ACE-FTS retrievals (version 3.0) have shown that the slight positive stratospheric bias has been removed and the large mesospheric differences have been decreased but are still present. Possible sources are being investigated at the time of writing. Additional work is ongoing to resolve the differences between the SR and SS retrievals for ACE-MAESTRO. These validated ACE ozone measurements will be a valuable dataset to continue the long-standing record of occultation measurements from space and will play a role in monitoring stratospheric ozone recovery.

2577

2578

References

Barret, B., De Mazière, M., and Demoulin, P.: Retrieval and characterization of ozone profiles from solar infrared spectra at the Jungfraujoch, J. Geophys. Res., 107, 4788–4803, doi:10.1029/2001JD001298, 2002. 2604

Barret, B., De Mazière, M., and Demoulin, P.: Correction to "Retrieval and characterization of ozone profiles from solar infrared spectra at the Jungfraujoch", J. Geophys. Res., 108(D12), 4372, doi:10.1029/2003JD003809, 2003. 2604

Barret, B., Ricaud, P., Santee, M. L., Attié, J.-L., Urban, J., Le Flochmoën, E., Berthet, G., Murtagh, D., Eriksson, P., Jones, A., de La Noë, J., Dupuy, E., Froidevaux, L., Livesey, N. J., Waters, J. W., and Filipiak, M. J.: Intercomparison of trace gases profiles from the Odin/SMR

2579

and Aura/MLS limb sounders, J. Geophys. Res., 111, D21302, doi:10.1029/2006JD007305, 2006. 2553

Bernath, P. F., McElroy, C. T., Abrams, M. C., Boone, C. D., Butler, M., Camy-Peyret, C., Carleer, M., Clerbaux, C., Coheur, P.-F., Colin, R., DeCola, P., De Mazière, M., Drummond, J. R., Dufour, D., Evans, W. F. J., Fast, H., Fussen, D., Gilbert, K., Jennings, D. E., Llewellyn, E. J., Lowe, R. P., Mahieu, E., McConnell, J. C., McHugh, M., McLeod, S. D., Michaud, R., Midwinter, C., Nassar, R., Nichitiu, F., Nowlan, C., Rinsland, C. P., Rochon, Y. J., Rowlands, N., Semeniuk, K., Simon, P., Skelton, R., Sloan, J. J., Soucy, M.-A., Strong, K., Tremblay, P., Turnbull, D., Walker, K. A., Walkty, I., Wardle, D. A., Wehrle, V., Zander, R., and Zou, J.: Atmospheric Chemistry Experiment (ACE): Mission overview, Geophys. Res. Lett., 32, L15S01, doi:10.1029/2005GL022386, 2005. 2518, 2519, 2520

Bhatt, P. P., Remsberg, E. E., Gordley, L. L., McInerney, J. M., Brackett, V. G., and Russell III, J. M.: An evaluation of the quality of Halogen Occultation Experiment ozone profiles in the lower atmosphere, J. Geophys. Res., 104(D8), 9261–9276, doi:10.1029/1999JD900058, 1999. 2532

Bird, J. C., Pal, S. R., Carswell, A. I., Donovan, D. P., Manney, G. L., Harris, J. M., and Uchino, O.: Observations of ozone structures in the Arctic polar vortex, J. Geophys. Res., 102(D9), 10 785–10 800, doi:10.1029/96JD03787, 1997. 2565

Blumenstock, T., Kopp, G., Hase, F., Hochschild, G., Mikuteit, S., Raffalski, U., and Ruhnke, R.: Observation of unusual chlorine activation by ground-based infrared and microwave spectroscopy in the late Arctic winter 2000/01, Atmos. Chem. Phys., 6, 897–905, 2006, http://www.atmos-chem-phys.net/6/897/2006/. 2603

Boone, C. D., Nassar, R., Walker, K. A., Rochon, Y., McLeod, S. D., Rinsland, C. P., and Bernath, P. F.: Retrievals for the Atmospheric Chemistry Experiment Fourier-transform spectrometer, Appl. Opt., 44(33), 7218–7231, 2005. 2520

Borchi, F., Pommereau, J.-P., Garnier, A., and Pinharanda, M.: Evaluation of SHADOZ sondes, HALOE and SAGE II ozone profiles at the tropics from SAOZ UV-Vis remote measurements onboard long duration balloons, Atmos. Chem. Phys., 5, 1381–1397, 2005, http://www.atmos-chem-phys.net/5/1381/2005/. 2531

Borchi, F. and Pommereau, J.-P.: Evaluation of ozonesondes, HALOE, SAGE II and III, Odin-OSIRIS and -SMR, and ENVISAT-GOMOS, -SCIAMACHY and -MIPAS ozone profiles in the tropics from SAOZ long duration balloon measurements in 2003 and 2004, Atmos. Chem. Phys., 7, 2671–2690, 2007,

2580

http://www.atmos-chem-phys.net/7/2671/2007/. 2558

Bovensmann, H., Burrows, J. P., Buchwitz, M., Frerick, J., Noël, S., Rozanov, V. V., Chance, K. V., and Goede, A. P. H.: SCIAMACHY: Mission objectives and measurement modes, J. Atmos. Sci., 56(2), 127–150, 1999. 2519, 2551

Bourassa, A. E., Degenstein, D. A., and Llewellyn, E. J.: SaskTran: A Spherical Geometry Radiative Transfer Code for Measurements of Limb Scattered Sunlight, J. Quant. Spectrosc. Radiat. Trans., 109(1), 52–73, 2008. 2538

Boyd, I. S., Parrish, A. D., Froidevaux, L., von Clarmann, T., Kyrölä, E., Russell III, J. M., and Zawodny, J. M.: Ground-based microwave ozone radiometer measurements compared with Aura-MLS v2.2 and other instruments at two NDACC sites, J. Geophys. Res., 112, D24S33, doi:10.1029/2007JD008720, 2007. 2554, 2568, 2570

Bracher, A., Bovensmann, H., Bramstedt, K., Burrows, J. P., von Clarmann, T., Eichmann, K.-U., Fischer, H., Funke, B., Gil-Lpez, S., Glatthor, N., Grabowski, U., Höpfner, M., Kaufmann, M., Kellmann, S., Kiefer, M., Koukouli, M. E., A. Lindenb, Lpez-Puertas, M., Mengistu Tsidu, G., Milz, M., Noel, S., Rohen, G., Rozanov, A., Rozanov, V. V., von Savigny, C., Sinnhuber, M., Skupin, J., Steck, T., Stiller, G. P., Wang, D.-Y., Weber, M. and Wuttke, M. W.: Cross comparisons of O_3 and NO_2 measured by the atmospheric ENVISAT instruments GOMOS, MIPAS, and SCIAMACHY, Adv. Space Res., 36(5), 855–867, 2005. 2545

Brewer, A. and Milford, J.: The Oxford Kew ozone sonde, Proc. Roy. Soc. London, Ser. A, 256, 470–495, 1960. 2561

Brinksma, E. J., Bracher, A., Lokelma, D. E., Segers, A. J., Boyd, I. S., Bramstedt, K., Claude, H., Godin-Beekman, S., Hansen., G., Kopp, G., Leblanc, T., McDermid, I. S., Meijer, Y. J., Nakane, H., Parrish, A., von Savigny, C., Stebel, K., Swart, D. P. J., Taha, G., and Piters, A. J. M.: Geophysical validation of SCIAMACHY Limb Ozone Profiles, Atmos. Chem. Phys., 6, 197–209, 2006,
http://www.atmos-chem-phys.net/6/197/2006/. 2551, 2552

Brühl, C., Drayson, S. R., Russell, J. M. III, Crutzen, P. J., McInerney, J. M., Purcell, P. N., Claude, H., Gernandt, H., McGee, T. J., McDermid, I. S., and Gunson, M. R.: Halogen Oc-cultation Experiment ozone channel validation, J. Geophys. Res., 101(D6), 10 217–10 240, doi:10.1029/95JD020310, 1996. 2532

Canty, T., Pickett, H. M., Salawitch, R. J., Jucks, K. W., Traub, W. A., and Waters, J. W.: Strato-spheric and mesospheric HO_x: results from Aura-MLS and FIRS-2, Geophys. Res. Lett., 33, L12802, doi:10.1029/2006GL025964, 2006. 2557

2581

Carswell, A. I., Pal, S. R., Steinbrecht, W., Whiteway, J. A., Ulitsky, A., and Wang, T. Y.: Lidar measurements of the middle atmosphere, Can. J. Phys., 69, 1076–1086, 1991. 2565

Ceccherini, S., Belotti, C., Carli, B., Raspollini, P., and Ridolfi, M.: MIPAS new measurement scenario: enhanced vertical resolution and regularization, in Proceedings of "Atmospheric Science Conference" SP-628, ESA-ESRIN Frascati, Italy, 8–12 May 2006. 2549

Ceccherini, S., Belotti, C., Carli, B., Raspollini, P., and Ridolfi, M.: Technical Note: Regular-ization performances with the error consistency method in the case of retrieved atmospheric profiles, Atmos. Chem. Phys., 7, 1435–1440, 2007,
http://www.atmos-chem-phys.net/7/1435/2007/. 2549

Chabrillat, S. and Fonteyn, D.: Modeling long-term changes of mesospheric temperature and chemistry, Adv. Space Res., 32(9), 1689–1700, 2003. 2546

Chu, W. P., McCormick, M. P., Lenoble, J., Brogniez, C., and Pruvost, P.: SAGE II inversion algorithm, J. Geophys. Res., 94(D6), 8339–8351, doi:10.1029/89JD00113, 1989. 2530

Cofield, R. E. and Stek, P. C.: Design and field-of-view calibration of 114–660 GHz optics of the Earth Observing System Microwave Limb Sounder, IEEE Trans. Geosci. Remote Sens., 44(5), 1166–1181, doi:10.1109/TGRS.2006.873234, 2006. 2553

Connor, B. J., Parrish, A., Tsou, J.-J., and McCormick, M. P.: Error analysis for the ground-based microwave ozone measurements during STOIC, J. Geophys. Res., 100(D5), 9283–9292, doi:10.1029/94JD00413, 1995. 2569, 2570

Cortesi, U., Lambert, J.-C., De Clercq, C., Bianchini, G., Blumenstock, T., Bracher, A., Castelli, E., Catoire, V., Chance, K. V., De Mazière, M., Demoulin, P., Godin-Beekmann, S., Jones, N., Jucks, K., Keim, C., Kerzenmacher, T., Kuellmann, H., Kuttippurath, J., Iarlori, M., Liu, G. Y., Liu, Y., McDermid, I. S., Meijer, Y. J., Mencaraglia, F., Mikuteit, S., Oelhaf, H., Piccolo, C., Pirre, M., Raspollini, P., Ravegnani, F., Reburn, W. J., Redaelli, G., Remedios, J. J., Sembhi, H., Smale, D., Steck, T., Taddei, A., Varotsos, C., Vigouroux, C., Waterfall, A., Wetze, G., and Wood, S.: Geophysical validation of MIPAS-ENVISAT operational ozone data, Atmos. Chem. Phys., 7, 4807–4867, 2007,
http://www.atmos-chem-phys.net/7/4807/2007/. 2521, 2522, 2547, 2548

Donovan, D. P., Bird, J. C., Whiteway, J. A., Duck, T. J., Pal, S. R., and Carswell, A. I.: Lidar observations of stratospheric ozone and aerosol above the Canadian high arctic during the 1994–95 winter, Geophys. Res. Lett., 22(24), 3489–3492, 1995. 2565

Dudhia, A., Jay, V. L., and Rodgers, C. D.: Microwindow selection for high-spectral-resolution sounders, Appl. Opt., 41, 3665–3673, 2002. 2548

2582

Fischer, H., Birk, M., Blom, C., Carli, B., Carlotti, M., von Clarmann, T., Delbouille, L., Dudhia, A., Ehhalt, D., Endemann, M., Flaud, J.-M., Gessner, R., Kleinert, A., Koopmann, R., Langen, J., López-Puertas, M., Mosner, P., Nett, H., Oelhaf, H., Perron, G., Remedios, J., Ridolfi, M., Stiller, G., and Zander, R.: MIPAS: an instrument for atmospheric and climate research, Atmos. Chem. Phys. Discuss., 7, 8795-8893, 2007, http://www.atmos-chem-phys-discuss.net/7/8795/2007/. 2547

Flittner, D. E., Bhartia, P. K., and Herman, B. M.,: O_3 profiles retrieved from limb scatter measurements: Theory, Geophys. Res. Lett., 27(17), 2601–2604, doi:10.1029/1999GL011343, 2000. 2538

Forbes, J. M., Russell, J., Miyahara, S., Zhang, X., Palo, S., Mlynczak, M., Mertens, C. J., and Hagan, M. E.: Troposphere-thermosphere tidal coupling as measured by the SABER instrument on TIMED during July–September 2002, J. Geophys. Res., 111, A10S06, doi:10.1029/2005JA011492, 2006. 2542

Fraser, A., Goutail, F., Strong, K., Bernath, P. F., Boone, C., Daffer, W. H., Drummond, J. R., Dufour, D. G., Kerzenmacher, T. E., Manney, G. L., McElroy, C. T., Midwinter, C., McLinden, C. A., Nichitiu, F., Nowlan, C. R., Walker, J., Walker, K. A., Wu, H., and Zou, J.: Intercomparison of UV-visible measurements of ozone and NO2 during the Canadian Arctic ACE validation campaigns: 2004-2006, Atmos. Chem. Phys. Discuss., 7, 16 283–16 347, 2007. 2524, 2565

Froidevaux, L., Livesey, N. J., Read, W. G., Jiang, Y. B., Jimenez, C., Filipiak, M. J., Schwartz, M. J., Santee, M. L., Pumphrey, H. C., Jiang, J. H., Wu, D. L., Manney, G. L., Drouin, B. J., Waters, J. W., Fetzer, E. J., Bernath, P. F., Boone, C. D., Walker, K. A., Jucks, K. W., Toon, G. C., Margitan, J. J., Sen, B., Webster, C. R., Christensen, L. E., Elkins, J. W., Atlas, E., Lueb, R. A., and Hendershot, R.: Early validation analyses of atmospheric profiles from EOS MLS on the Aura satellite, IEEE Trans. Geosci. Remote Sens., 44(5), 1106–1121, doi:10.1109/TGRS.2006.864366, 2006. 2521, 2553

Froidevaux, L., Jiang, Y. B., Lambert, A., Livesey, N. J., Read, W. G., Waters, J. W., Browell, E. V., Hair, J. W., Avery, M. A., McGee, T. J., Twigg, L. W., Sumnicht, G. K., Jucks, K. W., Margitan, J. J., Sen, B., Stachnik, R. A., Toon, G. C., Bernath, P. F., Boone, C. D., Walker, K. A., Filipiak, M. J., Harwood, R. S., Fuller, R. A., Manney, G. L., Schwartz, M. J., Daffer, W. H., Drouin, B. J., Cofield, R. E., Cuddy, D. T., Jarnot, R. F., Knosp, B. W., Perun, V. S., Snyder, W. V., Stek, P. C., Thurstans, R. P., and Wagner, P. A.: Validation of Aura Microwave Limb Sounder stratospheric ozone measurements, J. Geophys. Res., 112, in press, 2008. 2521, 2522, 2531, 2532, 2554

2583

Fu, D., Walker, K. A., Mittermeier, R. L., Strong, K., Sung, K., Fast, H., Bernath, P. F., Boone, C. D., Daffer, W. H., Fogal, P., Kolonjari, F., Loewen, P., Manney, G. L., and Mikhailov, O.: Simultaneous atmospheric measurements using two Fourier transform infrared spectrometers at the Polar Environment Atmospheric Research Laboratory during spring 2006, and comparisons with the ACE-FTS, Atmos. Chem. Phys. Discuss., accepted, 2008. 2524, 2565

Fussen, D., Vanhellemont, F., Dodion, J., Bingen, C., Walker, K. A., Boone, C. D., McLeod, S. D., and Bernath, P. F.: Initial intercomparison of ozone and nitrogen dioxide number density profiles retrieved by the ACE-FTS and GOMOS occultation experiments, Geophys. Res. Lett., 32, L16S02, doi:10.1029/2005GL022468, 2005. 2521, 2545

Godin, S., Carswell, A. I., Donovan, D. P., Claude, H., Steinbrecht, W., McDermid, I. S., McGee, T. J., Gross, M. R., Nakane, H., Swart, D. P. J., Bergwerff, H. B., Uchino, O., von der Gathen, P., and Neuber, R.: Ozone differential absorption lidar algorithm intercomparison, Appl. Opt., 38(30), 6225–6236, 1999. 2563

Glatthor, N., von Clarmann, T., Fischer, H., Funke, B., Gil-López, S., Grabowski, U., Höpfner, M., Kellman, S., Linden, A., López-Puertas, M., Mengistu Tsidu, G., Milz, M., Steck, T., Stiller, G. P., and Wang, D.-Y.: Retrieval of stratospheric ozone profiles from MIPAS/ENVISAT limb emission spectra: a sensitivity study, Atmos. Chem. Phys., 6, 2767–2781, 2006, http://www.atmos-chem-phys.net/6/2767/2006/. 2550

Goldman, A., Paton-Walsh, C., Bell, W., Toon, G. C., Blavier, J. F., Sen, B., Coffey, M. T., Hannigan, J. W., and Mankin, W. G.: Network for the Detection of Stratospheric Change Fourier transform infrared intercomparison at Table Mountain Facility, November 1996, J. Geophys. Res., 104(D23), 30 481–30 503, 1999. 2603

Griffith, D. W. T., Jones, N. B., and Matthews, W. A.: Interhemispheric ratio and annual cycle of carbonyl sulphide (OCS) total column from ground-based FTIR spectra, J. Geophys. Res., 103(D7), 8447–8454, 1998. 2603

Gunson, M. R., Abbas, M. M., Abrams, M. C., Allen, M., Brown, L. R., Brown, T. L., Chang, A. Y., Goldman, A., Irion, F. W., Lowes, L. L., Mahieu, E., Manney, G. L., Michelsen, H. A., Newchurch, M. J., Rinsland, C. P., Salawitch, R. J., Stiller, G. P., Toon, G. C., Yung, Y. L., and Zander, R.: The Atmospheric Trace Molecule Spectroscopy (ATMOS) experiment: Deployment on the ATLAS Space Shuttle missions, Geophys. Res. Lett., 23(17), 2333, doi:10.1029/96GL01569, 1996. 2520

Haley, C. S., Brohede, S., Sioris, C. E., Griffioen, E., Murtagh, D. P., McDade, I. C., Eriksson, P., Llewellyn, E. J., Bazureau, A., and Goutail, F.: Retrievals of stratospheric O_3 and NO_2

2584

profiles from Odin/OSIRIS limb-scattered sunlight measurements, J. Geophys. Res., 109, D16303, doi:10.1029/2004JD004588, 2004. 2558

Haley, C. S. and Brohede, S.: Status of the Odin/OSIRIS Stratospheric O_3 and NO_2 Data Products, Can. J. Phys., 85(11), 1177–1194, 2007. 2538

Hauchecorne, A., Godin, S., Marchand, M., Heese, B., and Souprayen, C.: Quantification of the transport of chemical constituents from the polar vortex to midlatitudes in the lower stratosphere using the high-resolution advection model MIMOSA and effective diffusivity, J. Geophys. Res., 107(D20), 8289, doi:10.1029/2001JD000491, 2002. 2560

Hase, F.: Inversion von Spurengasprofilen aus hochaufgelösten bodengebundenen FTIR-Messungen in absorption, Wissenschaftliche Berichte Forschungszentrum Karlsruhe, FZKA 6512, ISSN 0947-8620, 2000. 2566

Hase, F., Hannigan, J. W., Coffey, M. T., Goldman, A., Höpfner, M., Jones, N. B., Rinsland, C. P., and Wood, S. W.: Intercomparison of retrieval codes used for the analysis of high-resolution, ground-based FTIR measurements, J. Quant. Spectrosc. Radiat. Transfer, 87, 25–52, 2004. 2566

Iyer, N., Zawodny, J. M., Thomason, L. W., and Burton, S. P.: Recent advances in SAGE II data processing: Version 6.2, Eos Trans. AGU, 84(46), Fall Meet. Suppl., Abstract A42C-0771, 2003. 2531

Jarnot, R. F., Perun, V. S., and Schwartz, M. J.: Radiometric and spectral performance and calibration of the GHz bands of EOS MLS, IEEE Trans. Geosci. Remote Sens., 44(5), 1131–1143, doi:10.1109/TGRS.2005.863714, 2006. 2553

Jiang, Y. B., Froidevaux, L., Lambert, A., Livesey, N. J., Read, W. G., Waters, J. W., Bojkov, B., Leblanc, T., McDermid, I. S., Godin-Beekman, S., Filipiak, M. J., Harwood, R. S., Fuller, R. A., Daffer, W. H., Drouin, B. J., Cofield, R. E., Cuddy, D. T., Jarnot, R. F., Knosp, B. W., Perun, V. S., Schwartz, M. J., Snyder, W. V., Stek, P. C., Thurstans, R. P., Wagner, P. A., Allaart, M., Andersen, S. B., Bodeker, G., Calpini, B., Claude, H., Coetzee, G., Davies, J., DeBacker, H., Dier, H., Fujiwara, M., Johnson, B., Kelder, H., Leme, N. P., König-Langlo, G., Kyrö, E., Laneve, G., Fook, L. S., Merrill, J., Morris, G., Newchurch, M., Oltmans, S., Parrondos, M. C., Posny, F., Schmidlin, F., Skrivankova, P., Stubi, R., Tarasick, D. W., Thompson, A. M., Thouret, V., Viatte, P., Vomel, H., von der Gathen, P., Yela, M., and Zablocki, G.: Validation of the Aura Microwave Limb Sounder ozone by ozonesonde and lidar measurements, J. Geophys. Res., 112, D24S34, doi:10.1029/2007JD008776, 2007. 2554

Johnson, D. G., Jucks, K. W., Traub, W. A., and Chance, K. V.: Smithsonian stratospheric far-

2585

infrared spectrometer and data reduction system, J. Geophys. Res., 100(D2), 3091–3106, doi:10.1029/94JD02685, 1995. 2556, 2557

Jones, A., Murtagh, D., Urban, J., Eriksson, P., and Rösevall, J.: Intercomparison of Odin/SMR ozone measurements with MIPAS and balloonsonde data, Can. J. Phys., 85, 1111–1123, 2007. 2541, 2572

Jucks, K. W., Johnson, D. G., Chance, K. V., Traub, W. A., Margitan, J. M., Stachnik, R., Sasano, Y., Yokota, T., Kanzawa, H., Shibasaki, K., Suzuki, M., and Ogawa, T.: SValidation of ILAS v5.2 data with FIRS-2 balloon observations, J. Geophys. Res., 107(D24), 8207, doi:10.1029/2001JD000578, 2002. 2557

Kaiser, J. W. and Burrows, J. P.: Fast weighting functions for retrievals from limb scattering measurements, J. Quant. Spectrosc. Radiat. Transfer, 77(3), 273–283, 2003. 2551

Kaiser, J. W., von Savigny, C., Eichmann, K. U., Noël, S., Bovensmann, H., Frerick, J., and Burrows, J. P.: Satellite-pointing retrieval from atmospheric limb-scattering of solar UV-B radiation, Can. J. Phys., 82(12), 1041–1052, 2004. 2551

Kar, J., Trepte, C. R., Thomason, L. W., Zawodny, J. M., Cunnold, D. M., and Wang, H. J.: On the tropospheric measurements of ozone by the Stratospheric Aerosol and Gas Experiment II (SAGE II, version 6.1) in the tropics, Geophys. Res. Lett., 29(24), 2208, doi:10.1029/2002GL016241, 2002. 2531

Kar, J., McElroy, C. T., Drummond, J. R., Zou, J., Nichitiu, F., Walker, K. A., Randall, C. E., Nowlan, C. R., Dufour, D. G., Boone, C. D., Bernath, P. F., Trepte, C. R., Thomason, L. W., and McLinden, C.: Initial comparison of Ozone and NO_2 profiles from ACE-MAESTRO with Balloon and Satellite Data, J. Geophys. Res., 112, D16301, doi:10.1029/2006JD008242, 2007. 2522, 2523, 2535, 2537, 2562, 2574, 2607

Kasai, Y. J., Kagawa, A., Jones, N., Fujiwara, A., Seki, K., Murayama, Y., and Murcray, F.: Seasonal Variations of CO and HCN in the Troposphere Measured by Solar Absorption Spectroscopy Over Poker Flat, Alaska, Geophys. Res. Lett., 32, L19812, doi:10.1029/2005GL022826, 2005. 2603

Kazil, J., Kopp, E., Chabrillat, S., and Bishop, J.: The University of Bern Atmospheric Ion Model: Time-dependent modeling of the ions in the mesosphere and lower thermosphere, J. Geophys. Res., 108(D14), 4432, doi:10.1029/2001JD001276, 2003. 2546

Keckhut, P., McDermid, S., Swart, D., McGee, T., Godin-Beekmann, S., Adriani, A., Barnes, J., Baray, J.-L., Bencherif, H., Claude, H., di Sarra, A. G., Fiocco, G., Hansen, G., Hauchecorne, A., Leblanc, T., Lee, C. H., Pal, S., Mégie, G., Nakane, H., Neuber, R., Steinbrecht, W.,

2586

and Thayer, J.: Review of ozone and temperature lidar validations performed within the framework of the Network for the Detection of Stratospheric Change, J. Environ. Monit., 6, 721–733, doi:10.1039/b404256e, 2004. 2563

Kerzenmacher, T., Walker, K. A., Strong, K., Berman, R., Bernath, P. F., Boone, C. D., Drummond, J. R., Fast, H., Fraser, A., MacQuarrie, K., Midwinter, C., Sung, K., McElroy, C. T., Mittermeier, R. L., Walker, J., and Wu, H.: Measurements of O_3, NO_2 and Temperature during the 2004 Canadian Arctic ACE Validation Campaign, Geophys. Res. Lett., 32, L16S07, doi:10.1029/2005GL023032, 2005. 2521, 2523, 2565

Kobayashi, J. and Toyama, Y.: On various methods of measuring the vertical distribution of atmospheric ozone: (III) – Carbon iodine type chemical ozone sonde, Pap. Met. Geophys., 17, 113–126, 1966. 2561

Komhyr, W. D., Barnes, R. A., Brothers, G. B., Lathrop, J. A., and Opperman, D. P.: Electrochemical concentration cell ozonesonde performance evaluation during STOIC 1989, J. Geophys. Res., 100(D5), 9231–9244, doi:10.1029/94JD02175, 1995. 2561

Kouker, W., Offermann, D., Küll, V., Reddmann, T., Ruhnke, R., and Franzen, A.: Streamers observed by the CRISTA experiment and simulated in the KASIMA model, J. Geophys. Res., 104(D13), 16 405–16 418, doi:10.1029/1999JD900177, 1999. 2550

Kuttippurath, J., Bremer, H., Burrows, J., Kleinböhl, A., Küllmann, H., Künzi, K., Notholt, J., Sinnhuber, M., von Savigny, C., Lautié, N., Murtagh, D., Urban, J., Milz, M., Stiller, G., Petelina, S., de La Noë, J., Le Flochmoën, E., and Ricaud, P.: Intercomparison of ozone profile measurements from ASUR, SCIAMACHY, MIPAS, OSIRIS, and SMR, J. Geophys. Res., 112, D09311, doi:10.1029/2006JD007830, 2007. 2555

Kyrölä, E., Tamminen, J., Leppelmeier, G. W., Sofieva, V., Hassinen, S., Bertaux, J.-L., Hauchecorne, A., Dalaudier, F., Cot, C., Korablev, O., Hembise, O., Barrot, G., Mangin, A., Théodore, B., Guirlet, M., Etanchaud, F., Snoeij, P., Koopman, R., Saavedra, L., Fraisse, R., Fussen, D., and Vanhellemont, F.: GOMOS on Envisat: An overview, Adv. Space Res., 33, 1020–1028, doi:10.1016/S0273-1177(03)00590-8, 2004. 2544

Kyrölä, E., Tamminen, J., Leppelmeier, G. W., Sofieva, V., Hassinen, S., Bertaux, J.-L., Hauchecorne, A., Dalaudier, F., Fussen, D., Vanhellemont, F., Fanton d'Andon, O., Barrot, G., Mangin, A., Théodore, B., Guirlet, M., Snoeij, P., Koopman, R., Saavedra, L., and Meijer, Y. J.: Nighttime ozone profiles in the stratosphere and mesosphere by the Global Ozone Monitoring by Occultation of Stars on Envisat, J. Geophys. Res., 111, D24306, doi:10.1029/2006JD00577193, 2006. 2545

Lamsal, L. N., Weber, M., Tellmann, S., and Burrows, J. P.: Ozone column classified climatology of ozone and temperature profiles based on ozonesonde and satellite data, J. Geophys. Res., 109, D20304, doi:10.1029/2004JD004680, 2004. 2552

Livesey, N. J., Van Snyder, W., Read, W. J., and Wagner, P. A.: Retrieval algorithms for the EOS Microwave Limb Sounder (MLS), IEEE Trans. Geosci. Remote Sens., 44(5), 1144–1155, doi:10.1109/TGRS.2006.872327, 2006. 2553

Llewellyn, E. J., Lloyd, N. D., Degenstein, D. A., Gattinger, R. L., Petelina, S. V., Bourassa, A. E., Wiensz, J. T., Ivanov, E. V., McDade, I. C., Solheim, B. H., McConnell, J. C., Haley, C. S., von Savigny, C., Sioris, C. E., McLinden, C. A., Griffioen, E., Kaminski, J., Evans, W. F. J., Puckrin, E., Strong, K., Wehrle, V., Hum, R. H., Kendall, D. J. W., Matsushita, J., Murtagh, D. P., Brohede, S., Stegman, J., Witt, G., Barnes, G., Payne, W. F., Piché, L., Smith, K., Warshaw, G., Deslauniers, D.-L., Marchand, P., Richardson, E. H., King, R. A., Wevers, I., McCreath, W., Kyrölä, E., Oikarinen, L., Leppelmeier, G. W., Auvinen, H., Mégie, G., Hauchecorne, A., Lefèvre, F., de La Nöe, J., Ricaud, P., Frisk, U., Sjoberg, F., von Scheele, F., and Nordh, L.: The OSIRIS instrument on the Odin spacecraft, Can. J. Phys., 82(6), 411–422, 2004. 2537

Lucke, R. L., Korwan, D. R., Bevilacqua, R. M., Hornstein, J. S., Shettle, E. P., Chen, D. T., Daehler, M., Lumpe, J. D., Fromm, M. D., Debrestian, D., Neff, B., Squire, M., König-Langlo, G., and Davies, J.: The Polar Ozone and Aerosol Measurement (POAM) III instrument and early validation results, J. Geophys. Res., 104(D15), 18 785–18 800, doi:10.1029/1999JD900235, 1999. 2519, 2533

Lumpe, J. D., Bevilacqua, R. M., Hoppel, K. W., and Randall, C. E.: POAM III retrieval algorithm and error analysis, J. Geophys. Res., 107(D21), 4575, doi:10.1029/2002JD002137, 2002. 2534

Lumpe, J. D., Fromm, M., Hoppel, K. W., Bevilacqua, R. M., Randall, C. E., Browell, E. V., Grant, W. B., McGee, T., Burris, J., Twigg, L., Richard, E. C., Toon, G. C., Margitan, J. J., Sen, B., Pfeilsticker, K., Boesch, H., Fitzenberger, R., Goutail, F., and Pommereau, J. P.: Comparison of POAM III ozone measurements with correlative aircraft and balloon data during SOLVE, J. Geophys. Res., 108(D5), 8316, doi:10.1029/2001JD000472, 2003. 2558

Manney, G. L., Toon, G. C., and Zawodny, J. M.: Comparison of satellite ozone observations in coincident air masses in early November 1994, J. Geophys. Res., 106(D9), 9923–9944, doi:10.1029/2000JD900826, 2001. 2530, 2532

Manney, G. L., Daffer, W. H., Strawbridge, K. B., Walker, K. A., Boone, C. D., Bernath, P. F.,

Kerzenmacher, T., Schwartz, M. J., Strong, K., Sica, R. J., Kruger, K., Pumphrey, H. C., Froidevaux, L., Lambert, A., Santee, M. L., Livesey, N. J., Remsberg, E. E., Mlynczak, M. G., and Russell III, J. M.: The high arctic in extreme winters: vortex, temperature, and MLS and ACE-FTS trace gas evolution, Atmos. Chem. Phys. Discuss., 7, 10235–10285, 2007a. 2523, 2565

Manney, G. L., Daffer, W. H., Zawodny, J. M., Bernath, P. F., Hoppel, K. W., Walker, K. A., Knosp, B. W., Boone, C. D., Remsberg, E. E., Santee, M. L., Harvey, V. L., Pawson, S., Jackson, D. R., Deaver, L., McElroy, C. T., McLinden, C. A., Drummond, J. R., Pumphrey, H. C., Lambert, A., Schwartz, M. J., Froidevaux, L., McLeod, S. D., Takacs, L. L., Suarez, M. J., Trepte, C. R., Cuddy, D. C., Livesey, N. J., Harwood, R. S., and Waters, J. W.: Solar occultation satellite data and derived meteorological products: sampling issues and comparisons with Aura MLS J. Geophys. Res., 112, D24S50, doi:10.1029/2007JD008709, 2007b. 2574

Mauldin III, L. E., Zaun, N. H., McCormick, M. P., Guy, J. H., and Vaughn, W. R.: Stratospheric Aerosol and Gas Experiment II instruments: A functional description, Opt. Eng., 24, 307–312, 1985. 2519, 2530

McElroy, C. T., Nowlan, C. R., Drummond, J. R., Bernath, P. F., Barton, D. V., Dufour, D. G., Midwinter, C., Hall, R. B., Ogyu, A., Ullberg, A., Wardle, D. I., Kar, J., Zou, J., Nichitiu, F., Boone, C. D., Walker, K. A., and Rowlands, N.: The ACE-MAESTRO instrument on SCISAT: Description, performance, and preliminary results, Appl. Opt., 46(20), 4341–4356, 2007. 2518, 2522, 2523

McElroy, C. T.: A spectroradiometer for the measurement of direct and scattered solar irradiance from on-board the NASA ER-2 high-altitude research aircraft, Geophys. Res. Lett., 22(11), 1361–1364, doi:10.1029/95GL01391, 1995a. 2522

McElroy, C. T., Midwinter, C., Barton, D. V., and Hall, R. B.: A comparison of J-values from the composition and photodissociative flux measurement with model calculations, Geophys. Res. Lett., 22(11), 1365–1368, doi:10.1029/95GL01392, 1995b. 2522

McHugh, M., Magill, B., Walker, K. A., Boone, C. D., Bernath, P. F., and Russell III, J. M.: Comparisons of atmospheric retrievals from ACE and HALOE, Geophys. Res. Lett., 32, L15S10, doi:10.1029/2005GL022403, 2005. 2521, 2573

McPeters, R. D., Janz, S. J., Hilsenrath, E., Brown, T. L., Flittner, D. E., and Heath, D. F.: The retrieval of O_3 profiles from limb scatter measurements: Results from the Shuttle Ozone Limb Sounding Experiment, Geophys. Res. Lett., 27(17), 2597–2600, doi:10.1029/1999GL011342, 2000. 2538

2589

Meijer, Y. J., Swart, D. P. J., Allaart, M., Andersen, S. B., Bodeker, G., Boyd, I., Braathen, G., Calisesi, Y., Claude, H., Dorokhov, V., von der Gathen, P., Gil, M., Godin-Beekmann, S., Goutail, F., Hansen, G., Karpetchko, A., Keckhut, P., Kelder, H. M., Koelemeijer, R., Kois, B., Koopman, R. M., Kopp, G., Lambert, J.-C., Leblanc, T., McDermid, I. S., Pal, S., Schets, H., Stubi, R., Suortti, T., Viscont G., and Yela, M.: Pole-to-pole validation of Envisat GOMOS ozone profiles using data from ground-based and balloon sonde measurements, J. Geophys. Res., 109, D23305, doi:10.1029/2004JD004834, 2004. 2545

Mertens, C. J.: Retrieval of mesospheric and lower thermospheric kinetic temperature from measurements of CO_2 15 μm Earth limb emission under non-LTE conditions, Geophys. Res. Lett., 28(7), 1391–1394, doi:10.1029/2000GL012189, 2001. 2542

Mertens, C. J., Schmidlin F. J., Goldberg R. A., Remsberg E. E., Pesnell W. D., Russell III, J. M., Mlynczak M. G., Wintersteiner P. P., Picard R. H., Winick J. R., and Gordley, L. L.: SABER observations of mesospheric temperatures and comparison with falling spheres measurements taken during the 2002 summer MaCWAVE campaign, Geophys. Res. Lett., 31, L03105, doi:10.1029/2003GL018605, 2004. 2542

Moreau, G., Robert, C., Catoire, V., Chartier, M., Camy-Peyret, C., Huret, N., Pirre, M., Pomathiod, L., and Chalumeau, G.: SPIRALE: a multispecies in situ balloon-borne instrument with six tunable diode laser spectrometers, Appl. Opt., 44(28), 5972–5989, 2005. 2559, 2560

Morris, G. A., Gleason, J. F., Russell III, J. M., Schoeberl, M. R., and McCormick, M. P.: A comparison of HALOE V19 with SAGE II V6.00 ozone observations using trajectory mapping, J. Geophys. Res., 107(D13), 4177, doi:10.1029/2001JD000847, 2002. 2530

Murtagh, D. P., Frisk, U., Merino, F., Ridal, M., Jonsson, A., Stegman, J., Witt, G., Eriksson, P., Jiménez, C., Mégie, G., de la Noë, J., Ricaud, P., Baron, P., Pardo, J. R., Hauchecorne, A., Llewellyn, E. J., Degenstein, D. A., Gattinger, R. L., Lloyd, N. D., Evans, W. F. J., McDade, I. C., Haley, C. S., Sioris, C., von Savigny, C., Solheim, B. H., McConnell, J. C., Strong, K., Richardson, E. H., Leppelmeier, G. W., Kyrölä, E., Auvinen, H., and Oikarinen, L.: An overview of the Odin atmospheric mission, Can. J. Phys., 80, 309–319, 2002. 2537

Nakajima, H., Suzuki, M., Matsuzaki, A., Ishigaki, T., Waragai, K., Mogi, Y., Kimura, N., Araki, N., Yokota, T., Kanzawa, H., Sugita, T., and Sasano, Y.: Characteristics and performance of the Improved Limb Atmospheric Spectrometer (ILAS) in orbit, J. Geophys. Res., 107(D24), 8213, doi:10.1029/2001JD001439, 2002. 2557

Nazaryan, H. and McCormick, M. P.: Comparisons of Stratospheric Aerosol and Gas Experiment (SAGE II) and Solar Backscatter Ultraviolet Instrument (SBUV/2) ozone profiles and

2590

trend estimates, J. Geophys. Res., 110, D17302, doi:10.1029/2004JD005483, 2005. 2531

Parrish, A., Connor, B. J., Chu, W. P., Tsou, J.-J., and McDermid, I. S.: Ground-based microwave monitoring of stratospheric ozone, J. Geophys. Res., 97(D2), 2541–2546, doi:10.1029/91JD02914, 1992. 2569

5 Parrish, A.: Millimeter-wave remote sensing of ozone and trace constituents in the stratosphere, Proc. IEEE, 82, 1915–1929, 1994. 2569

Paton-Walsh, C., Bell, W., Gardiner, T., Swann, N., Woods, P., Notholt, J., Schutt, H., Galle, B., Arlander, W., and Mellqvist, J.: An uncertainty budget for ground-based Fourier transform infrared column measurements of HCl, HF, N2O, and HNO3, deduced from results of side-
10 by-side instrument intercomparisons, J. Geophys. Res., 102, 867–887, 1997. 2603

Petelina, S. V., Llewellyn, E. J., Degenstein, D. A., Lloyd, N. D., Gattinger, R. L., Haley, C. S., von Savigny, C., Griffioen, E., McDade, I. C., Evans, W. F. J., Murtagh, D. P., and de La Noë, J.: Comparison of the Odin/OSIRIS stratospheric ozone profiles with coincident POAM III and ozonesonde measurements, Geophys. Res. Lett., 31, L07105, doi:10.1029/2003GL019299,
15 2004. 2538

Petelina, S. V., Llewellyn, E. J., Walker, K. A., Degenstein, D. A., Boone, C. D., Bernath, P. F., Haley, C. S., von Savigny, C., Lloyd, N. D., and Gattinger, R. L.: Validation of ACE-FTS stratospheric ozone profiles against Odin/OSIRIS measurements, Geophys. Res. Lett., 32, L15S06, doi:10.1029/2005GL022377, 2005a. 2521, 2538

20 Petelina, S. V., Degenstein, D. A., Llewellyn, E. J., Lloyd, N. D., Mertens, C. J., Mlynczak, M. G., and Russell III, J. M.: Thermal conditions for PMC existence derived from Odin/OSIRIS and TIMED/SABER data, Geophys. Res. Lett., 32, L17813, doi:10.1029/2005GL023099, 2005b. 2542

Pickett, H. M.: Microwave Limb Sounder THz module on Aura, IEEE. Trans. Geosci. Remote
25 Sens., 44(5), 1122–1130, 2006. 2553

Pommereau, J. P. and Piquard, J.: Ozone, nitrogen dioxide and aerosol vertical distributions by UV-visible solar occultation from balloons, Geophys. Res. Lett, 21(13), 1227–1230, 1994. 2558

Pougatchev, N. S. and Rinsland, C. P.: Spectroscopic study of the seasonal variation of carbon
30 monoxide vertical distribution above Kitt Peak, J. Geophys. Res., 100, 1409–1416, 1995. 2566

Pougatchev, N. S., Connor, B. J., and Rinsland, C. P.: Infrared measurements of the ozone vertical distribution above Kitt Peak, J. Geophys. Res., 100, 16 689–16 697, 1995. 2566

2591

Randall, C. E., Rusch, D. W., Bevilacqua, R. M., Hoppel, K. W., Lumpe, J. D., Shettle, E., Thompson, E., Deaver, L., Zawodny, J., Kyrö, E., Johnson, B., Kelder, H., Dorokhov, V. M., König-Langlo, G., and Gil, M.: Validation of POAM III ozone: comparison with ozonesonde and satellite data, J. Geophys. Res., 108(D12), 4367, doi:10.1029/2002JD002944, 2003.
5 2531, 2532, 2534

Raspollini, P., Belotti, C., Burgess, A., Carli, B., Carlotti, M., Ceccherini, S., Dinelli, B. M., Dudhia, A., Flaud, J.-M., Funke, B., Höpfner, M., López-Puertas, M., Payne, V., Piccolo, C., Remedios, J. J., Ridolfi, M., and Spang, R.: MIPAS level 2 operational analysis, Atmos. Chem. Phys., 6, 5605–5630, 2006,
10 http://www.atmos-chem-phys.net/6/5605/2006/. 2541, 2547, 2548

Reber, C. A., Trevathan, C. E., McNeal, R. J., and Luther, M. R.: The Upper Atmosphere Research Satellite (UARS) Mission, J. Geophys. Res. 98(D6), 10 643–10 647, 1993. 2532

Redelsperger, J.-L., Thorncroft, C. D., Diedhiou, A., Lebel, T., Parker, D. J., and Polcher, J.: African Monsoon Multidisciplinary Analysis: An international research project and field cam-
15 paign, Bull. Amer. Meteor. Soc., 87, 1739-1746, doi:10.1175/BAMS-87-12-1739, 2006. 2558

Ridolfi, M., Carli, B., Carlotti, M., von Clarmann, T., Dinelli, B. M., Dudhia, A., Flaud, J.-M., Höpfner, M., Morris, P. E., Raspollini, P., Stiller, G., and Wells, R. J.: Optimised forward model and retrieval scheme for MIPAS near-real-time data processing, Appl. Opt., 39(8), 1323–1340, 2000. 2547, 2548

20 Rinsland, C. P., Jones, N. B., Connor, B. J., Logan, J. A., Pougatchev, N. S., Goldman, A., Murcray, F. J., Stephen, T. M., Pine, A. S., Zander, R., Mahieu, E., and Demoulin, P.: Northern and southern hemisphere ground-based infrared spectroscopic measurements of tropospheric carbon monoxide and ethane, J. Geophys. Res., 103, 28 197–28 217, 1998. 2566

Rodgers, C. D.: Inverse Methods for Atmospheric Sounding – Theory and Practise, in: Series
25 on Atmospheric, Oceanic and Planetary Physics, World Scientific (publisher), vol. 2, 2000. 2539, 2541, 2553, 2555, 2567, 2569

Rodgers, C. D. and Connor, B. J.: Intercomparison of remote sounding instruments, J. Geophys. Res., 108(D3), 4116, doi:10.1029/2002JD002299, 2003. 2528

Roth, C. Z., Degenstein, D. A., Bourassa, A. E., and Llewellyn, E. J.: The retrieval of vertical
30 profiles of the ozone number density using Chappuis band absorption information and a multiplicative algebraic reconstruction technique, Can. J. Phys., 85(11), 1225–1243, 2007. 2538

Rothman, L. S., Jacquemart, D., Barbe, A., Benner, D. C., Birk, M., Brown, L. R., Carleer,

2592

M. R., Chackerian Jr., C., Chance, K., Coudert, L. H., Dana, V., Malathy Devi, V., Flaud, J.-M., Gamache, R. R., Goldman, A., Hartmann, J.-M., Jucks, K. W., Maki, A. G., Mandin, J.-Y., Massie, S. T., Orphal, J., Perrin, A., Rinsland, C. P., Smith, M. A. H., Tennyson, J., Tolchenov, R. N., Toth, R. A., Vander Auwera, J., Varanasi, P., and Wagner, G.: The HITRAN 2004 molecular spectroscopic database, J. Quant. Spectrosc. Radiat. Transfer, 96, 139–204, doi:10.1016/j.jqsrt.2004.10.008, 2005. 2521, 2560

Russell III, J. M., Gordley, L. L., Park, J. H., Drayson, S. R., Hesketh, W. D., Cicerone, R. J., Tuck, A. F., Frederick, J. E., Harries, J. E., and Crutzen, P. J.: The Halogen Occultation Experiment, J. Geophys. Res., 98(D6), 10 777–10 797, doi:10.1029/93JD00799, 1993. 2519, 2532

Russell III, J. M., Mlynczak, M. G., Gordley, L. L., Tansock, J., and Esplin, R.: An overview of the SABER experiment and preliminary calibration results, Proc. SPIE Int. Soc. Opt. Eng., 3756, 277–288, 1999. 2542

SAGE III ATBD Team: SAGE III Algorithm Theoretical Basis Document (ATBD) for transmission level 1b products version 2.1, NASA Langley Res. Cent. (LaRC), Hampton, Virginia, 2002a. 2519, 2535

SAGE III ATBD Team: SAGE III Algorithm Theoretical Basis Document (ATBD): Lunar and solar algorithm, NASA Langley Res. Cent. (LaRC), Hampton, Virginia, 2002b. 2536

Schneider, N., Selsis, F., Urban, J., Lezeaux, O., de La Noë, J., and Ricaud, P.: Seasonal and diurnal ozone variations: observations and modeling, J. Atmos. Chem., 50, 25–47, 2005. 2526, 2573

Schneider, M., Blumenstock, T., Chipperfield, M., Hase, F., Kouker, W., Reddmann, T., Ruhnke, R., Cuevas, E., and Fischer, H.: Subtropical trace gas profiles determined by ground-based FTIR spectroscopy at Izaña (28° N, 16° W): Five year record, error analysis, and comparison with 3D-CTMs, Atmos. Chem. Phys., 5, 153–167, 2005, http://www.atmos-chem-phys.net/5/153/2005/. 2603

Senten, C., De Mazière, M., Dils, B., Hermans, C., Kruglanski, M., Neefs, E., Scolas, F., Vandaele, A. C., Vanhaelewyn, G., Vigouroux, C., Carleer, M., Coheur, P. F., Fally, S., Barret, B., Baray, J. L., Delmas, R., Leveau, J., Metzger, J. M., Mahieu, E., Boone, C., Walker, K. A., Bernath, P. F., and Strong, K.: Technical Note: New ground-based FTIR measurements at Île de La Réunion: Observations, error analysis, and comparisons with independent data, Atmos. Chem. Phys. Discuss., 8, 827–891, 2008, http://www.atmos-chem-phys-discuss.net/8/827/2008/. 2603

2593

Schoeberl, M. R., Douglass, A. R., Hilsenrath, E., Bhartia, P. K., Beer, R., Waters, J. W., Gunson, M. R., Froidevaux, L., Gille, J. C., Barnett, J. J., Levelt, P. F., and DeCola, P.: Overview of the EOS Aura mission, IEEE Trans. Geosci. Remote Sens., 44(5), 1066–1074, 2006. 2553

Sica, R. J., Izawa, M. R. M., Walker, K. A., Boone, C. D., Petelina, S. V., Argall, P. S., Bernath, P. F., Burns, G. B., Catoire, V., Collins, R. L., Daffer, W. H., DeClercq, C., Fan, Z. Y., Firanski, B. J., French, W. J. R., Gérard, P., Gerding, M., Granville, J., Innis, J. L., Keckhut, P., Kerzenmacher, T., Klekociuk, A. R., Kyrö, E., Lambert, J.-C., Llewellyn, E. J., Manney, G. L., McDermid, I. C., Mizutani, K., Murayama, Y., Piccolo, C., Raspollini, P., Ridolfi, M., Robert, C., Steinbrecht, W., Strawbridge, K. B., Strong, K., Stübi, R., and Thurairajah, B.: Validation of the Atmospheric Chemistry Experiment (ACE) version 2.2 temperature using ground-based and space-borne measurements, Atmos. Chem. Phys., 8, 35–62, 2008, http://www.atmos-chem-phys.net/8/35/2008/. 2542, 2565

Smit, H. G. J., Sträter, W., Johnson, B. J., Oltmans, S. J., Davies, J., Tarasick, D. W., Hoegger, B., Stubi, R., Schmidlin, F. J., Northam, T., Thompson, A. M., Witte, J. C., Boyd, I. S., and Posny, F.: Assessment of the performance of ECC-ozonesondes under quasi flight conditions in the environmental simulation chamber: insights from the Jülich Ozone Sonde Intercomparison Experiment (JOSIE), J. Geophys. Res., 112, D19306, doi:10.1029/2006JD007308, 2007. 2561

Stratospheric Processes And their Role in Climate (SPARC): Assessment of trends in the vertical distribution of ozone, SPARC report No. 1, in: WMO Global Ozone Res. and Monit. Project Rep. 43, edited by: Harris, N., Hudson, R., and Phillips, C., World Meteorol. Org., Geneva, 1998. 2530, 2561

Steck, T., von Clarmann, T., Fischer, H., Funke, B., Grabowski, U., Höpfner, M., Kellmann, S., Kiefer, M., Linden, A., Stiller, G. P., Wang, D. Y., Allaart, M., Blumenstock, T., von der Gathen, P., Hansen, G., Hase, F., Hochschild, G., Kopp, G., Kyrölä, E., Oelhaf, H., Raffalski, U., Redondas Marrero, A., Remsberg, E., Russell III, J. M., Stebel, K., Steinbrecht, W., Wetzel, G., Yela, M., and Zhang, G.: Bias determination and precision validation of ozone profiles from MIPAS-Envisat retrieved with the IMK-IAA processor, Atmos. Chem. Phys., 7, 3639–3662, 2007, http://www.atmos-chem-phys.net/7/3639/2007/. 2532, 2550

Sung, K., Skelton, R., Walker, K. A., Boone, C. D., Fu, D., and Bernath, P. F.: N_2O and O_3 arctic column amounts from PARIS-IR observations: Retrievals, characterization and error

2594

analysis, J. Quant. Spectrosc. Rad. Transfer, 107, 385–406, 2007. 2523, 2565

Sussmann, R. and Borsdorff, T.: Technical note: Interference errors in infrared remote sounding of the atmosphere, Atmos. Chem. Phys., 7, 3537–3557, 2007, http://www.atmos-chem-phys.net/7/3537/2007/. 2603

Thompson, A. M., Witte, J. C., McPeters, R. D., Oltmans, S. J., Schmidlin, F. J., Logan, J. A., Fujiwara, M., Kirchhoff, V. W. J. H., Posny, F., Coetzee, G. J. R., Hoegger, B., Kawakami, S., Ogawa, T., Johnson, B. J., Vömel, H., and Labow, G.: Southern Hemisphere Additional Ozonesondes (SHADOZ) 1998-2000 tropical ozone climatology: 1. Comparison with Total Ozone Mapping Spectrometer (TOMS) and ground-based measurements, J. Geophys. Res., 108(D2), 8238, doi:10.1029/2001JD000967, 2003a. 2601

Thompson, A. M., Witte, J. C., Oltmans, S. J., Schmidlin, F. J., Logan, J. A., Fujiwara, M., Kirchhoff, V. W. J. H., Posny, F., Coetzee, G. J. R., Hoegger, B., Kawakami, S., Ogawa, T., Fortuin, J. P. F., and Kelder, H. M.: Southern Hemisphere Additional Ozonesondes (SHADOZ) 1998-2000 tropical ozone climatology: 2. Tropospheric variability and the zonal wave-one, J. Geophys. Res., 108(D2), 8241, doi:10.1029/2002JD002241, 2003b. 2601

Thompson, A. M., Witte, J. C., Smit, H. G. J., Oltmans, S. J., Johnson, B. J., Kirchhoff, V. W. J. H., and Schmidlin, F. J.: Southern Hemisphere Additional Ozonesondes (SHADOZ) 1998-2004 tropical ozone climatology: 3. Instrumentation, station-to-station variability, and evaluation with simulated flight profiles, J. Geophys. Res., 112, D03304, doi:10.1029/2005JD007042, 2007a. 2601

Thompson, A. M., Stone, J. B., Witte, J. C., Miller, S. K., Pierce, R. B., Chatfield, R. B., Oltmans, S. J., Cooper, O. R., Loucks, A. L., Taubman, B. F., Johnson, B. J., Joseph, E., Kucsera, T. L., Merrill, J. T., Morris, G. A., Hersey, S., Forbes, G., Newchurch, M. J., Schmidlin, F. J., Tarasick, D. W., Thouret, V., and Cammas, J.-P.: Intercontinental Chemical Transport Experiment Ozonesonde Network Study (IONS) 2004: 1. Summertime upper troposphere/lower stratosphere ozone over northeastern North America, J. Geophys. Res., 112, D12S12, doi:10.1029/2006JD007441, 2007b. 2601

Thompson, A. M., Stone, J. B., Witte, J. C., Miller, S. K., Oltmans, S. J., Kucsera, T. L., Ross, K. L., Pickering, K. E., Merrill, J. T., Forbes, G., Tarasick, D. W., Joseph, E., Schmidlin, F. J., McMillan, W. W., Warner, J., Hintsa, E. J., and Johnson, J. E.: Intercontinental Chemical Transport Experiment Ozonesonde Network Study (IONS) 2004: 2. Tropospheric ozone budgets and variability over northeastern North America, J. Geophys. Res., 112, D12S13, doi:10.1029/2006JD007670, 2007c. 2601

2595

Urban, J., Lautié, N., Le Flochmoën, E., Jiménez, C., Eriksson, P., de La Noë, J., Dupuy, E., Ekström, M., El Amraoui, L., Frisk, U., Murtagh, D., Olberg, M., and Ricaud, P.: Odin/SMR observations of stratospheric trace gases: Level 2 processing of ClO, N_2O, O_3, and HNO_3, J. Geophys. Res., 110, D14307, doi:10.1029/2004JD005741, 2005. 2540, 2541

Vigouroux, C., De Mazière, M., Errera, Q., Chabrillat, S., Mahieu, E., Duchatelet, P., Wood, S., Smale, D., Mikuteit, S., Blumenstock, T., Hase, F., and Jones, N.: Comparisons between ground-based FTIR and MIPAS N_2O and HNO_3 profiles before and after assimilation in BAS-COE, Atmos. Chem. Phys., 7, 377–396, 2007, http://www.atmos-chem-phys.net/7/377/2007/. 2567

von Clarmann, T., Grabowski, U., Höpfner, M., Kellmann, S., Kiefer, M., Linden, A., Mengistu Tsidu, G., Milz, M., Steck, T., Stiller, G. P., Wang, D. Y., Fischer, H., Funke, B., Gil-López, S., and López-Puertas, M.: Retrieval of temperature and tangent altitude pointing from limb emission spectra recorded from space by the Michelson Interferometer for Passive Atmospheric Sounding (MIPAS), J. Geophys. Res., 108(D23), 4736, doi:10.1029/2003JD003602, 2003. 2547, 2550

von Koenig, M., Bremer, H., Eyring, V., Goede, A., Hetzheim, H., Kleipool, Q., Kuellmann H., and Künzi, K.: An airborne submm radiometer for the observation of stratospheric trace gases: Microwave Radiometry and Remote Sensing of the Earth's Surface and Atmosphere, edited by: Pampaloni, P. and Paloscia, S., VSP Utrecht, 409–415, 2000. 2555

von Savigny, C., Haley, C. S., Sioris, C. E., McDade, I. C., Llewellyn, E. J., Degenstein, D., Evans, W. F. J., Gattinger, R. L., Griffioen, E., Kyrölä, E., Lloyd, N. D., McConnell, J. C., McLinden, C. A., Mégie, G., Murtagh, D. P., Solheim, B., and Strong, K.: Stratospheric ozone profiles retrieved from limb scattered sunlight radiance spectra measured by the OSIRIS instrument on the Odin satellite, Geophys. Res. Lett., 30(14), 1755–1758, doi:10.1029/2002GL016401, 2003. 2538

von Savigny, C., Rozanov, A., Bovensmann, H., Eichmann, K.-U., Noël, S., Rozanov, V. V., Sinnhuber, B.-M., Weber, M., and Burrows, J. P.: The ozone hole break-up in September 2002 as seen by SCIAMACHY on ENVISAT, J. Atmosph. Sci., 62(3), 721–734, 2005a. 2551

von Savigny, C., Kaiser, J. W., Bovensmann, H., Burrows, J. P., McDermid, I. S., and Leblanc, T.: Spatial and temporal characterization of SCIAMACHY limb pointing errors during the first three years of the mission, Atmos. Chem. Phys., 5, 2593–2602, 2005b. 2551

Walker, K. A., Randall, C. E., Trepte, C. R., Boone, C. D., and Bernath, P. F.: Initial validation comparisons for the Atmospheric Chemistry Experiment (ACE-FTS), Geophys. Res. Lett.,

2596

32, L16S04, doi:10.1029/2005GL022388, 2005. 2521, 2523, 2565, 2573

Wang, H. J., Cunnold, D. M., Thomason, L. W., Zawodny, J. M., and Bodeker, G. E.: Assessment of SAGE II version 6.1 ozone data quality, J. Geophys. Res., 107(D23), 4691, doi:10.1029/2002JD002418, 2002. 2531

Wang, H. J., Cunnold, D. M., Thomason, L. W., and Zawodny, J. M.: SAGE III solar ozone measurements: Initial results, Geophys. Res. Lett., 33, L03805, doi:10.1029/2005GL025099, 2006. 2536

Wang, P. H., Cunnold, D. M., Trepte, C. R., Wang, H. J., Jing, P., Brackett, V. G., Zawodny, J. M., and Bodeker, G. E.: Ozone variability in the midlatitude upper troposphere and lower stratosphere diagnosed from a monthly SAGE II climatology relative to the tropopause, J. Geophys. Res., 111, D21304, doi:10.1029/2005JD006108, 2006. 2531

Waters, J. W., Froidevaux, L., Harwood, R. S., Jarnot, R. F., Pickett, H. M., Read, W. G., Siegel, P. H., Cofield, R. E., Filipiak, M. J., Flower, D. A., Holden, J. R., Lau, G. K., Livesey, N. J., Manney, G. L., Pumphrey, H. C., Santee, M. L., Wu, D. L., Cuddy, D. T., Lay, R. R., Loo, M. S., Perun, V. S., Schwartz, M. J., Stek, P. C., Thurstans, R. P., Boyles, M. A., Chandra, K. M., Chavez, M. C., Chen, G.-S., Chudasama, B. V., Dodge, R., Fuller, R. A., Girard, M. A., Jiang, J. H., Jiang, Y., Knosp, B. W., LaBelle, R. C., Lam, J. C., Lee, K. A., Miller, D., Oswald, J. E., Patel, N. C., Pukala, D. M., Quintero, O., Scaff, D. M., Van Snyder, W., Tope, M. C., Wagner, P. A., and Walch, M. J.: The Earth Observing System Microwave Limb Sounder (EOS MLS) on the Aura satellite, IEEE Trans. Geosci. Remote Sens., 44(5), 1075–1092, doi:10.1109/TGRS.2006.873771, 2006. 2553

Wiacek, A., Taylor, J. R., Strong, K., Saari, R., Kerzenmacher, T., Jones, N. B., and Griffith, D. W. T.: Ground-Based solar absorption FTIR spectroscopy: characterization of retrievals and first results from a novel optical design instrument at a New NDACC Complementary Station, J. Atmos. Oceanic Technol., 24(3), 432–448, 2007. 2603

WMO (World Meteorological Organization): Scientific assessment of ozone depletion: 2006, WMO Global Ozone Res. and Monit. Project, Rep. 50, World Meteorol. Org., Geneva, 2007. 2518

Zander, R., Mahieu, E., Demoulin, P., Duchatelet, P., Roland, G., Servais, C., De Mazière, M., Reimann, S., and Rinsland, C. P.: Our changing atmosphere: Evidence based on long-term infrared solar observations at the Jungfraujoch since 1950, Sci. Total Environ., 391, 184–195, 2008. 2603

2597

Table 1. Summary of the coincidence characteristics for the instruments and data products used in the statistical analyses. The full comparison period, latitude range and number of coincidences are presented in columns 2–4. Columns 5–8 give the mean and 1-σ standard deviation for: great circle distance, differences in latitude, longitude and time between the ACE and correlative measurements. For instruments which have multiple retrieval codes, these are noted in parentheses in column 1.

Instrument	Period	Latitude range	Approx. # events	Distance [km]	Latitude diff. [°]	Longitude diff. [°]	Time diff. [mins]
SAGE II	2004/08/09–2005/05/06	70° S–66° N	230	449±234	−1.4±1.9	0.1±5.9	−7±31
HALOE	2004/07/05–2005/08/17	53° S–67° N	50	382±222	0.4±2.2	2.4±5.8	38±46
POAM III	2004/03/16–2005/11/30	86° S–72° N	380	395±165	0.6±3.1	0.5±5.5	16±53
SAGE III	2004/02/21–2005/10/09	65° S–83° N	650	328±177	−0.0±2.4	0.3±5.7	−10±31
OSIRIS (York)	2004/02/24–2006/08/31	80° S–86° N	910	458±231	0.2±2.9	−0.6±5.6	1±66
OSIRIS (SaskMART)	2004/03/02–2006/08/05	79° S–86° N	1220	463±229	0.1±2.9	−0.6±5.6	2±67
SMR	2004/02/21–2006/08/31	82° S–82° N	1160	438±219	0.2±2.8	−0.2±5.7	−1±68
SABER	2004/03/02–2006/07/31	85° S–85° N	6210	366±158	−0.1±2.8	−0.2±5.6	0±68
GOMOS	2004/04/06–2005/12/08	72° S–80° N	1810	317±122	−0.1±2.0	0.5±41.7	54±438
MIPAS (ESA f.r.)[a]	2004/02/21–2004/03/26	70° N–80° N	140	190±65	−0.5±1.3	−0.4±43.7	68±292
MIPAS (ESA r.r.)[b]	2005/01/27–2006/05/04	85° S–86° N	160	401±225	−0.1±2.8	0.4±5.4	96±210
MIPAS (IMK-IAA)	2004/02/21–2004/03/26	30° N–80° N	680	276±146[c] 315±159[d]	−0.2±1.7[c] −0.2±2.2[d]	1.8±9.3[c] −2.2±7.3[d]	−304±79[c] 340±98[d]
SCIAMACHY	2004/03/01–2004/12/31	80° S–80° N	730	339±120	0.6±2.3	−0.1±8.3	−84±233
Aura-MLS	2004/09/16–2007/05/23	80° S–86° N	3180	359±156	0.4±2.9	1.5±5.8	12±68
ASUR	2005/01/24–2005/02/07	60° N–70° N	40	645±225	0.3±3.6	1.7±12.0	208±113
Ozonesondes[e]	2004/02/22–2006/08/03	78° S–83° N	380	478±210	0.4±3.8	0.1±4.9	8±728
NDACC Ozonesondes + lidars[f]	2004/02/21–2006/08/19	71° S–83° N	250	305±135	1.4±1.1	7.7±6.5	302±180
Eureka DIAL	2004/02/21–2006/02/23	76° N–81° N	10	279±123	−1.7±1.1	−2.4±10.1	417±56

2598

a ESA data product for full resolution MIPAS measurements. See text for details.
b ESA data product for reduced resolution MIPAS measurements. See text for details.
c ACE vs. MIPAS daytime measurements.
d ACE vs. MIPAS nighttime measurements.
5 e Statistical analyses presented in Sect. 6.5.
f Detailed NDACC study described in Sect. 6.6.

2599

Table 2. List of the ozonesonde stations which provided data for the analyses, including location (column 2) and operating agency (column 3). The type of sensor used by each station is indicated in column 5. The source of the data used for these studies is indicated in column 6. In column 1, normal font indicates the stations included only in the statistical comparisons (Sect. 6.5); bold font shows the stations used in the studies presented in Sects. 6.5 and 6.6; emphasized font applies to stations used in the detailed NDACC study described in Sect. 6.6.

Station	Coordinates	Agency	GAW ID	Type	Source
Alert	82.5° N, 62.3° W	MSC	CAN	ECC	WOUDC/MSC[a]
Eureka	80.1° N, 86.4° W	MSC	CAN	ECC	WOUDC/MSC[a]
Ny Ålesund	78.9° N, 11.9° E	AWI	NOR	ECC	WOUDC/AWI[a]
Thule	76.5° N, 68.7° W	DMI	GRL	ECC	DMI[a]
Resolute	74.7° N, 95.0° W	MSC	CAN	ECC	WOUDC/MSC[a]
Summit	72.60° N, 38.50° W	NOAA-CMDL	GRL	ECC	NDACC
Scoresbysund	70.5° N, 22.0° W	DMI	DNK	ECC	DMI[a]
Sodankylä	67.37° N, 26.67° E	FMI	FIN	ECC	NDACC
Keflavik	63.97° N, 22.60° E	INTA	ISL	ECC	NDACC
Orlandet	63.42° N, 9.24° E	NILU	NOR	ECC	NDACC
Jokioinen	60.82° N, 23.48° E	FMI	FIN	ECC	NDACC
Churchill	58.8° N, 94.7° W	MSC	CAN	ECC	NDACC
Edmonton	53.6° N, 114.1° W	MSC	CAN	ECC	WOUDC/MSC[a]
Goose Bay	53.3° N, 60.4° E	MSC	CAN	ECC	WOUDC/MSC[a]
Legionowo	52.4° N, 21.0° E	PIMWM	POL	ECC	WOUDC
Lindenberg	52.2° N, 14.1° E	DWD	DEU	ECC	WOUDC
Vanscoy	52.1° N, 107.2° W	MSC	CAN	ECC	WOUDC
Debilt	52.1° N, 5.1° E	KNMI	NLD	ECC	WOUDC
Uccle	50.8° N, 4.4° E	RMI	BEL	ECC	WOUDC
Bratts Lake (Regina)	50.2° N, 104.7° W	MSC	CAN	ECC	IONS[b]
Prague	50.0° N, 14.5° E	CHMI	CZE	ECC	WOUDC
Kelowna	49.9° N, 119.4° W	MSC	CAN	ECC	IONS[b]
Hohenpeißenberg	47.8° N, 11.0° E	DWD	DEU	B.-M.	WOUDC
Payerne	46.5° N, 6.6° E	MeteoSwiss	CHE	ECC	WOUDC
Egbert	44.2° N, 79.8° W	MSC	CAN	ECC	IONS[b]/WOUDC
Sable Island	44.0° N, 60.0° W	MSC	CAN	ECC	IONS[b]
Haute-Provence	43.94° N, 5.71° E	CNRS	FRA	ECC	NDACC
Yarmouth	43.9° N, 66.1° W	MSC	CAN	ECC	IONS[b]

Table 2. Continued.

Station	Coordinates	Agency	GAW ID	Type	Source
Sapporo	43.1° N, 141.3° E	JMA	JPN	C.-I.	WOUDC
Madrid	40.8° N, 12.2° W	INME	ESP	ECC	WOUDC
Boulder	40.03° N, 105.25° W	NOAA-CMDL	USA	ECC	IONS[b]/NDACC
Trinidad Head	40.5° N, 3.7° W	NOAA-CMDL	USA	ECC	IONS[b]
Wallops Island	37.9° N, 75.5° W	NASA-WFF	USA	ECC	IONS[b]
Tateno (Tsukuba)	36.1° N, 140.1° E	JMA	JPN	C.-I.	WOUDC
Isfahan	32.5° N, 51.4° E	MDI	IRN	ECC	WOUDC
Honk Kong Obs.	22.3° N, 114.2° E	HKO	HKG	ECC	WOUDC
Paramaribo	5.8° N, 55.2° W	KNMI	SUR	ECC	SHADOZ[c]
Nairobi	1.3° S, 36.8° E	MeteoSwiss	KEN	ECC	SHADOZ[c]
Malindi	3° S, 40.2° E	CRPSM	KEN	ECC	SHADOZ[c]
Maxaranguape (Natal)	5.4° S, 35.4° W	INPE	BRA	ECC	SHADOZ[c]
American Samoa	14.3° S, 170.6° W	NOAA-CMDL	ASM	ECC	SHADOZ[c]
Irene	25.9° S, 28.2° E	SAWS	ZAF	ECC	SHADOZ[c]
Lauder	45.0 ° S, 169.7° E	NIWA	NZL	ECC	WOUDC/NIWA[a]
Marambio	64.2° S, 56.7° W	FMI	ATA	ECC	WOUDC
Dumont d'Urville	66.67° S, 140.01° E	CNRS	ATA	ECC	NDACC
Davis	68.6° S, 78.0° E	ABM	ATA	ECC	WOUDC/AAD[a]
Syowa	69° S, 39.6° E	JMA	JPN	C.-I.	WOUDC
Neumayer	70.7° S, 8.3° W	AWI	ATA	ECC	WOUDC/AWI[a]
McMurdo	77.85° S, 166.67° E	UWYO	ATA	ECC	NDACC
Belgrano	77.87° S, 34.63° W	INTA	ATA	ECC	NDACC

[a] Data obtained from the WOUDC database (http://www.woudc.org/). In the case of missing data (e.g., in 2006), the corresponding results were provided directly by the station P.I.
[b] Summer 2004 sounding was part of the IONS protocol optimized for Aura validation (Thompson et al., 2007b,c); data available at http://croc.gsfc.nasa.gov/intex/ions.html.
[c] Data acquired from the SHADOZ archive (http://croc.gsfc.nasa.gov/shadoz/; Thompson et al., 2003a,b, 2007a).

2601

Table 3. Name, location and operating agency for the lidar stations which provided data for the detailed NDACC analyses (Sect. 6.6).

Station	Coordinates	Agency
Eureka	80.05° N, 86.42° W	MSC
Ny-Ålesund	78.91° N, 11.88° E	AWI
Andoya	69.28° N, 16.02° E	NILU
Hohenpeißenberg	47.8° N, 11.02° E	DWD
Haute-Provence	43.94° N, 5.71° E	CNRS

Table 4. List of the FTIR stations which provided data for the analyses (Sect. 6.8). The latitude and longitude of the station are provided, together with the altitude above sea level in meters (m a.s.l.). The coincidence criteria used in this study are indicated for each station (column 5). References describing the stations, measurements and analyses are given in column 6.

Station	Location	Coordinates	Alt. [m a.s.l.]	Coincidence Criteria	Reference
Thule	Greenland	76.5° N, 68.7° W	225	±24 h, 1000 km	Goldman et al. (1999)
Kiruna	Sweden	67.8° N, 20.4° E	420	±12 h, 500 km	Blumenstock et al. (2006)
Poker Flat	Alaska	65.1° N, 147.4° W	610	±24 h, 1000 km	Kasai et al. (2005)
Harestua	Norway	60.2° N, 10.8° E	600	±24 h, 1000 km	Paton-Walsh et al. (1997)
Zugspitze	German Alps	47.4° N, 11° E	2962	±24 h, 1000 km	Sussmann and Borsdorff (2007)
Jungfraujoch	Swiss Alps	46.5° N, 8.0° E	3580	±48 h, 1000 km	Zander et al. (2007)
Toronto	Canada	43.7° N, 79.4° W	174	±48 h, 1000 km	Wiacek et al. (2007)
Izaña	Canary Islands	28.3° N, 16.5° W	2367	±24 h, 1000 km	Schneider et al. (2005)
La Réunion	Indian Ocean	20.9° S, 55.5° E	50	±24 h, ±10° lat., ±15° lon.	Senten et al. (2008)
Wollongong	Australia	34.5° S, 150.9° E	30	±24 h, 1000 km	Griffith et al. (1998)

Table 5. Results of the comparisons between ACE-FTS, ACE-MAESTRO and the ground-based FTIRs. The microwindow(s) used in the FTIR retrievals are listed in column 2. For each ACE/FTIR instrument pair, the number of comparison pairs, the vertical range used to calculate the partial columns, the corresponding degrees of freedom (DOFS) and the mean difference and 1-σ standard deviation of the mean are indicated. The retrieval code (with version number) and spectroscopic database used by each station are given in the footnotes.

FTIR Station[a]	Microwindows[b,c] [cm^{-1}]	ACE-FTS				ACE-MAESTRO			
		# of pairs	Range [km]	DOFS FTIR	Mean diff. ±Std. Dev.	# of pairs	Range [km]	DOFS FTIR	Mean diff. ±Std. Dev.
Thule	1130.0–1133.00	48	12.2–41.1	2.8	−9.1±6.4	41	12.2–41.1	2.8	−0.7±16.4
Kiruna	782.56–782.86 788.85–789.37 993.30–993.80 1000.00–1005.00[d]	27	14.3–46.7	3.3	3.2±4.7	27	13.2–46.7	3.4	−4.6±5.8
Poker Flat	3051.29–3051.90	12	10–38	3.1	−0.4±4.9	10	11–38	3.0	−8.7±4.7
Harestua	1000.00–1005.00[d]	60	15.5–46.9	2.7	2.6±9.9	52	14.7–46.9	2.9	−0.5±10.8
Zugspitze	1000.00–1005.00[d]	25	15.4–36.3	1.8	3.7±6.2	22	14.7–36.3	2.0	−2.0±6.0
Jungfraujoch	1000.00–1005.00[d]	32	15.4–42.4	~2.5	−9.9±6.5	29	14.2–42.4	~2.5	−3.7±4.7
Toronto	3045.10–3045.35	54	17.8–40.9	1.7	1.7±5.6	39	16.3–40.9	1.8	−5.2±6.0
Izaña	782.56–782.86 788.85–789.37 993.30–993.80 1000.00–1005.00[d]	10	14.3–46.7	3.9	6.3±1.9	7	14.3–46.7	3.9	1.4±3.8
La Réunion	1000.00–1005.00[d]	4	16.6–44.9	3.0	3.2±4.6	4	15.4–44.9	3.1	−1.1±6.2
Wollongong	1002.58–1003.50 1003.90–1004.40 1004.58–1005.00	7	14–42	2.8	1.2±10.3	5	12–42	3.1	−6.6±16.4

[a] Retrieval codes: PROFITT92 is used in Kiruna and Izaña. The other stations use SFIT2: Thule (v3.92b), Toronto, La Réunion and Wollongong (v3.92), Jungfraujoch (v3.91), Zugspitze (v3.90), Harestua (v3.81) and Poker Flat (v3.7).

[b] Spectroscopic linelist: HITRAN 2001 for Kiruna and Izaña. All other stations use HITRAN 2004.

[c] When multiple microwindows are listed for a station, they are fitted simultaneously during the retrieval process.

[d] The 1000.00–1005.00 cm^{-1} microwindow was selected following the studies of Barret et al. (2002, 2003), for use within the European project UFTIR: "Time series of Upper Free Troposphere observations from a European ground-based FTIR network" (http://www.nilu.no/uftir/).

Table 6. List of instruments used in comparisons with the MWRs at Mauna Loa and Lauder. The retrieval version number (column 2) and number of coincident pairs for Mauna Loa (column 3) and Lauder (column 4) are listed. All available measurements from 2004–end of 2006 were used with the exceptions noted below. Note, the MWR located at Lauder had a receiver failure at the end of 2003, with regular measurements commencing again in May 2004.

Instrument	Version	No. of pairs Mauna Loa	Lauder
ACE-FTS	2.2 Update	14	29
ACE-MAESTRO	1.2	11–12	26–29
SAGE II[a]	6.20	19–20	29
HALOE[b]	19	32	43
Aura-MLS[c]	2.2	780–781	514
GOMOS[d]	6.0f	56–87	52–64
MIPAS[e]	4.62/4.65	53–76	11
Lidar (Mauna Loa)	5.0	79–405	–
Lidar (Lauder)	7.0	–	82–142

[a] Measurements ended in August 2005.
[b] Measurements ended in November 2005.
[c] Measurements began in September 2004.
[d] Instrument offline from January–August 2005 due to an instrument anomaly.
[e] Full resolution measurements from January–March 2004 (version 4.62) and reduced resolution measurements from August–September 2004 (version 4.65) used in comparison.

2605

Table 7. Summary of results for the ACE-FTS and ACE-MAESTRO profile comparisons with correlative measurements. For cases when the SR and SS comparisons were performed separately or when only one type of occultation was used, the fractional differences are labeled this way. SR/SS is used when the comparison was not separated by occultation type. Columns 2–5: for ACE-FTS, number of comparison pairs, continuous altitude range in which the relative difference is globally within ±10%, typical (estimated by visual examination of the numerical values) and maximum percent differences in this range. Columns 6–9: same information for ACE-MAESTRO.

Instrument	ACE-FTS Number of events	Range [km]	Typical diff.	Maximum diff.	ACE-MAESTRO Number of events	Range [km]	Typical diff.	Maximum diff.
SAGE II	99 (SR)	19–42	+5%	+10%	199 (SR)	15–58	±3%	−12%
	30 (SS)	15–46	+4%	+12%	30 (SS)	15–48	±2%	+9.9%
HALOE	8 (SR)	19–40	+7%	+13%	8 (SR)	15–39	±6%	+15.4%
	41 (SS)	16–40	+6%	+12%	40 (SS)	12–40	±4%	−10.6%
POAM III[a]	131 (SR)	13–40	+5%	+12%	74 (SR)	18–44	−7%	−13.9%
	245 (SS)	16–43	+4%	+10%	104 (SS)	16–40	±4%	−13.2%
SAGE III[a]	37 (SR)	13–48	±3%	−9.2%	12 (SR)	15–53	−7%	±12.5%
	611 (SS)	10–44	+2%	+8%	695 (SS)	15–40	±4%	+10.6%
OSIRIS (York)	913 (SR/SS)	10–41	+7%	+11%	439 (SR)	16–40	+7%	+11.9%
	–	–	–	–	548 (SS)	15–42	±3%	+10.2%
OSIRIS (SaskMART)	1219 (SR/SS)	9–48	+4%	−10%	489 (SR)	16–59	±4%	±6.5%
	–	–	–	–	635 (SS)	16–49	±3%	±10.5%
SMR[b]	1161 (SR/SS)	19–42	+15%	+20%	393 (SR)	20–46	+14%	+20.5%
	–	–	–	–	705 (SS)	19–41	+11%	+20.3%
GOMOS	1812 (SR/SS)	12–42	+5%	+10.4%	–	–	–	–
MIPAS (ESA f.r.)	138 (SS)	11–41	±5%	+9.6%	–	–	–	–
MIPAS (ESA r.r.)	160 (SR/SS)	13–45	±3%	−10%	–	–	–	–
MIPAS (IMK-IAA, night)	333 (SS)	8–45	+2%	+10.7%	–	–	–	–
MIPAS (IMK-IAA, day)	348 (SS)	8–43	±4%	+8.4%	–	–	–	–
SCIAMACHY	734 (SR/SS)	17–41[c]	±4%	+16.2%	–	–	–	–
SABER	6210 (SR/SS)	18–50	±3%	+9.7%	2830 (SR)	20–52	±4%	−9.5%
	–	–	–	–	3383 (SS)	19–44	±2%	+9.6%
Aura-MLS	3178 (SR/SS)	12–43	+4%	+10.2%	1254 (SR)	19–48	+5%	+10.9%
	–	–	–	–	1910 (SS)	18–40	±5%	±10.9%
ASUR	39 (SR)	18–40	+4%	+10.9%	37 (SR)	20–46	±3%	+10.6%
Ozonesondes[d]	376 (SR/SS)	11–36	+5%	+10.4%	151 (SR)	15–33	+4%	+9.6%
	–	–	–	–	311 (SS)	15–38	±3%	−9.5%
Ozonesondes (NDACC)[e]	~200 (SR/SS)	11–30	±1%	−6.3%	~200 (SR/SS)	15–30	−5%	−9.8%
Lidars (NDACC)[e]	~50 (SR/SS)	10–42	±2%	+9.4%	~50 (SR/SS)	15–41	−5%	−9.0%
Eureka DIAL[b]	10 (SS)	14–34	−8%	−11.9%	8 (SS)	12–38	−15%	−20.0%
Lauder MWR	29 (SR/SS)	20–44	+5%	+10.8%	29 (SR/SS)	20–46	±2%	+14.0%
Mauna Loa MWR	14 (SR/SS)	20–42	+4%	+7.7%	12 (SR/SS)	20–42	±3%	−7.6%

2606

[a] For comparisons of ACE-MAESTRO with POAM III and SAGE III, results are taken from Kar et al. (2007).

[b] Comparisons with SMR: altitude range with differences of +10 to +20% for ACE-FTS (+5 to 20% for ACE-MAESTRO); Comparisons of ACE-MAESTRO with the Eureka lidar: range with abs(differences) lower than 20%.

[c] Range restricted to the levels recommended for the SCIAMACHY limb-scattering measurements.

[d] Results from the statistical analyses presented in Sect. 6.5.

[e] Results from the detailed NDACC study of Sect. 6.6.

5

2607
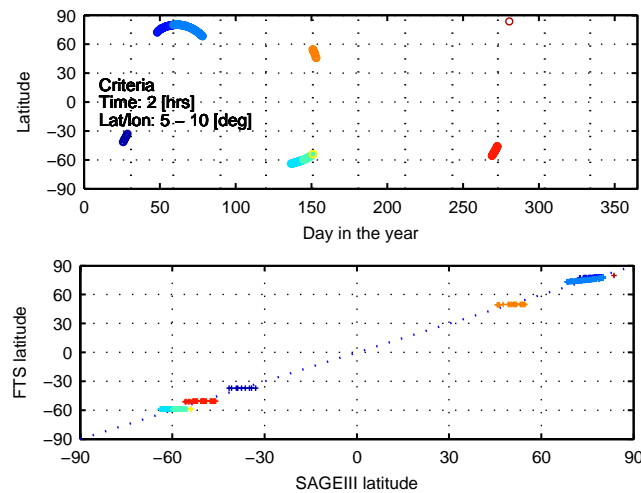
Fig. 1. Top panel: Latitude coverage of the ACE-FTS occultations coincident with SAGE III observations in 2005 (coincidence criteria: ±2 h, ±5° in latitude and ±10° in longitude). The x-axis grid lines indicate the separation by months. There are no coincidences for the tropics or subtropics. Bottom panel: Comparison of the ACE-FTS and SAGE III latitudes for the same coincidences. The dotted line indicates equal latitudes for both instruments. Symbols and colours correspond to those used in the top panel.
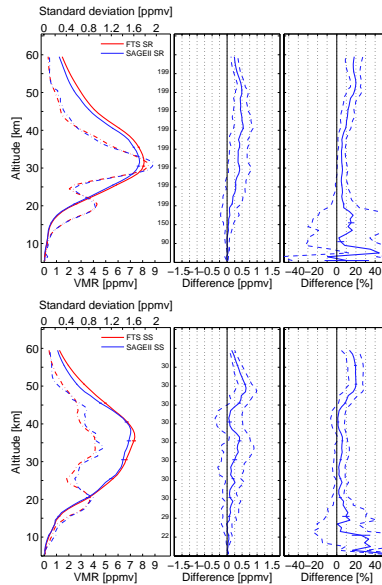
Fig. 2. Mean profiles and differences for the ACE-FTS – SAGE II coincidences. Results are shown for ACE-FTS SR (top panel) and SS (bottom panel) observations. In each panel: Left: Mean VMR profiles from ACE-FTS and SAGE II (solid lines) and associated 1-σ standard deviations (dot-dashed lines). The uncertainty in the mean (standard deviation divided by the square root of the number of pairs) is shown every 5 km as horizontal "error" bars on the VMR profiles. The number of coincident pairs used is given every 5 km. Middle: Absolute differences (ACE-FTS–SAGE II) in ppmv (solid line), with corresponding standard deviations (dashed line), and uncertainty in the mean reported as error bars. Right: Fractional differences in percent (solid line) shown as 2×(ACE-FTS–SAGE II)/(ACE-FTS+SAGE II), standard deviations (dashed line), and uncertainty in the mean (error bars).
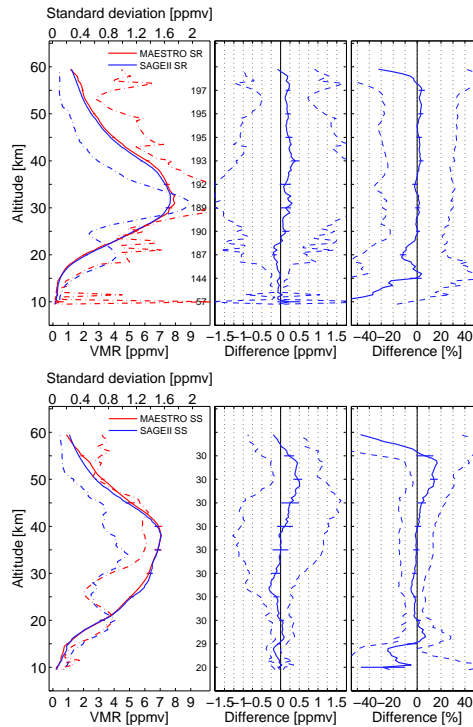
Fig. 3. Same as Fig. 2, but for the comparisons between ACE-MAESTRO and SAGE II. Top: comparison with ACE-MAESTRO SR observations; bottom: comparison with ACE-MAESTRO SS observations.
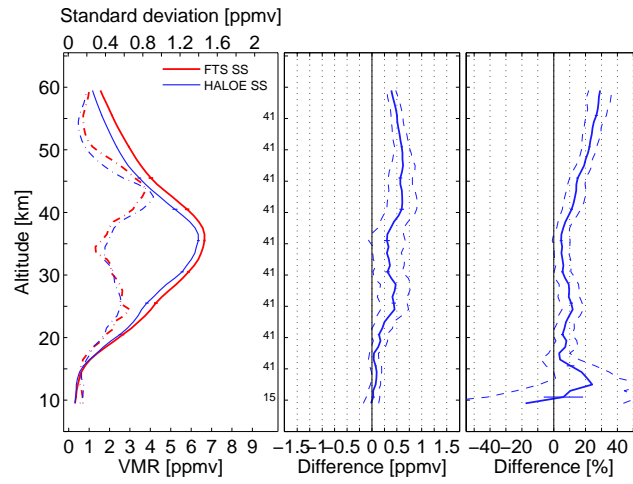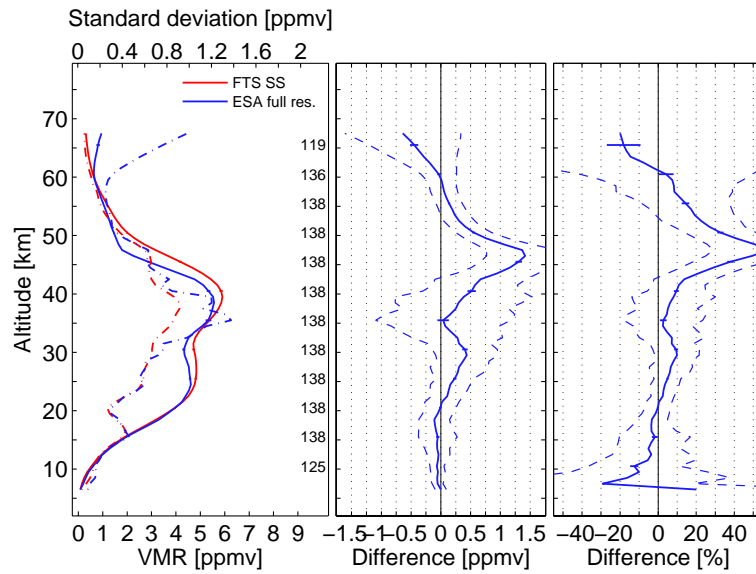
Fig. 4. Same as Fig. 2, but for the comparisons between ACE-FTS and HALOE. Because of the limited number of SR comparisons, results are shown for ACE-FTS SS observations only.

2611
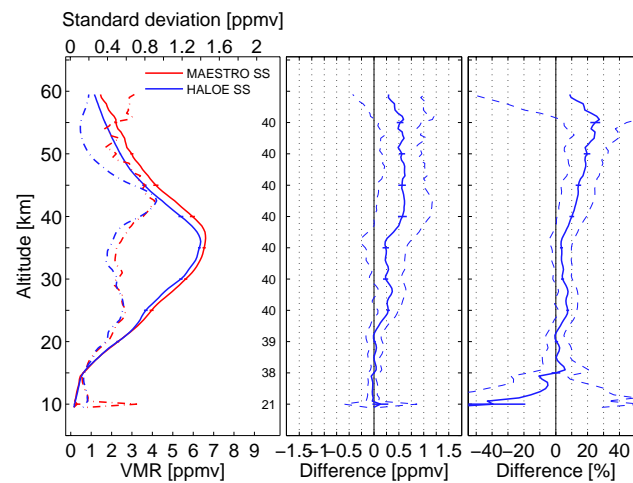
Fig. 5. Same as Fig. 2, but for the comparisons between ACE-MAESTRO and HALOE. Because of the limited number of SR comparisons, results are shown for ACE-MAESTRO SS observations only.

2612
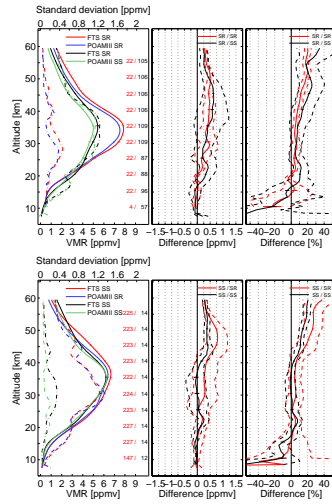
Fig. 6. Mean profiles and differences for the ACE-FTS – POAM III coincidences. Results are shown for ACE-FTS SR (top panel) and SS (bottom panel) observations. In each panel: Left: Mean VMR profiles from ACE-FTS and POAM III (solid lines) and associated 1-σ standard deviations (dot-dashed lines). POAM III SR (blue) mean profiles are paired with ACE-FTS (red) mean profiles and POAM III SS (green) are paired with ACE-FTS (black) mean profiles. The uncertainty in the mean is shown every 5 km by error bars on the VMR profiles. The number of coincident pairs used is given every 5 km. Middle: Absolute differences (ACE-FTS–POAM III) in ppmv (solid line), with corresponding standard deviations (dashed line), and uncertainty in the mean reported as error bars. The ACE-FTS – POAM III SR and ACE-FTS – POAM III SS differences are shown in red and black, respectively. Right: Fractional differences in percent (solid line) shown as 2×(ACE-FTS–POAM III)/(ACE-FTS+POAM III), standard deviations (dashed line), and uncertainty in the mean (error bars). The colour scheme used is the same as that used in the middle panel.

2613
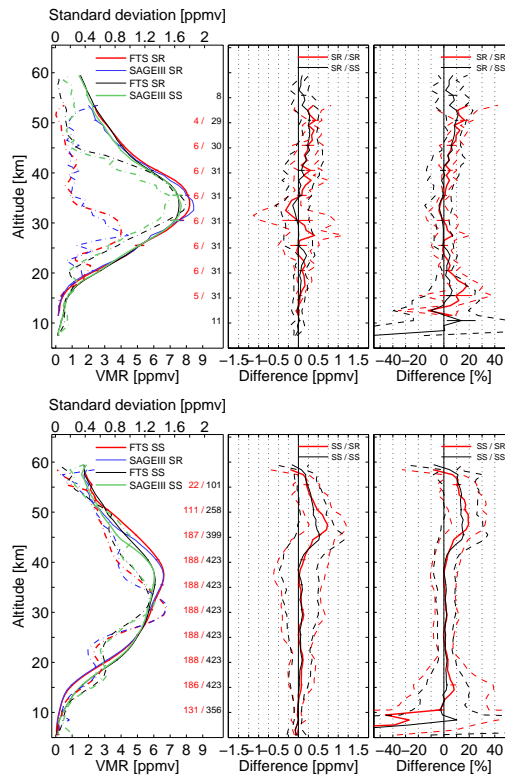
Fig. 7. Same as Fig. 6, but for the comparisons between ACE-FTS and SAGE III. Results are shown for ACE-FTS SR observations (top panel) and ACE-FTS SS observations (bottom panel).

2614
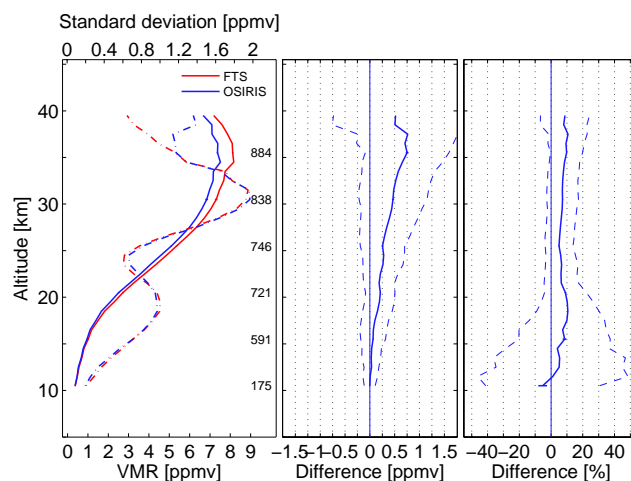
Fig. 8. Mean profiles and differences for the ACE-FTS – OSIRIS (York) coincidences. Results for ACE-FTS SR and SS observations are combined. Left: Mean VMR profiles from ACE-FTS and OSIRIS (York) (solid lines) and associated 1-σ standard deviations (dot-dashed lines). The uncertainty in the mean is shown every 5 km using error bars on the VMR profiles. The maximum number of coincident pairs is given every 5 km. Middle: Absolute differences (ACE-FTS – OSIRIS (York)) in ppmv (solid line), with corresponding standard deviations (dashed line), and uncertainty in the mean reported as error bars. Right: Fractional differences in percent (solid line) shown as 2×(ACE-FTS−OSIRIS (York))/(ACE-FTS+OSIRIS (York)), standard deviations (dashed line), and uncertainty in the mean (error bars).
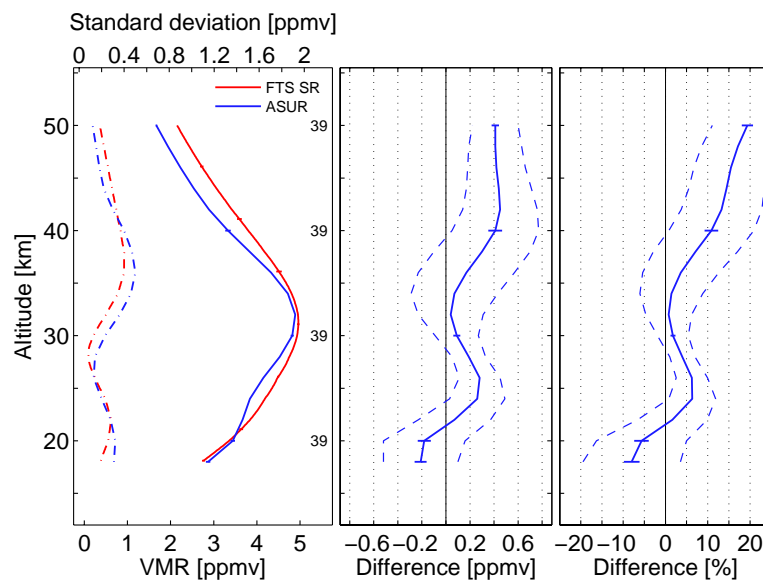
2615
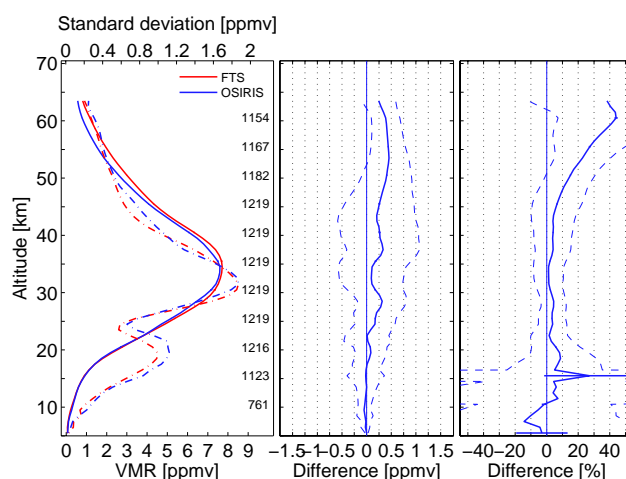
Fig. 9. Same as Fig. 8, but for the comparisons between ACE-FTS and OSIRIS (SaskMART).

2616
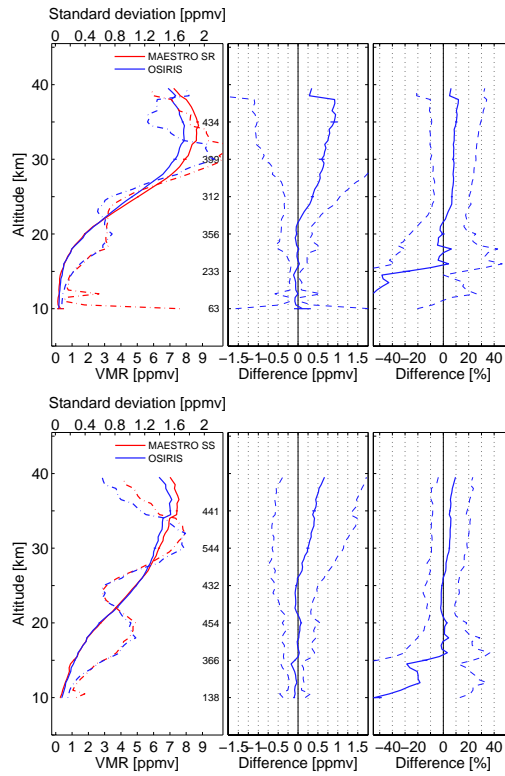
Fig. 10. Same as Fig. 2, but for the comparisons between ACE-MAESTRO and OSIRIS (York). Top: comparison with ACE-MAESTRO SR observations; bottom: comparison with ACE-MAESTRO SS observations.
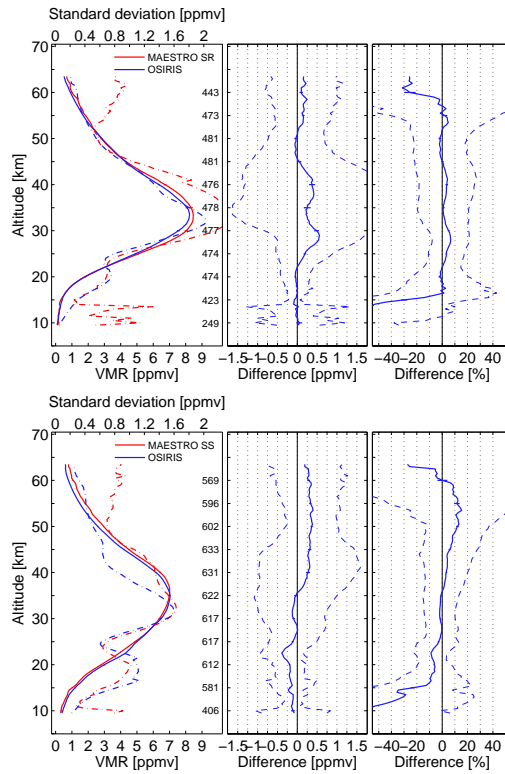
Fig. 11. Same as Fig. 2, but for the comparisons between ACE-MAESTRO and OSIRIS (SaskMART), for the ACE-MAESTRO SR (top panel) and SS (bottom panel) events.
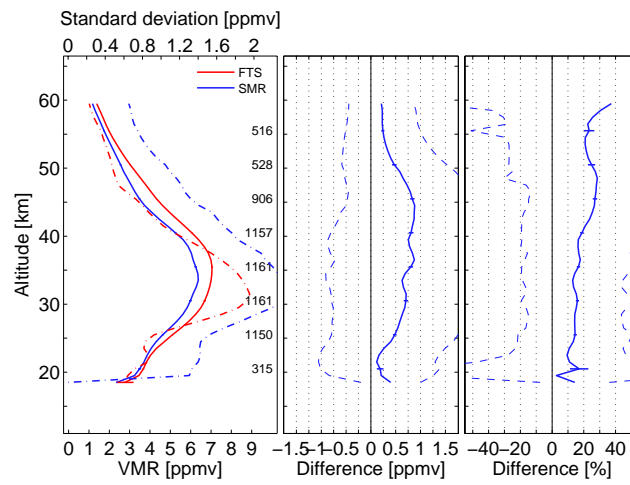
Fig. 12. Same as Fig. 8, but for the comparisons between ACE-FTS and SMR.
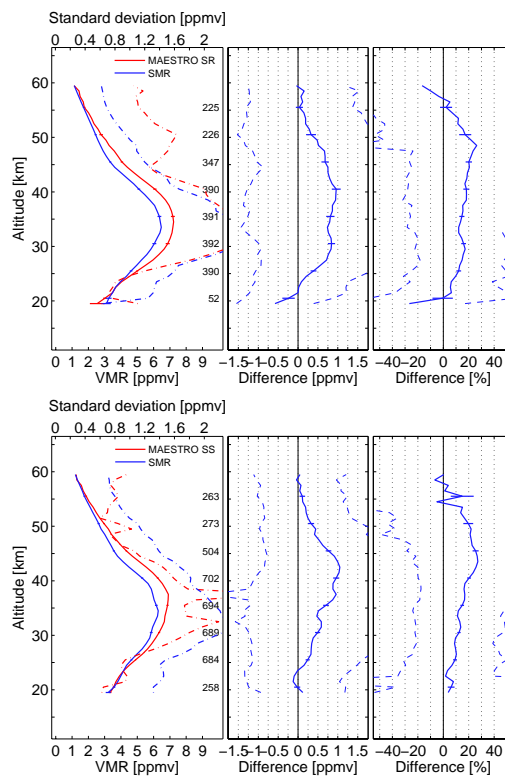
Fig. 13. Same as Fig. 2, but for the comparisons between ACE-MAESTRO and SMR. Top: comparison with ACE-MAESTRO SR observations; bottom: comparison with ACE-MAESTRO SS observations.

Fig. 14. Same as Fig. 8, but for the comparisons between ACE-FTS and SABER.

2621

Fig. 15. Same as Fig. 2, but for the comparisons between ACE-MAESTRO and SABER. Top: comparison with ACE-MAESTRO SR observations; bottom: comparison with ACE-MAESTRO SS observations.

2622
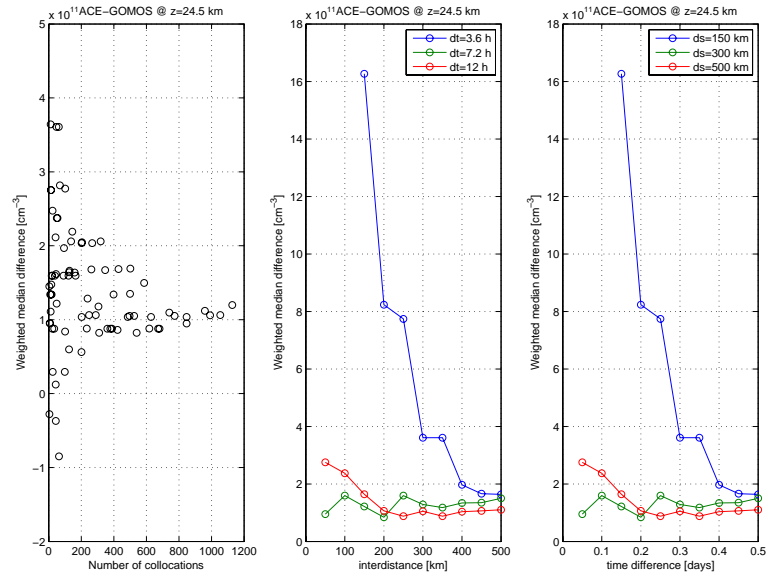
Fig. 16. Dependence of the weighted median difference, *m*, on the ACE-FTS – GOMOS co-incidence characteristics. In panels from left to right: variation of *m* relative to the number of coincident events, to the distance between the measurements and to the time difference. The altitude shown is 24.5 km.
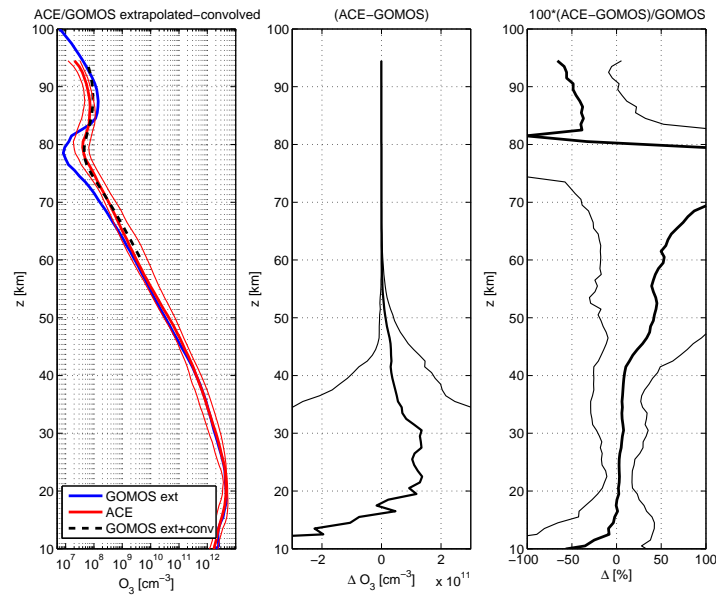
Fig. 17. Weighted median profiles and differences for the ACE-FTS and GOMOS coincidences. Left: Number density weighted median profiles (thick red) and associated 16 and 84 percentiles (thin red) for ACE-FTS. For GOMOS, the weighted median profile corrected by the SOCRATES model (thin blue line) and the corrected weighted median profile convolved with the emprical smoothing function (dashed black line) are shown. Middle: Weighted median profile (thick line) and associated 16 and 84 percentiles (thin lines) for the absolute differences between the ACE-FTS and corrected GOMOS profiles (ACE-FTS–GOMOS) in $cm^{-3} \times 10^{11}$. Right: Weighted median profile and 16 and 84 percentiles for the relative differences between ACE-FTS and the photochemically corrected GOMOS profiles expressed as (ACE-FTS–GOMOS)/GOMOS [%].

Standard deviation [ppmv]

Fig. 18. Same as Fig. 8, but for the comparisons between ACE-FTS and the MIPAS ozone product retrieved from the full resolution observations with the ESA operational processor v4.62.

2625

Standard deviation [ppmv]
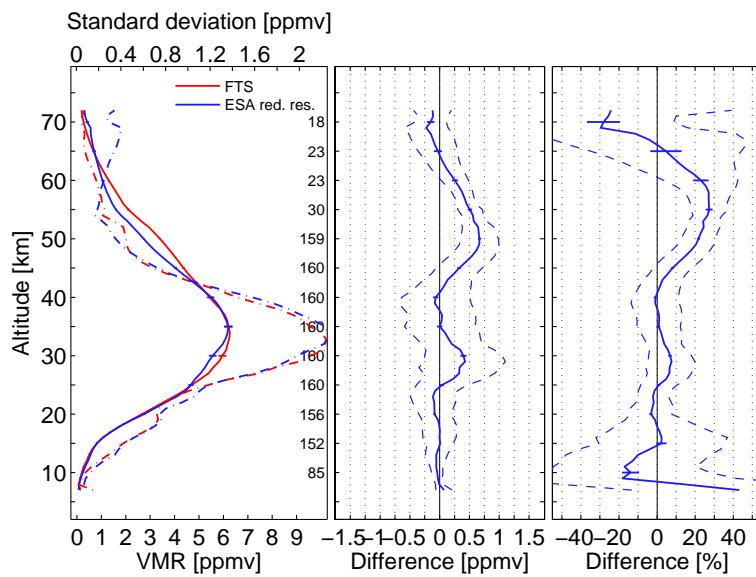
Fig. 19. Same as Fig. 8, but for the comparisons between ACE-FTS and the MIPAS ozone product retrieved from the reduced resolution observations with the ESA ML2PP/5.0 processor.
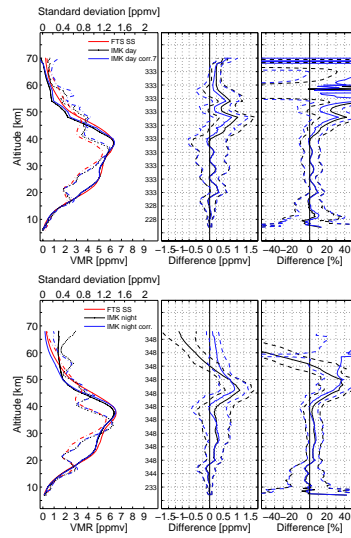
Fig. 20. Mean profiles and differences for the comparisons between ACE-FTS and the MIPAS ozone product retrieved from the full resolution observations with the IMK-IAA processor. Results are shown for MIPAS daytime (top panel) and nighttime (bottom panel) observations. In each panel: Left: Mean VMR profiles are shown for the ACE-FTS (red solid line), IMK-IAA original retrievals (black solid line) and IMK-IAA retrievals using the photochemical correction from KASIMA (blue solid line, see text). Middle: Absolute difference profiles (ACE-FTS−IMK-IAA) in ppmv for the IMK-IAA original retrievals (black) and the retrievals corrected with KASIMA (blue), with corresponding standard deviations (dashed line), and uncertainty in the mean reported as error bars. Right: Fractional differences in percent (solid line) shown as 2×(ACE-FTS−IMK-IAA)/(ACE-FTS+IMK-IAA), standard deviations (dashed line), and uncertainty in the mean (error bars) for comparisons with the IMK-IAA original retrievals (black) and the retrievals corrected with KASIMA (blue).

<div align="center">2627</div>
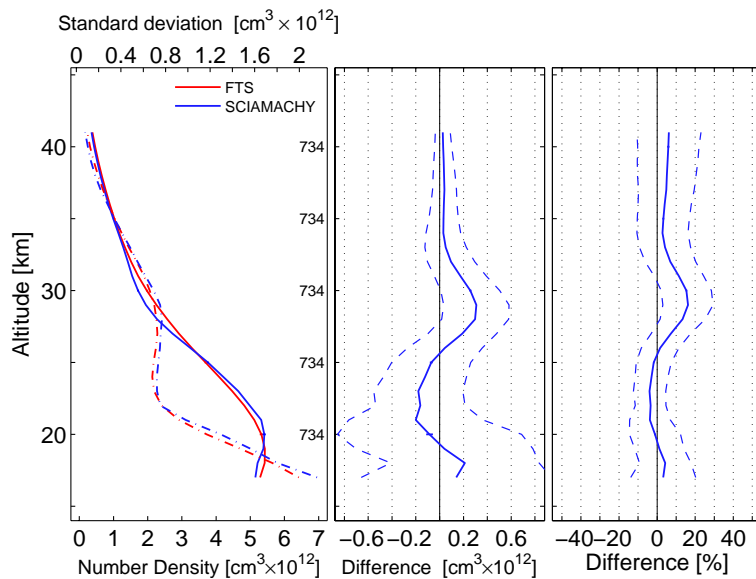
Fig. 21. Same as Fig. 8, but for the comparisons in number density between ACE-FTS and the SCIAMACHY IUP v1.63 ozone data product.

<div align="center">2628</div>
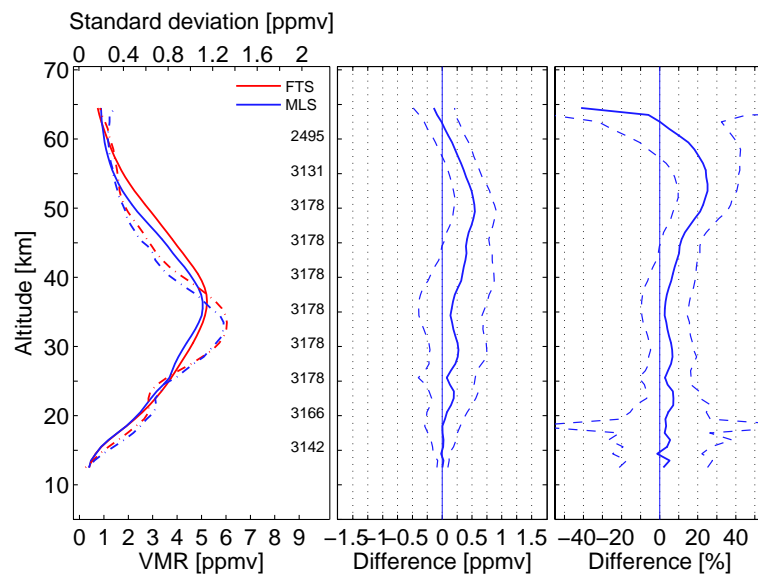
Fig. 22. Same as Fig. 8, but for the comparisons between ACE-FTS and Aura-MLS.

2629
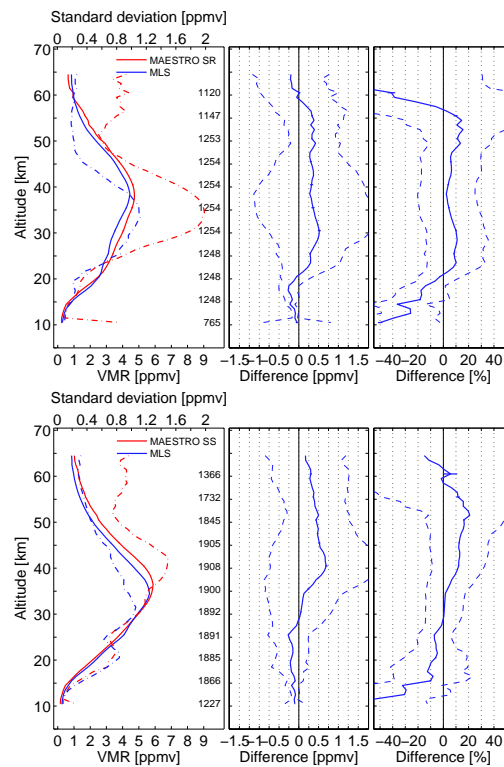
Fig. 23. Same as Fig. 2, but for the comparisons between ACE-MAESTRO and Aura-MLS. Top: comparison with ACE-MAESTRO SR observations; bottom: comparison with ACE-MAESTRO SS observations.

2630

Fig. 24. Same as Fig. 2, but for the comparisons between ACE-FTS and ASUR. Fractional differences are here expressed as (ACE-FTS−ASUR)/ACE-FTS [%].
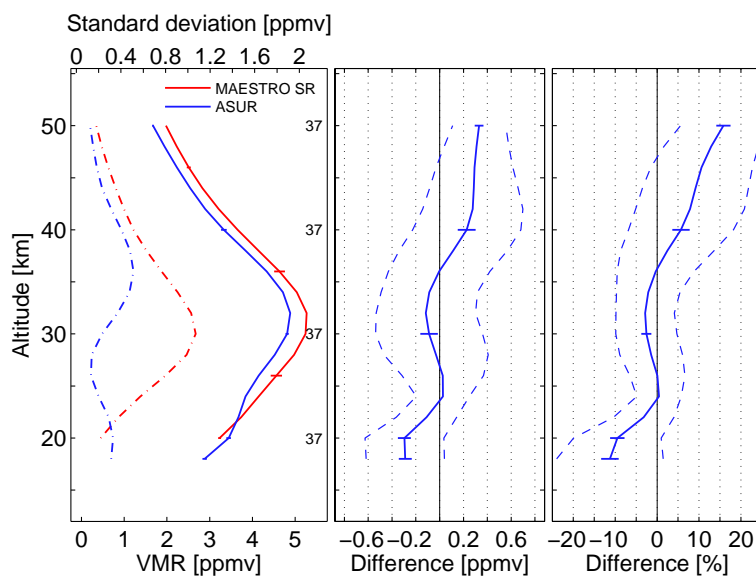
Fig. 25. Same as Fig. 2, but for the comparisons between ACE-MAESTRO and ASUR. Fractional differences are here expressed as (ACE-MAESTRO−ASUR)/ACE-MAESTRO [%].
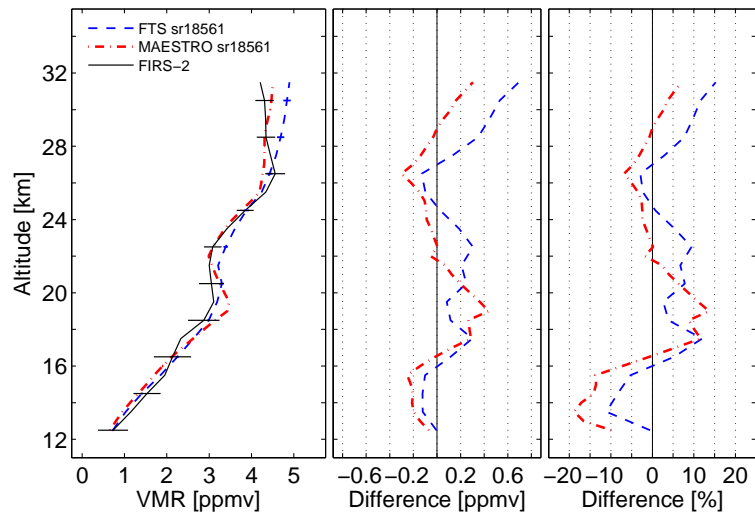
Fig. 26. Comparison of a profile from FIRS-2 on 24 January 2007 at 10:11 UT with profiles from ACE-FTS and ACE-MAESTRO SR occultation sr18561 obtained on 23 January 2007 at 08:25 UT. Left: Measured VMR profiles from FIRS-2 (solid black), ACE-FTS (dashed blue) and ACE-MAESTRO (dot-dashed red). Error bars show uncertainty estimate for FIRS-2 (see text). Middle: Absolute differences in ppmv for ACE-FTS − FIRS-2 (dashed blue) and ACE-MAESTRO − FIRS-2 (dot-dashed red). Right: Fractional differences 2×(ACE−FIRS-2)/(ACE+FIRS-2) in percent shown for comparison with ACE-FTS (dashed blue) and ACE-MAESTRO (dot-dashed red).

2633
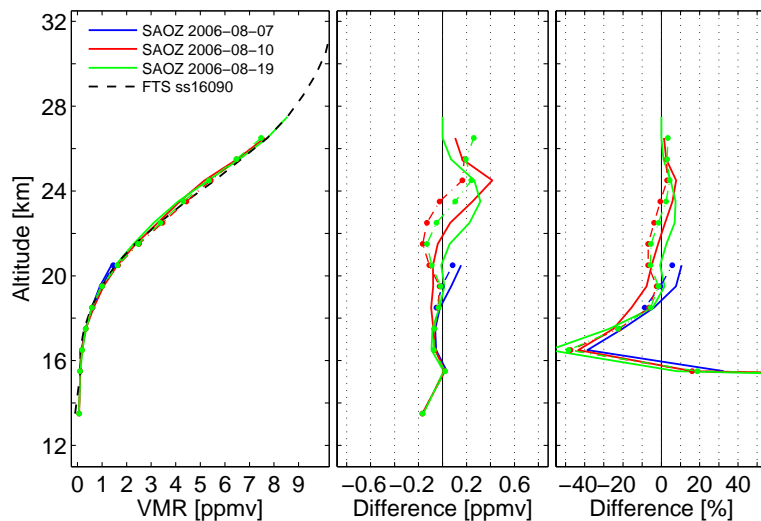
Fig. 27. Comparison of an ACE-FTS profile (ss16090, 8 August 2006 at 17:40 UT) with results from three spatially coincident SAOZ flights (7, 10 and 19 August 2006). Left: the ACE-FTS profile is shown in dashed black. SAOZ profiles obtained during ascent (solid lines) and during SS occultation (dotted curves) on 7, 10, and 19 August 2006 are shown in blue, red and green, respectively. Middle: Absolute differences for ACE-FTS − SAOZ (in ppmv) are shown using the same colour scheme as left panel. Right: Fractional differences (in percent) are given as 2×(ACE-FTS−SAOZ)/(ACE-FTS+SAOZ) using the same colour scheme as left and middle panels.

2634
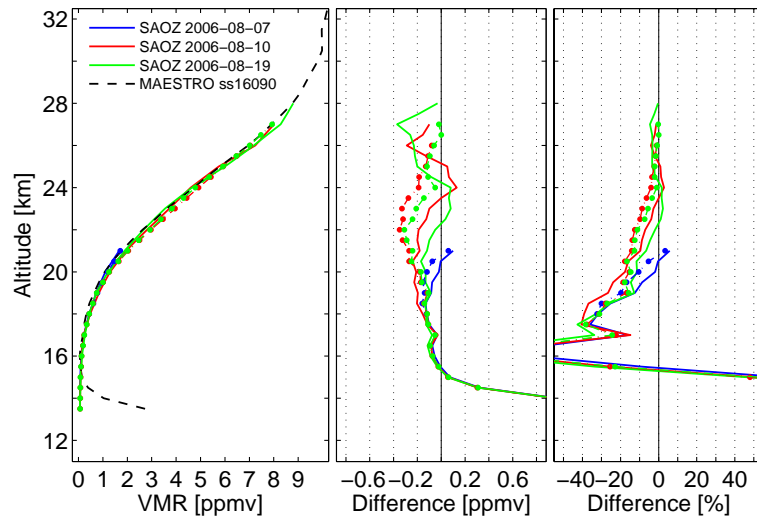
Fig. 28. Same as Fig. 27 but for ACE-MAESTRO and SAOZ.
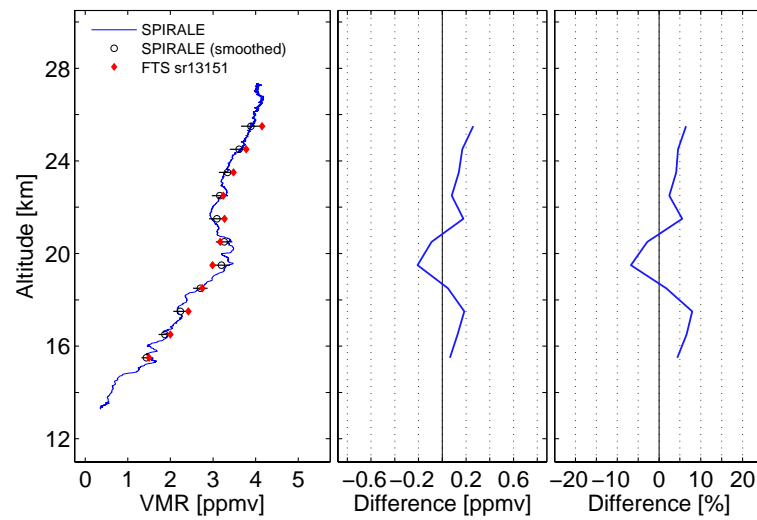
Fig. 29. SPIRALE profile measured on 20 January 2007 compared with ACE-FTS profile obtained from SR occultation sr13151 on 21 January 2007 at 08:00 UT. Left: VMR profiles from ACE-FTS (red diamonds) and SPIRALE (solid blue line) are shown along with the smoothed SPIRALE profile (black circles, see text). Uncertainties in the SPIRALE profiles are reported as error bars, however at some altitudes these are smaller than the width of the symbol. Middle: Absolute differences in ppmv, expressed as (ACE-FTS−SPIRALE(smoothed)). Right: Fractional differences in percent 2×(ACE-FTS−SPIRALE(smoothed))/(ACE-FTS+SPIRALE(smoothed)).
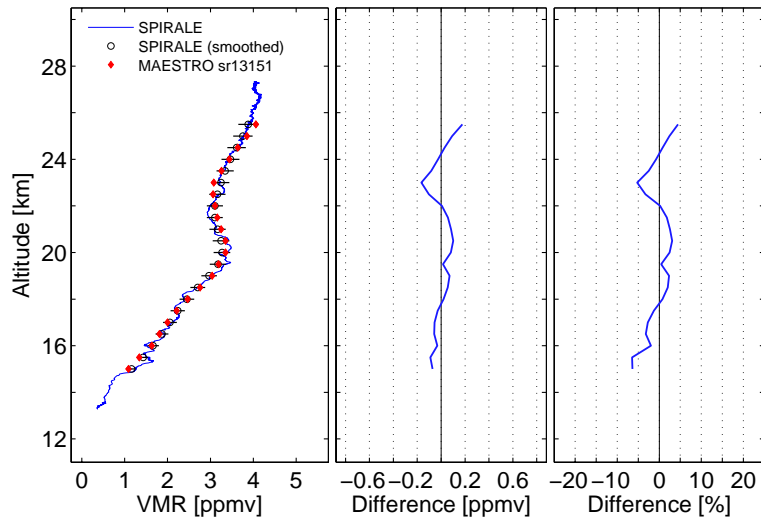
Fig. 30. Same as Fig. 29, but for comparison of ACE-MAESTRO and SPIRALE coincident profiles.
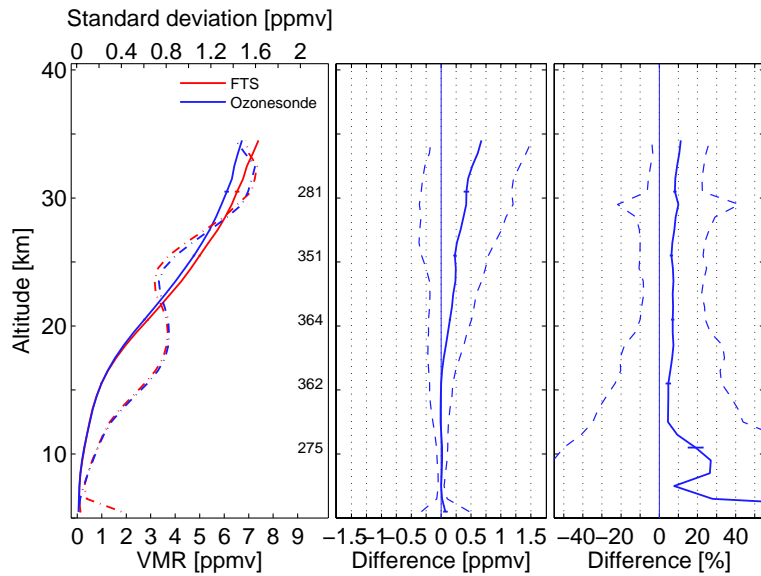
Fig. 31. Results of statistical comparisons of ACE-FTS and ozonesonde profiles. Left: Mean VMR profiles from ACE-FTS (solid red) and ozonesondes (solid black) are shown along with the 1-σ standard deviation of the mean (dot-dashed lines). The uncertainty in the mean is shown using error bars on the VMR profiles. The maximum number of coincident pairs is given every 5 km. Middle: Absolute differences (ACE-FTS−ozonesonde) in ppmv (solid line), with corresponding standard deviations (dashed line) and uncertainty in the mean shown as error bars every 5 km. Right: Fractional differences in percent (solid line) shown as (ACE-FTS−ozonesonde)/ozonesonde, standard deviations (dashed line), and uncertainty in the mean (error bars).
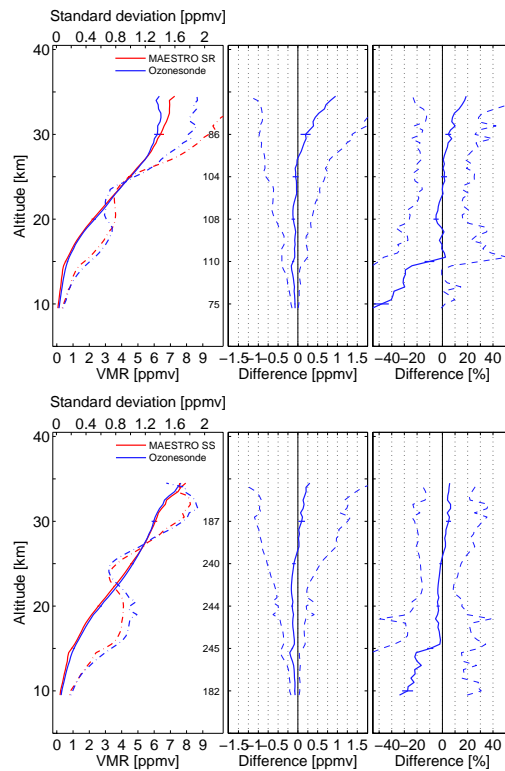
Fig. 32. Same as Fig. 2, but for statistical comparisons between ACE-MAESTRO and ozonesondes. Top (bottom) panel shows comparisons for ACE-MAESTRO SR (SS) occultations.

2639
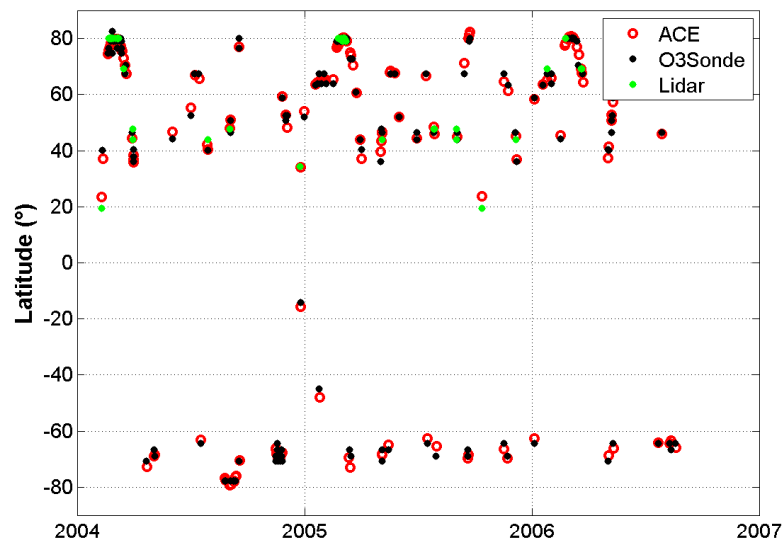
Fig. 33. Time and latitude coverage of the collocations between ACE and the NDACC ground-based ozone instruments for coincidence criteria of ±12 h and 500 km. Note, not all collocations noted here were used in calculations (see text).

2640
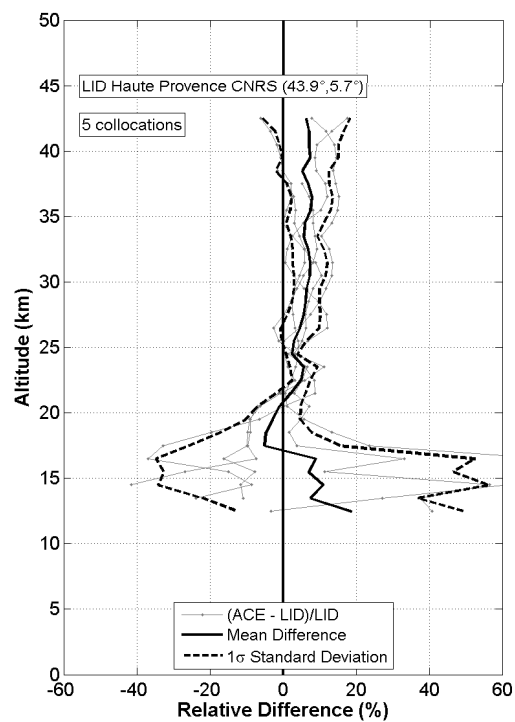
Fig. 34. Relative differences for each pair of coincident ACE-FTS and Haute-Provence lidar measurements plotted versus altitude (grey lines). Corresponding mean (solid black line) and 1-σ standard deviation (dashed line).

2641
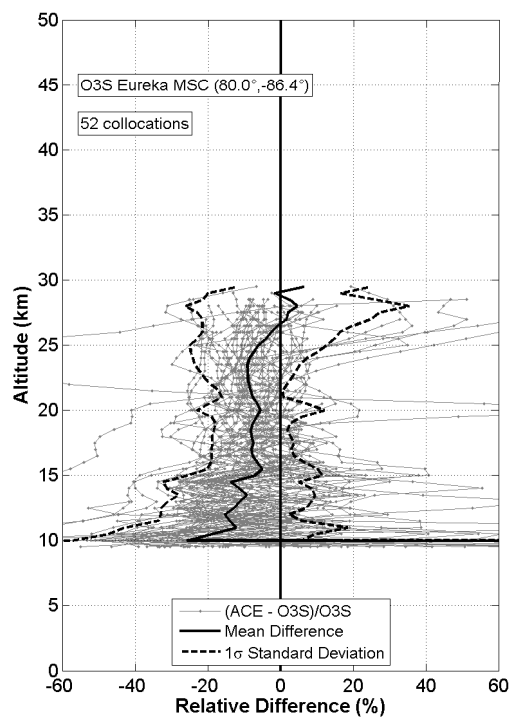
Fig. 35. Same as Fig. 34 but for comparison between ACE-MAESTRO and ozonesonde measurements at Eureka.

2642
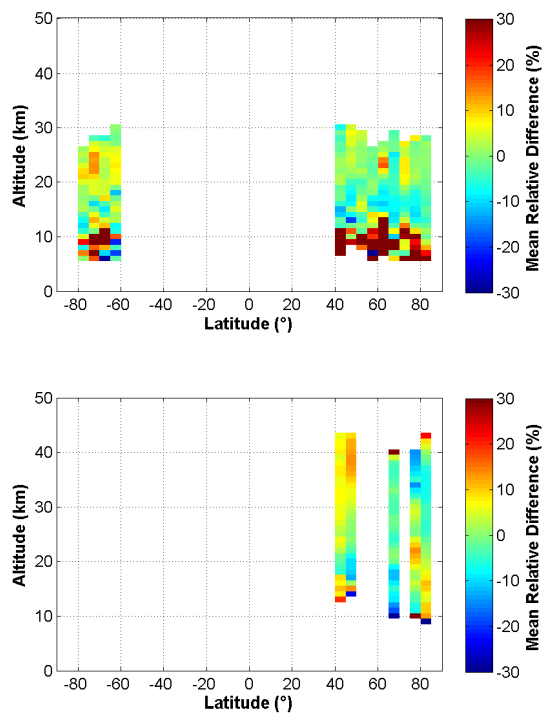
Fig. 36. Mean relative differences for comparisons between ACE-FTS and ozonesonde data, plotted versus altitude and latitude (top); same information as above for comparisons with lidar data (bottom).
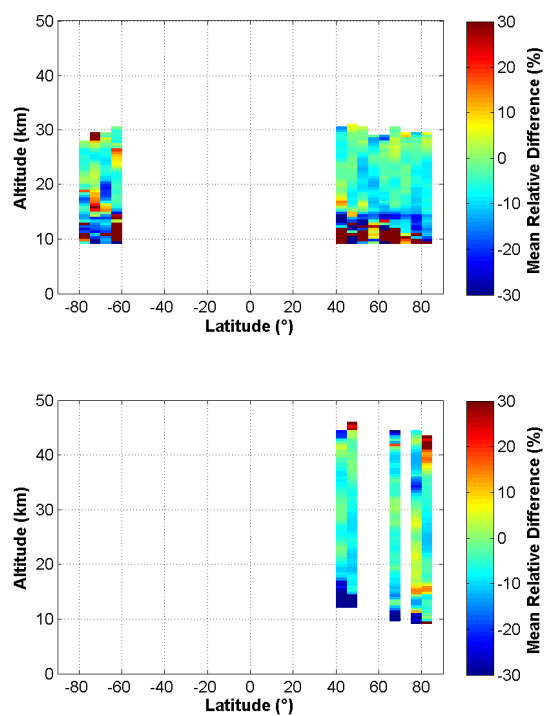
Fig. 37. Same as Fig. 36 but for differences between ACE-MAESTRO and ozonesonde (top) and lidar (bottom) data.
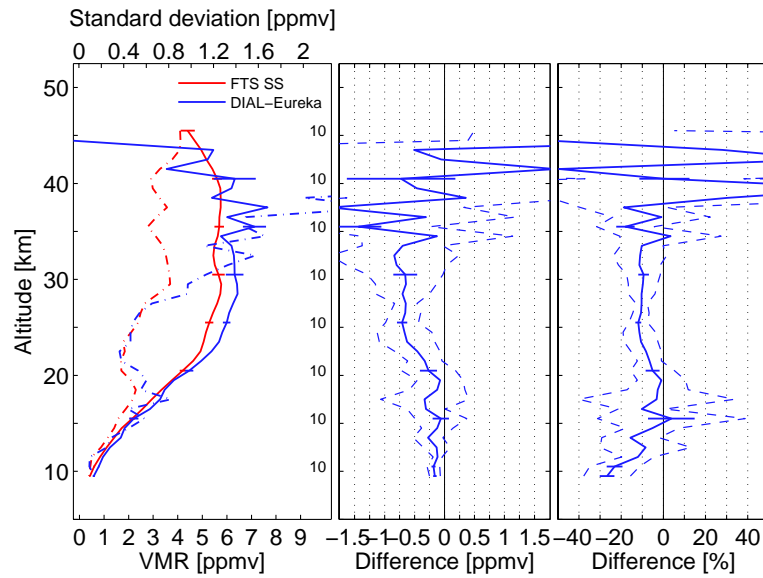
Fig. 38. Same as Fig. 2, but for the comparisons between ACE-FTS and the Eureka DIAL. All coincident ACE measurements were SS occultations.

2645
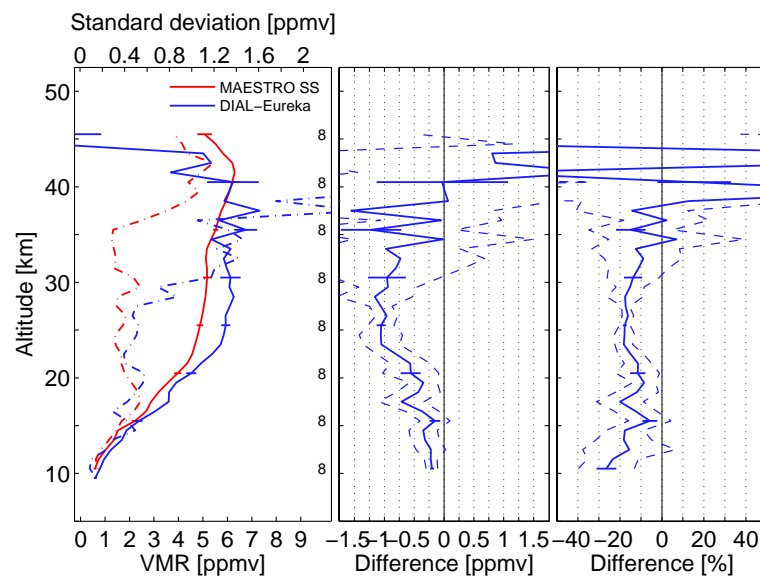
Fig. 39. Same as Fig. 2, but for the comparisons between ACE-MAESTRO and the Eureka DIAL. All coincident ACE measurements were SS occultations.
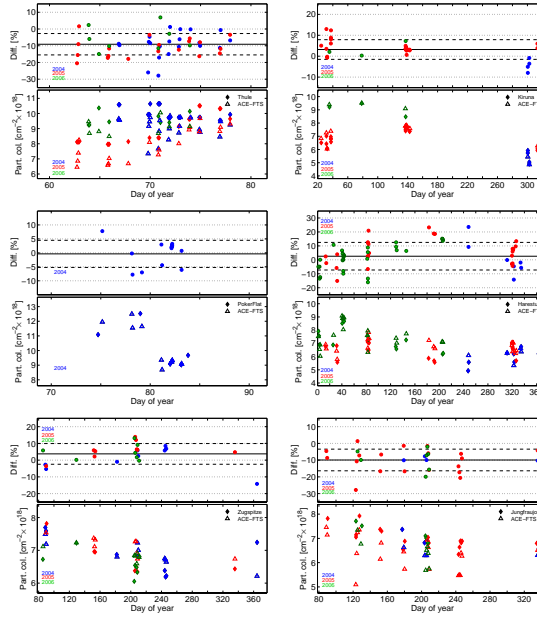
Fig. 40. Time series of ozone partial column comparisons for ACE-FTS with each ground-based FTIR instrument listed in Table 4. For each station, the bottom panel shows the partial column values for ACE-FTS (open triangles) and for the correlative FTIR measurements (filled diamonds). The top panel gives the relative differences between the partial column values for ACE-FTS and for the FTIR instruments, colour-coded according to the year of the observation: blue for 2004, red for 2005 and green for 2006. The horizontal black lines show the mean relative differences (solid) and the associated standard deviations (dashed). Note that the x- and y-axis scales used for each station are different.

2647
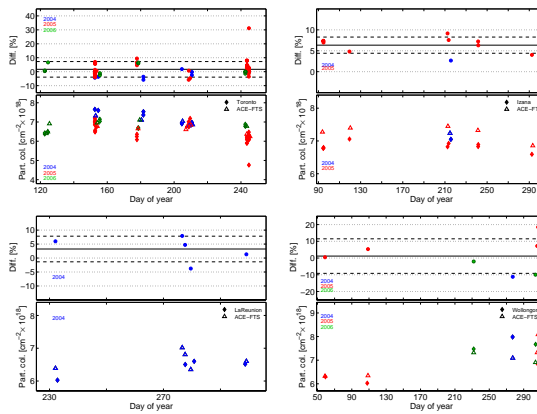
Fig. 40. Continued.

2648
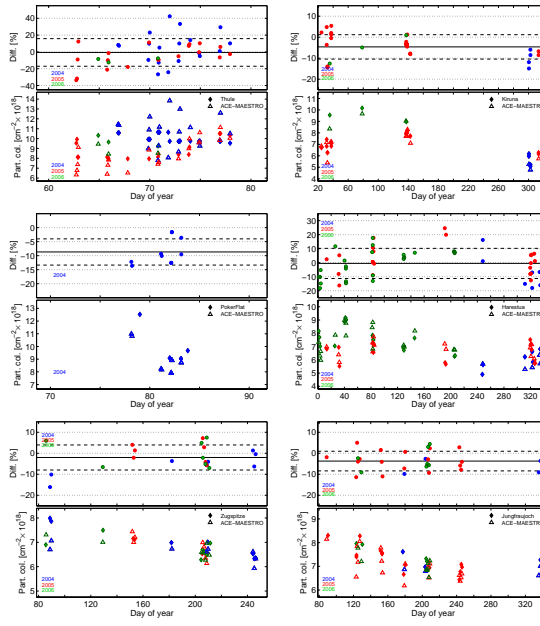
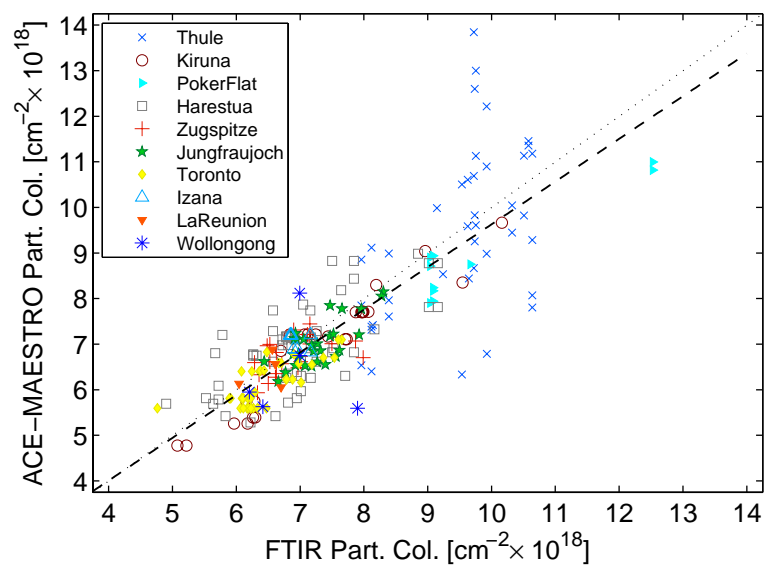**Fig. 41.** Same as Fig. 40 but for ACE-MAESTRO comparisons.
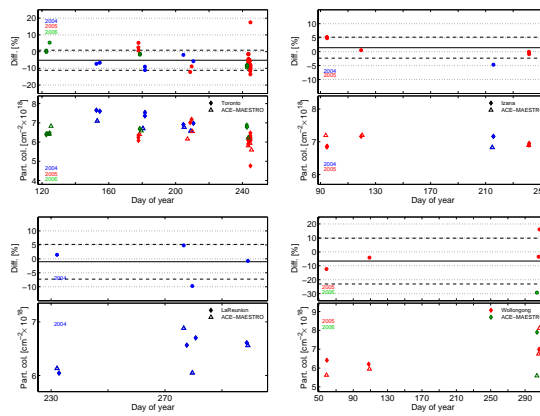
Fig. 41. Continued.
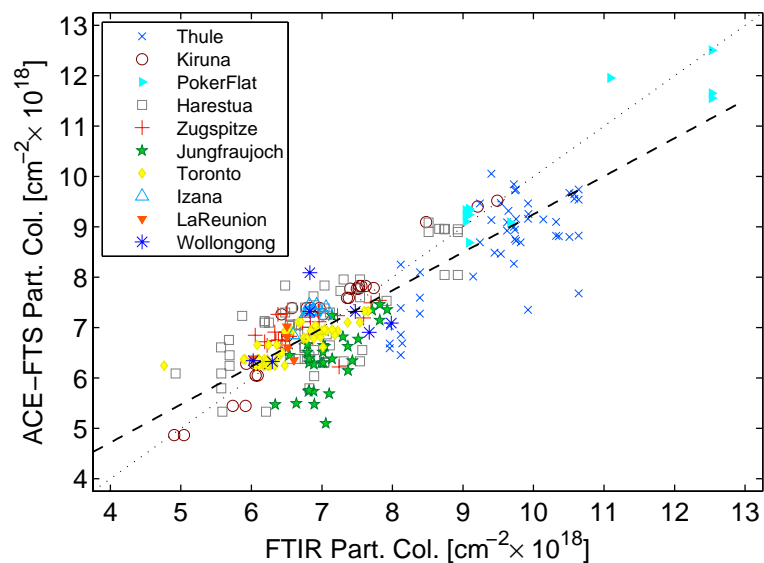
Fig. 42. Scatter plot of the ACE-FTS and ground-based FTIR partial columns of ozone shown in Fig. 40. The correlation value is 0.877. The least-squares linear fit of the data is also shown (dashed black).
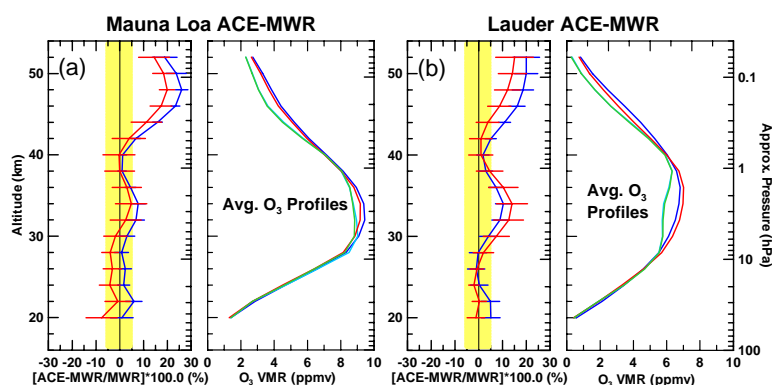
2651

**Fig. 43.** Same as Fig. 42 but for ACE-MAESTRO. The correlation value is 0.841.

Fig. 44. Mean profiles and fractional differences for the comparison of ACE-FTS and ACE-MAESTRO with the ground-based MWRs at Mauna Loa **(a)** and Lauder **(b)**. For each site: Left: Fractional differences ((ACE−MWR)/MWR) in percent shown for comparison with ACE-FTS (blue) and ACE-MAESTRO (red). Error bars indicate twice the uncertainty in the mean (2 × the 1-σ standard deviation divided by the square root of the number of pairs). Right: Mean VMR profiles from ACE-FTS (blue), ACE-MAESTRO (red) and the MWR mean profiles paired with ACE-FTS (green) and with ACE-MAESTRO (cyan). Approximate pressures corresponding to the altitudes are reported on the right-hand side.
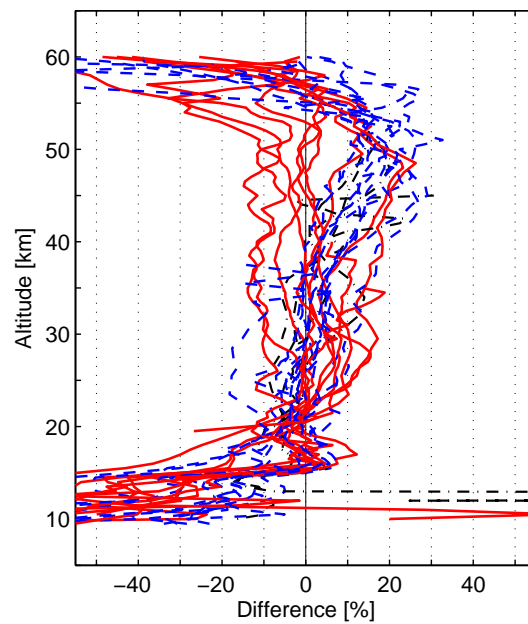
2653
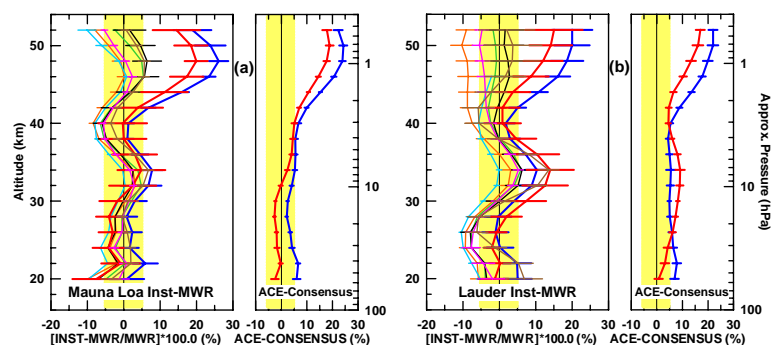
Fig. 45. Fractional differences for the comparison of the instruments listed in Table 6 with the ground-based MWRs and for the comparison of ACE-FTS and ACE-MAESTRO with the consensus profile at Mauna Loa **(a)** and Lauder **(b)**. For each site: Left: Fractional differences ((Instrument−MWR)/MWR) in percent shown for comparison with ACE-FTS (blue), ACE-MAESTRO (red), SAGE II (black), HALOE (orange), Aura-MLS (green), GOMOS (magenta), MIPAS (brown) and Lidar (light blue). Error bars indicate twice the uncertainty in the mean (2 × the 1-σ standard deviation divided by the square root of the number of pairs). Right: Fractional differences ((ACE−Consensus)/Consensus) in percent obtained by subtracting the average of the non-ACE difference profiles (left panel) from the ACE-MWR difference profiles. Fractional differences and 2 × the uncertainty in the mean (error bars) are shown for ACE-FTS (blue) and ACE-MAESTRO (red).
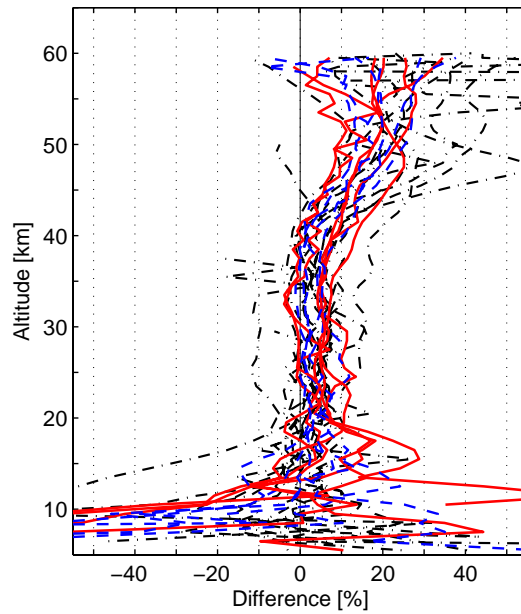
Fig. 46. Summary plot of the relative difference profiles for all statistical comparisons with ACE-FTS. Results are shown for ACE-FTS SR (solid red line) and SS (dashed blue line) when analyses were made separately. Relative difference profiles when no SR/SS separation was made are shown in black dot-dashed lines.

Fig. 47. Summary plot of the relative difference profiles for all statistical comparisons with ACE-MAESTRO. Results are separated between ACE-MAESTRO SR (solid red line) and SS (dashed blue line) occultations. The detailed NDACC study results are for the combined SR/SS results and are shown using the black dot-dashed lines.